Electronic Supplementary Material (ESI) for Inorganic Chemistry Frontiers.
This journal is © the Partner Organisations 2015

Enhancing the Photoluminescence Quantum Yields of Blue-Emitting Cationic Iridium(III) Complexes Bearing Bisphosphine Ligands

*Diego Rota Martir,[a] Ashu K. Bansal,[b] Vincent Di Mascio,[a] David B. Cordes,[a] Adam F. Henwood,[a] Alexandra M. Z. Slawin,[a] Paul C. J. Kamer,[a] Laura Martínez-Sarti,[c] Antonio Pertegás,[c] Henk J. Bolink,[c] Ifor D.W. Samuel,[b] and Eli Zysman-Colman[a]**

[a] Organic Semiconductor Centre, EaStCHEM School of Chemistry, University of St Andrews, St Andrews, Fife, UK, KY16 9ST, Fax: +44-1334 463808; Tel: +44-1334 463826; E-mail: eli.zysman-colman@st-andrews.ac.uk;
URL: http://www.zysman-colman.com
[b] Organic Semiconductor Centre, SUPA, School of Physics and Astronomy, University of St. Andrews, St. Andrews, Fife, KY16 9SS, UK; E-mail: idws@st-andrews.ac.uk
[c] Instituto de Ciencia Molecular, Universidad de Valencia, C/ Catedrático J. Beltrán, ES-46980 Paterna, Valencia, Spain. E-mail: henk.bolink@uv.es

SUPPORTING INFORMATION

Table of contents:

	Pages
Characterization of precursors and ligands	**S2**
Characterization of iridium dimers **D1** – **D4**	**S7**
Characterization of $[Ir(C^\wedge N)_2(P^\wedge P)]PF_6$ complexes, **1** - **4**	**S10**
Crystal structure data of complexes **2a**, **4c** and **1e**	**S38**
Supplementary optoelectronic data for complexes **1** – **4**	**S39**
Electroluminescent devices (LEECs)	**S52**

Characterization of Precursors and Ligand

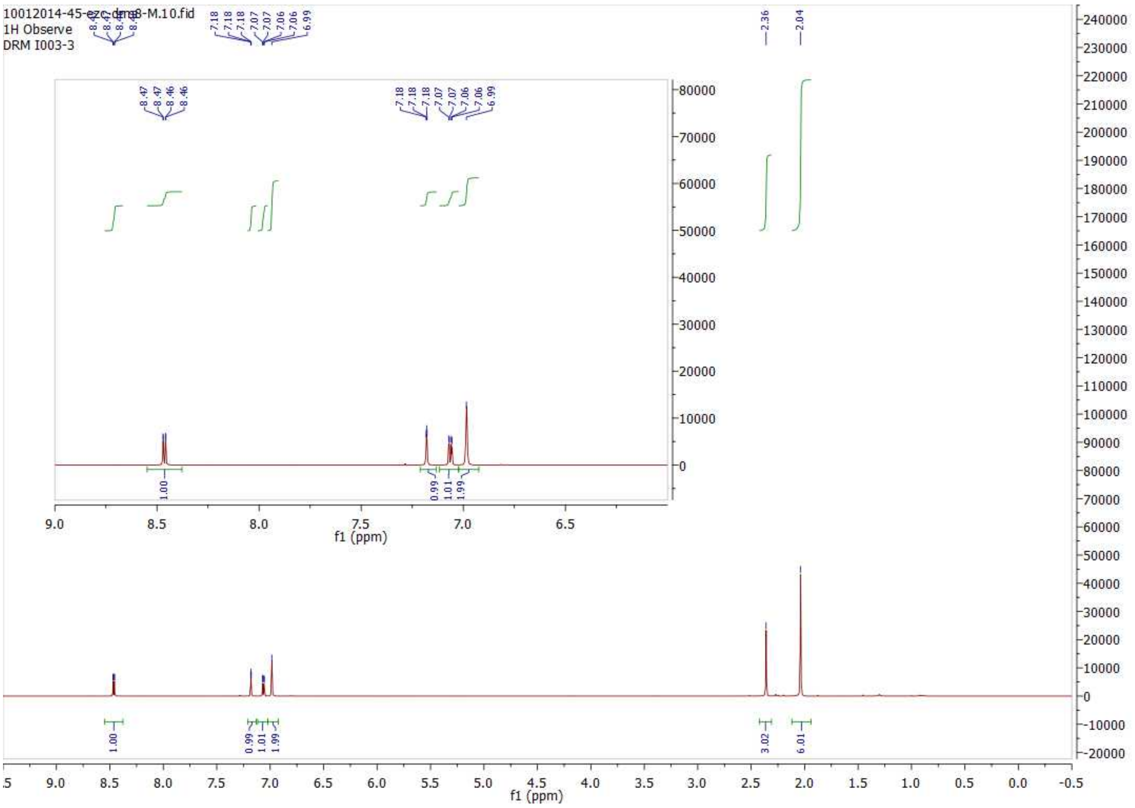

Figure **S1**. ^{1}H NMR spectra of **2-Chloro-4-(2,4,6-trimethylphenyl)pyridine** (**A**) in CD_3Cl

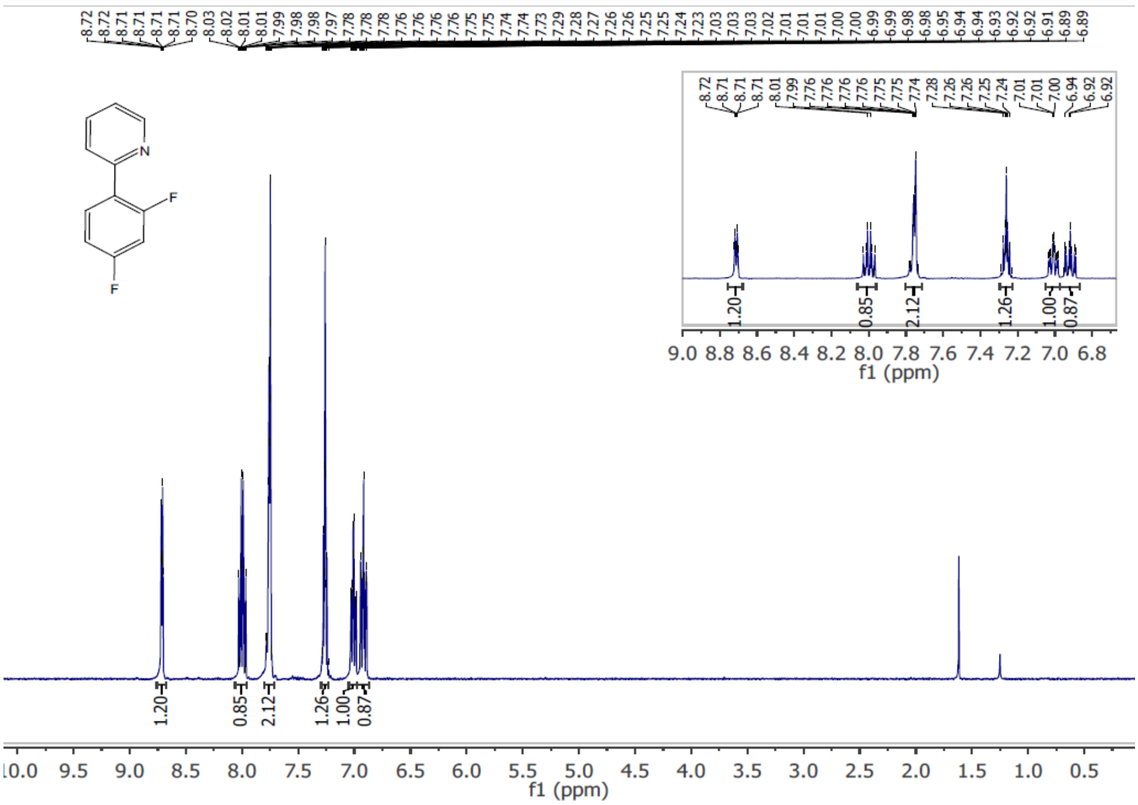

Figure **S2**. ^{1}H NMR spectrum of **2-(2,4-difluorophenyl)pyridine (dFppy)** in $CDCl_3$.

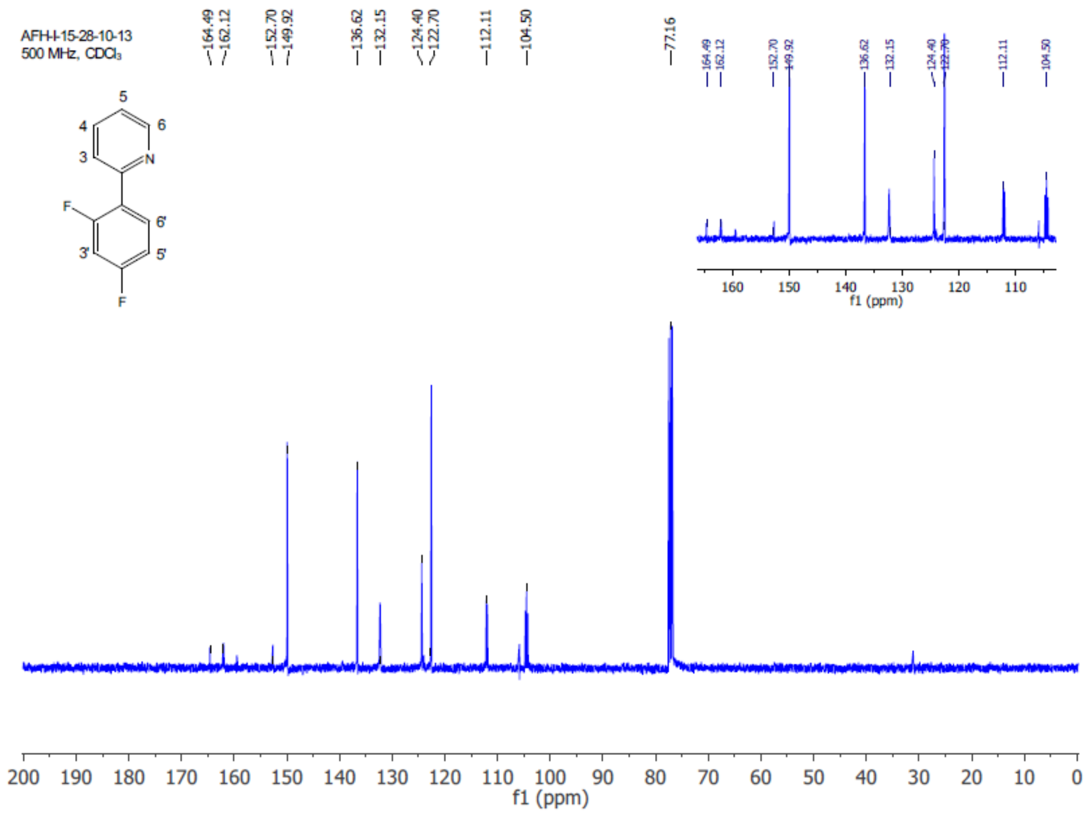

Figure **S3**. ^{13}C NMR spectrum of 2**-(2,4-difluorophenyl)pyridine (dFppy)** in $CDCl_3$.

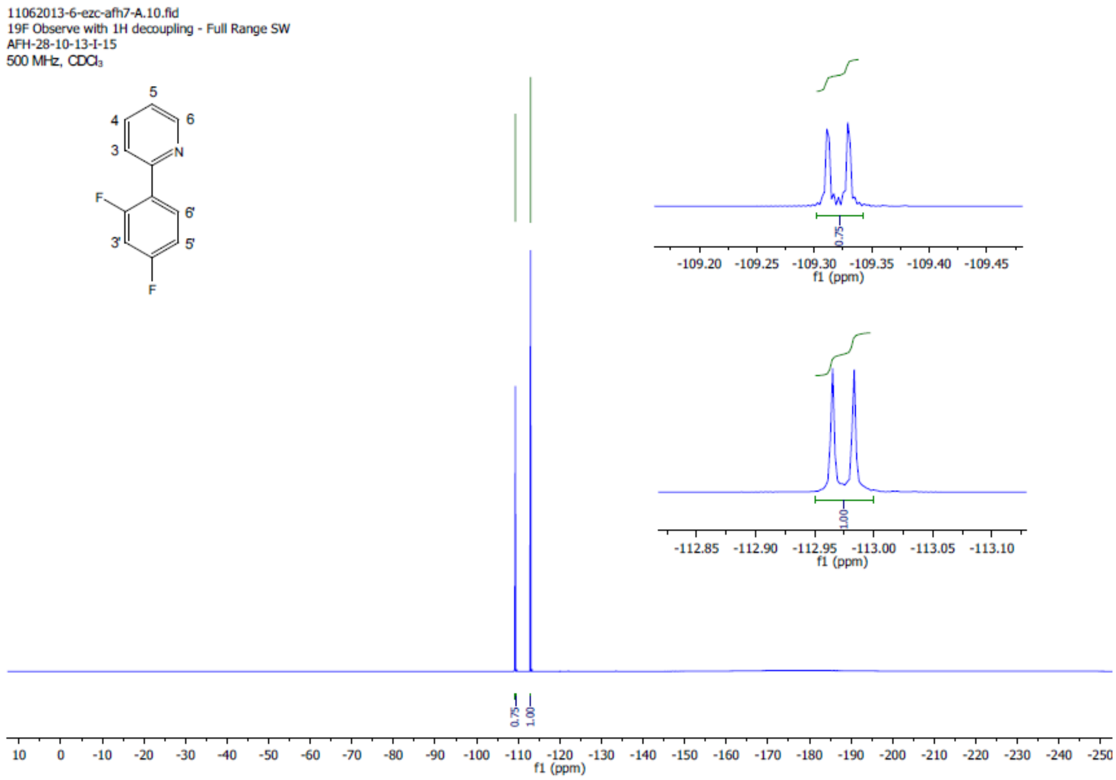

Figure **S4.** ^{19}F {^{1}H} NMR spectrum of **2-(2,4-difluorophenyl)pyridine (dFppy)** in $CDCl_3$.

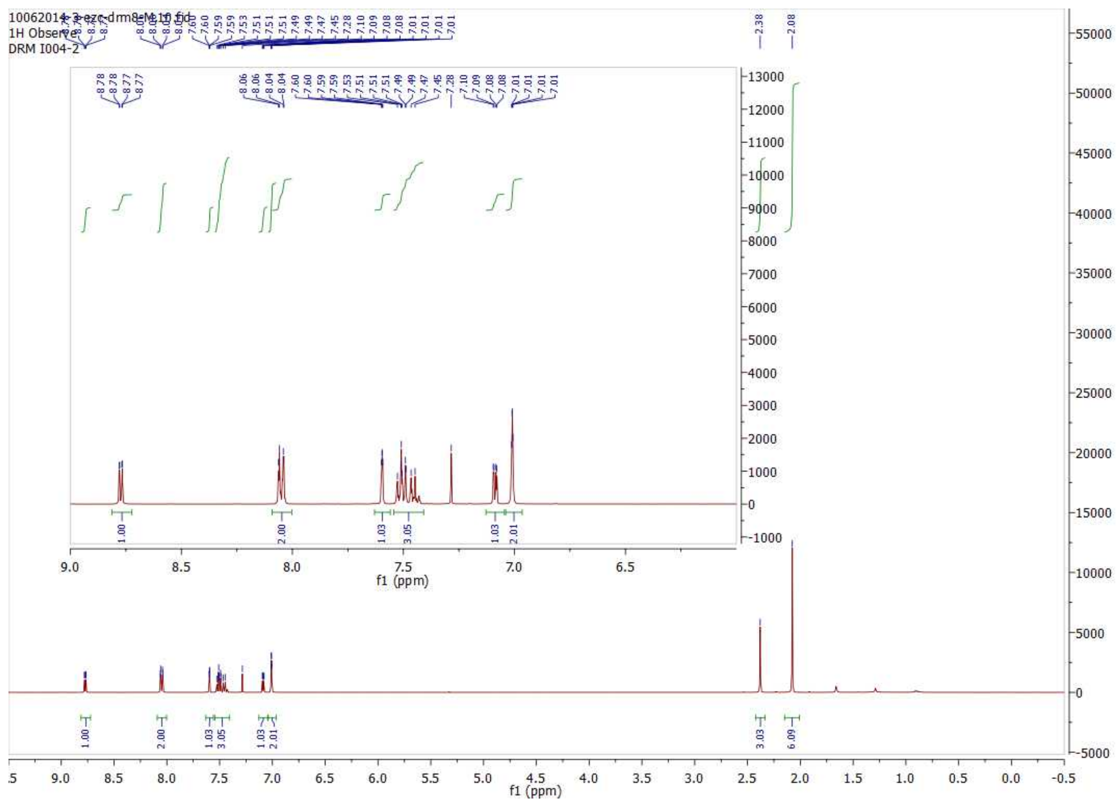

Figure **S5**. ^{1}H NMR spectra of **2-phenyl-4-(2,4,6-trimethylphenyl)pyridine (mesppy)** in $CDCl_3$.

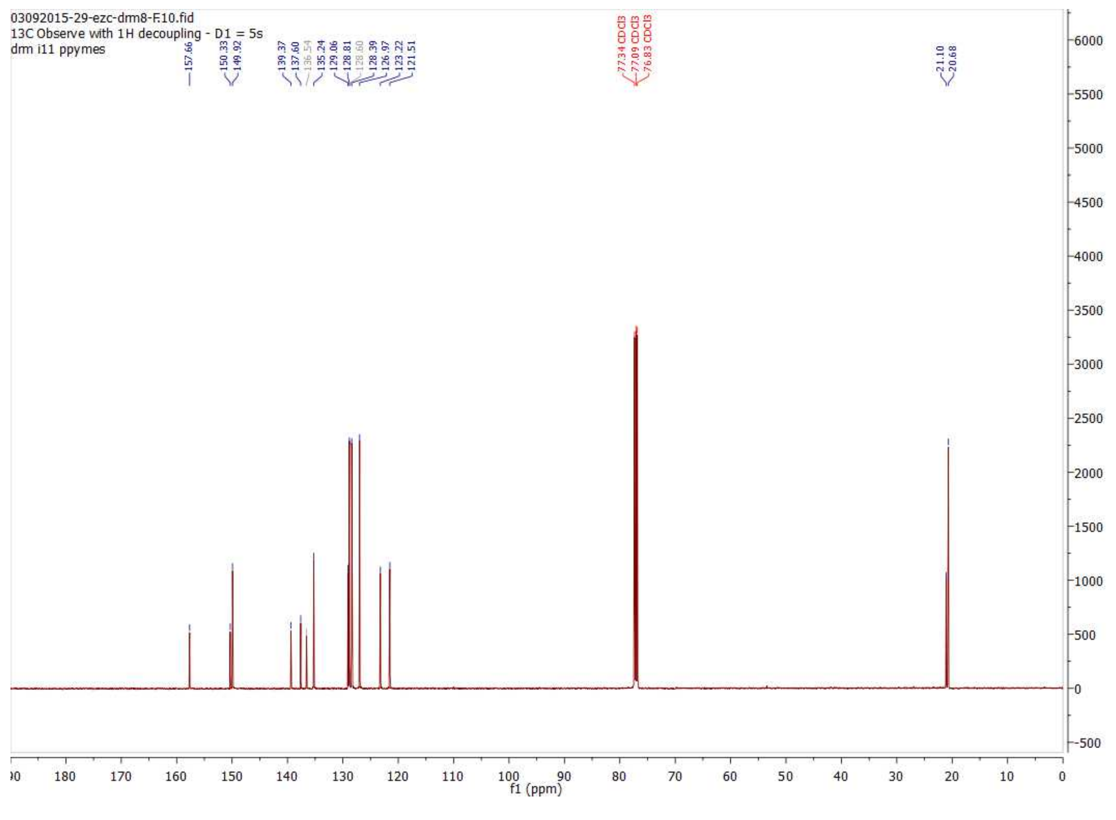

Figure **S6**. ^{13}C NMR spectra of **2-phenyl-4-(2,4,6-trimethylphenyl)pyridine (mesppy)** in $CDCl_3$

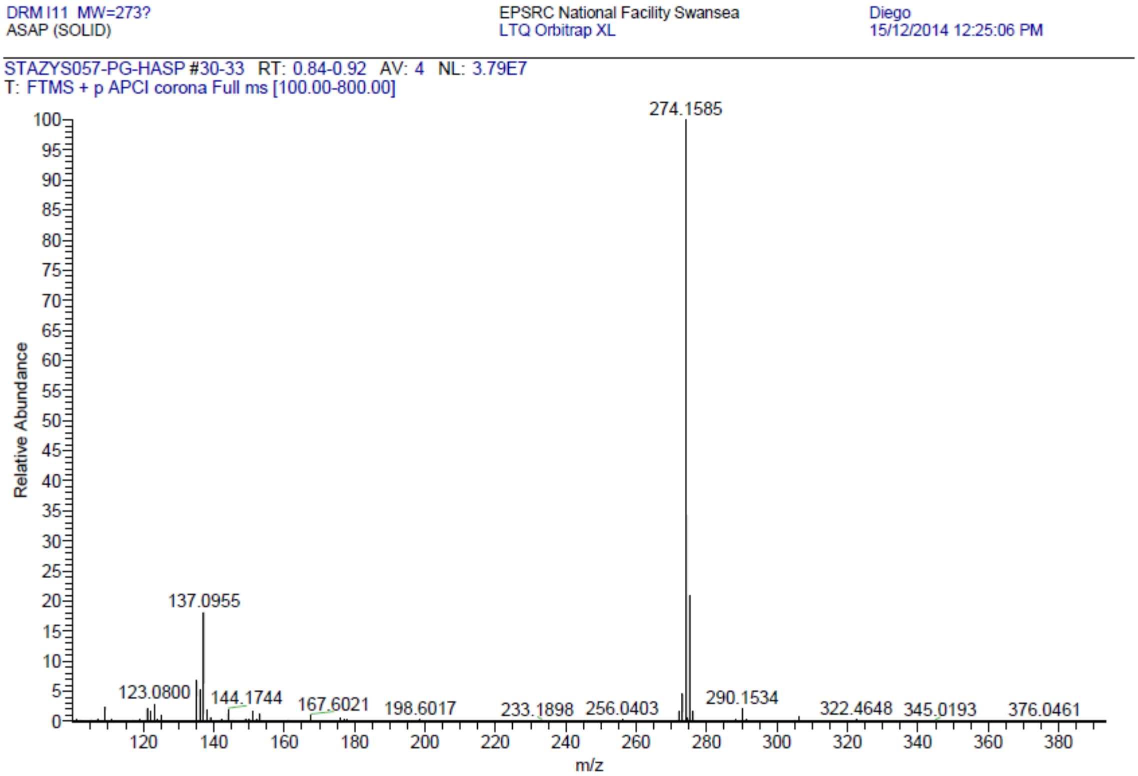

Figure **S7.** FT-MS spectra of **2-phenyl-4-(2,4,6-trimethylphenyl)pyridine (mesppy)**

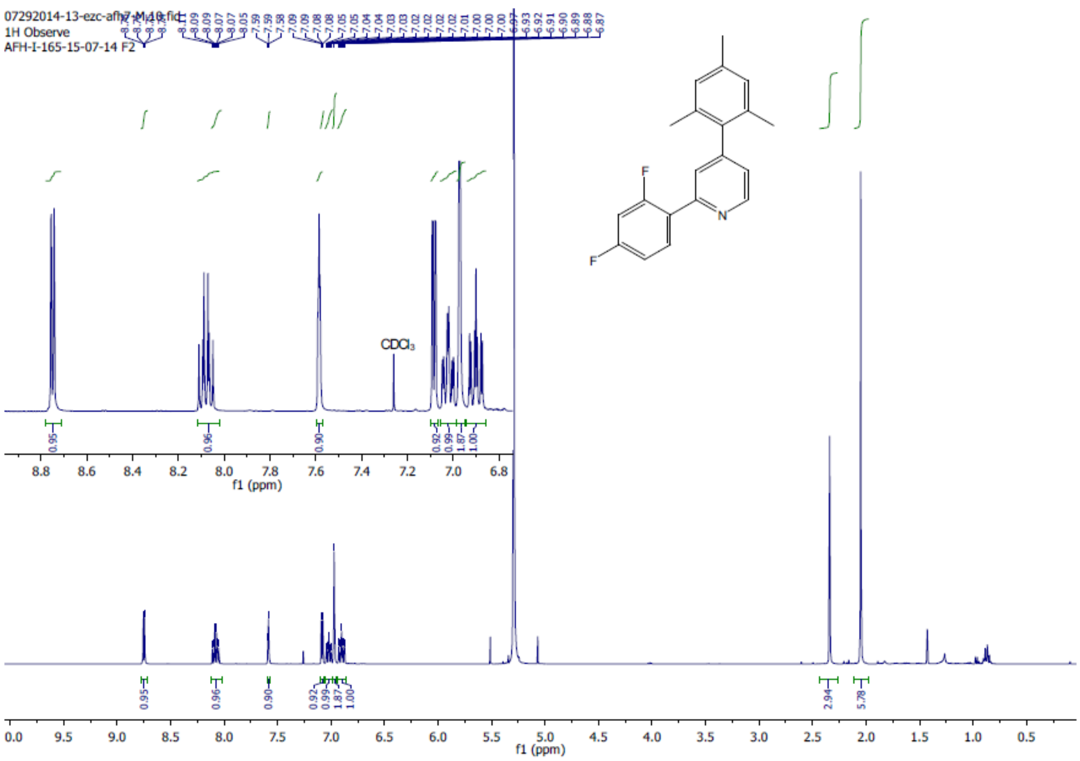

Figure **S8**. ^{1}H NMR spectrum of **2-(2,4-difluorophenyl)-4-(2,4,6-trimethylphenyl)pyridine (dFmesppy)** in $CDCl_3$.

Figure **S9**. ^{19}F NMR spectrum of **2-(2,4-difluorophenyl)-4-(2,4,6-trimethylphenyl)pyridine (dFmesppy)** in $CDCl_3$.

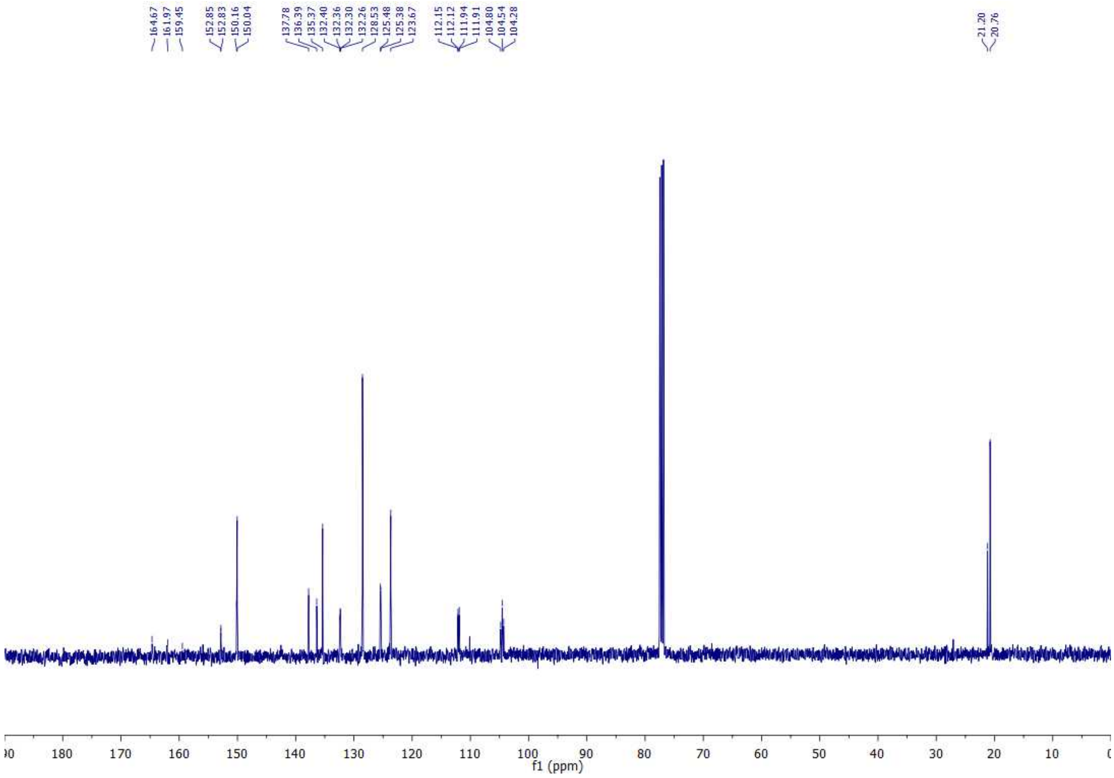

Figure **S10.** ^{13}C NMR spectrum of **2-(2,4-difluorophenyl)-4-(2,4,6-trimethylphenyl)pyridine (dFmesppy)** in $CDCl_3$.

Characterization of Iridium dimers

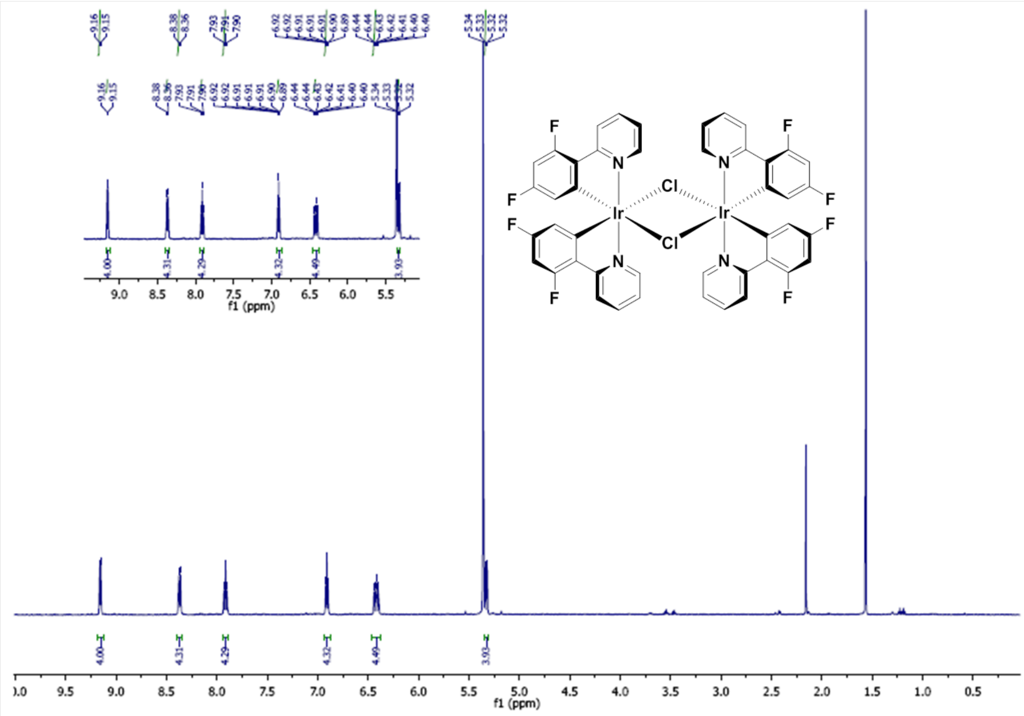

Figure **S11.** [1]H NMR spectrum of **tetrakis[2-(4',6'-difluorophenyl)-pyridinato-*N*,*C*[2']]-bis(*μ*-chloro)diiridium(III), [Ir(dFppy)$_2$(*μ*-Cl)]$_2$ (D2)** in CD_2Cl_2.

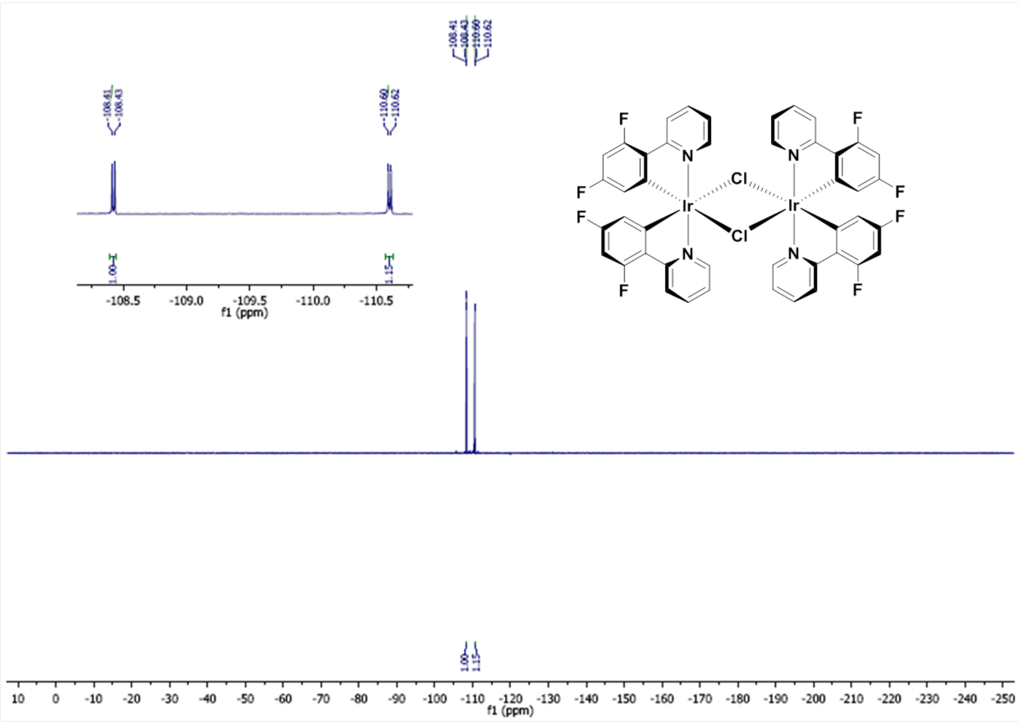

Figure **S12.** [19]F NMR spectrum of **tetrakis[2-(4',6'-difluorophenyl)-pyridinato-*N*,*C*[2']]-bis(*μ*-chloro)diiridium(III), [Ir(dFppy)$_2$(*μ*-Cl)]$_2$ (D2)** in CD_2Cl_2.

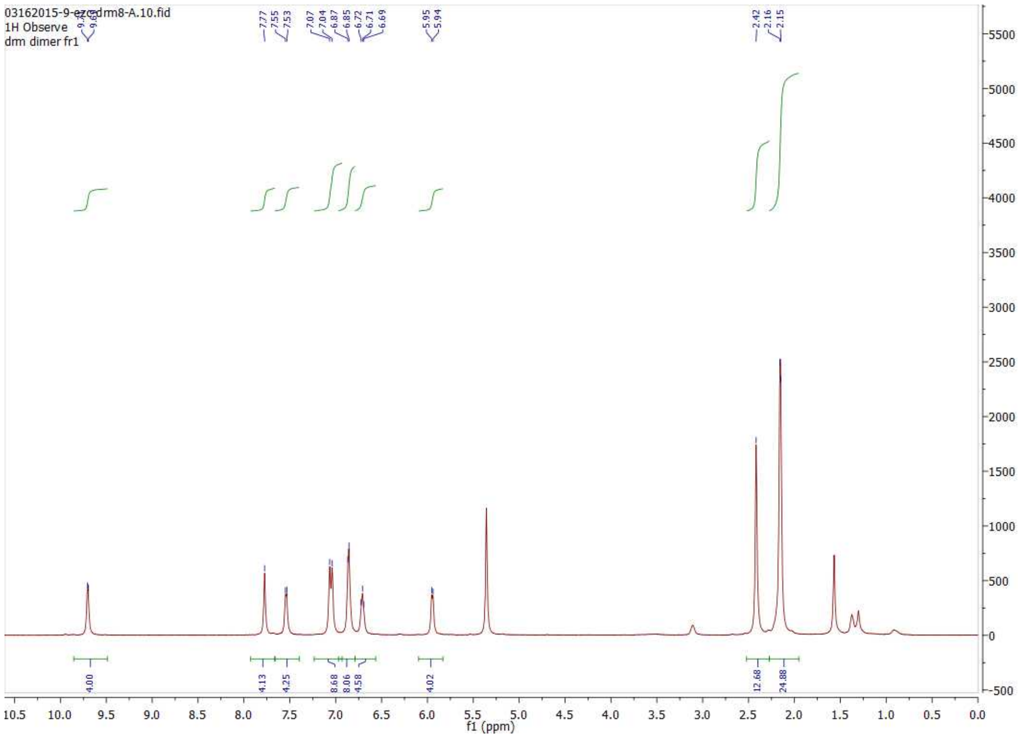

Figure **S13**. ^{1}H NMR spectrum of **tetrakis[2-(phenyl)-4-(2,4,6-trimethylphenyl)pyridinato-*N*,*C*$^{2'}$]-bis(*μ*-chloro)diiridium(III), [Ir(mesppy)$_2$(*μ*-Cl)]$_2$ (D3)** in CD_2Cl_2.

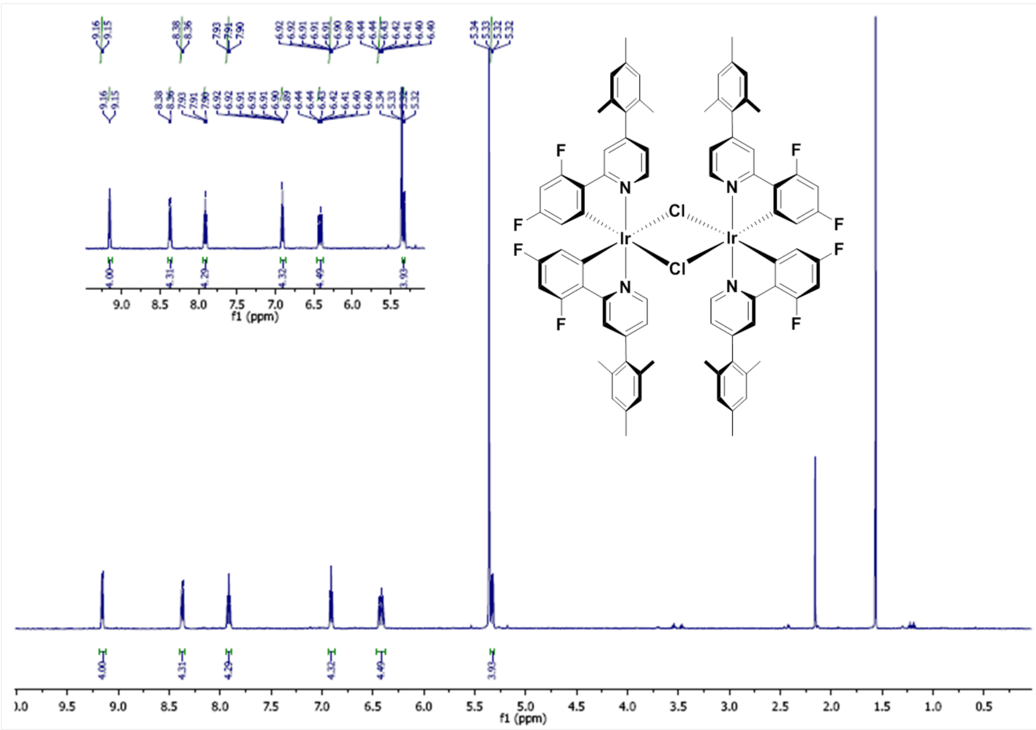

Figure **S14**. ^{1}H NMR spectrum of **tetrakis[2-(4',6'-difluorophenyl)-4-(2,4,6-trimethylphenyl)pyridinato-*N*,*C*$^{2'}$]-bis(*μ*-chloro)diiridium(III)**, **[Ir(dFmesppy)$_2$(*μ*-Cl)]$_2$ (D4)** in CD_2Cl_2.

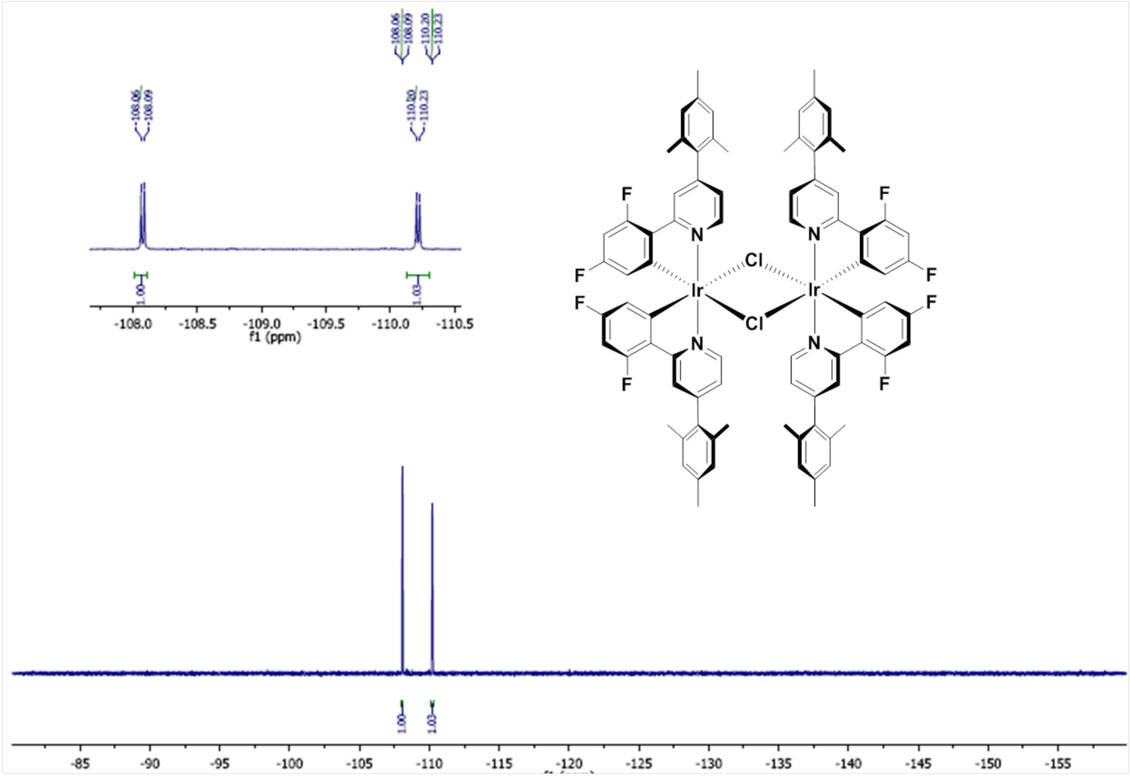

Figure **S15**. ^{19}F NMR spectrum of **tetrakis[2-(4',6'-difluorophenyl)-4-(2,4,6-trimethylphenyl)pyridinato-*N*,*C*$^{2'}$]-bis(μ-chloro)diiridium(III), [Ir(dFmesppy)$_2$(μ-Cl)]$_2$ (D4)** in CD_2Cl_2.

Characterization of $[Ir(C^\wedge N)_2(P^\wedge P)]PF_6$ complexes

Iridium(III)bis[2-phenylpyridinato]-4,5-bis(diphenylphosphino)-9,9-dimethylxanthenehexafluorophosphate, $[Ir(ppy)_2(xantphos)]PF_6$ (1a)

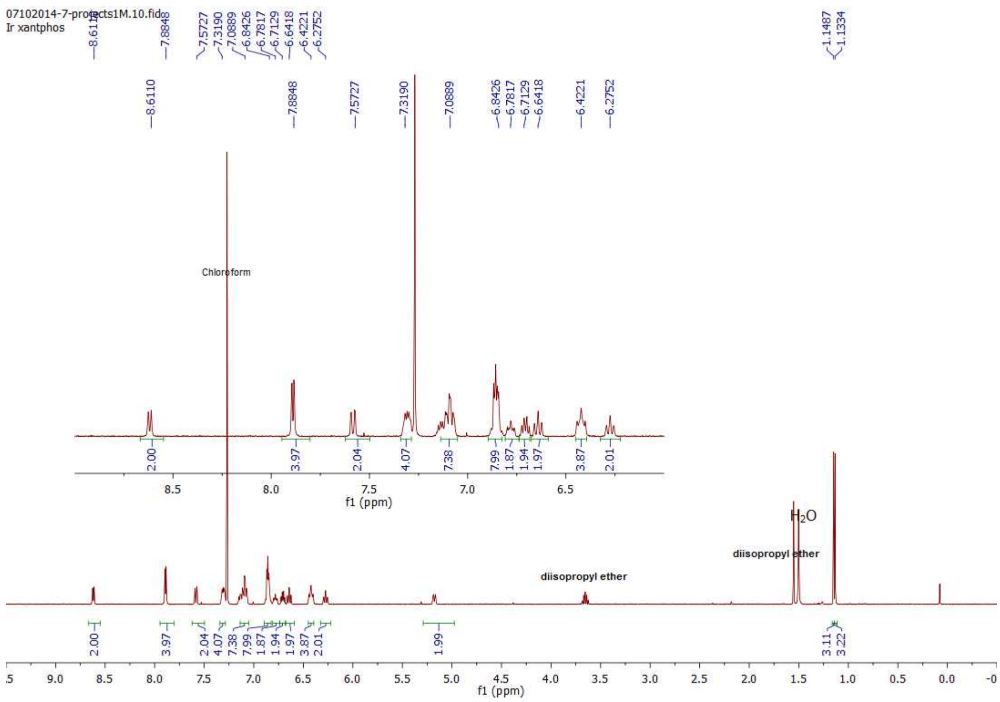

Figure **S16.** ^{1}H NMR spectrum of **$[Ir(ppy)_2(xantphos)]PF_6$ (1a)** in CD_2Cl_2.

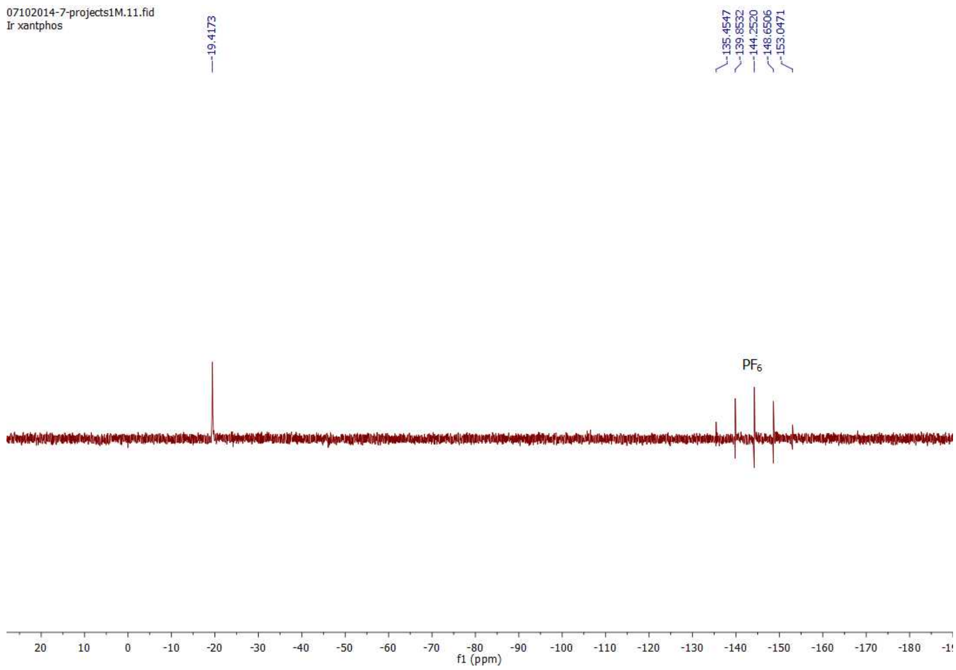

Figure **S17**. ^{31}P NMR spectrum of **$[Ir(ppy)_2(xantphos)]PF_6$ (1a)** in CD_2Cl_2.

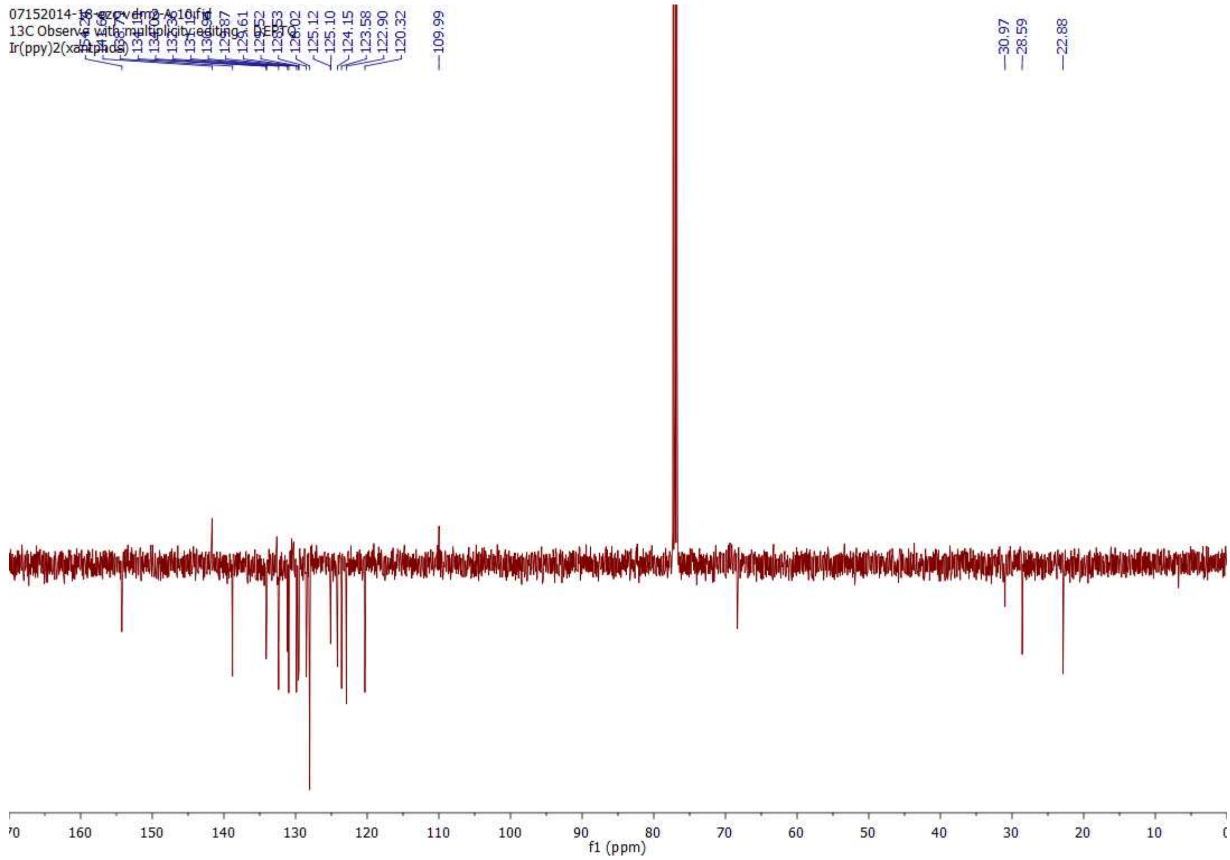

Figure **S18.** ^{13}C NMR spectrum of **[Ir(ppy)$_2$(xantphos)]PF$_6$ (1a)** in CD_2Cl_2.

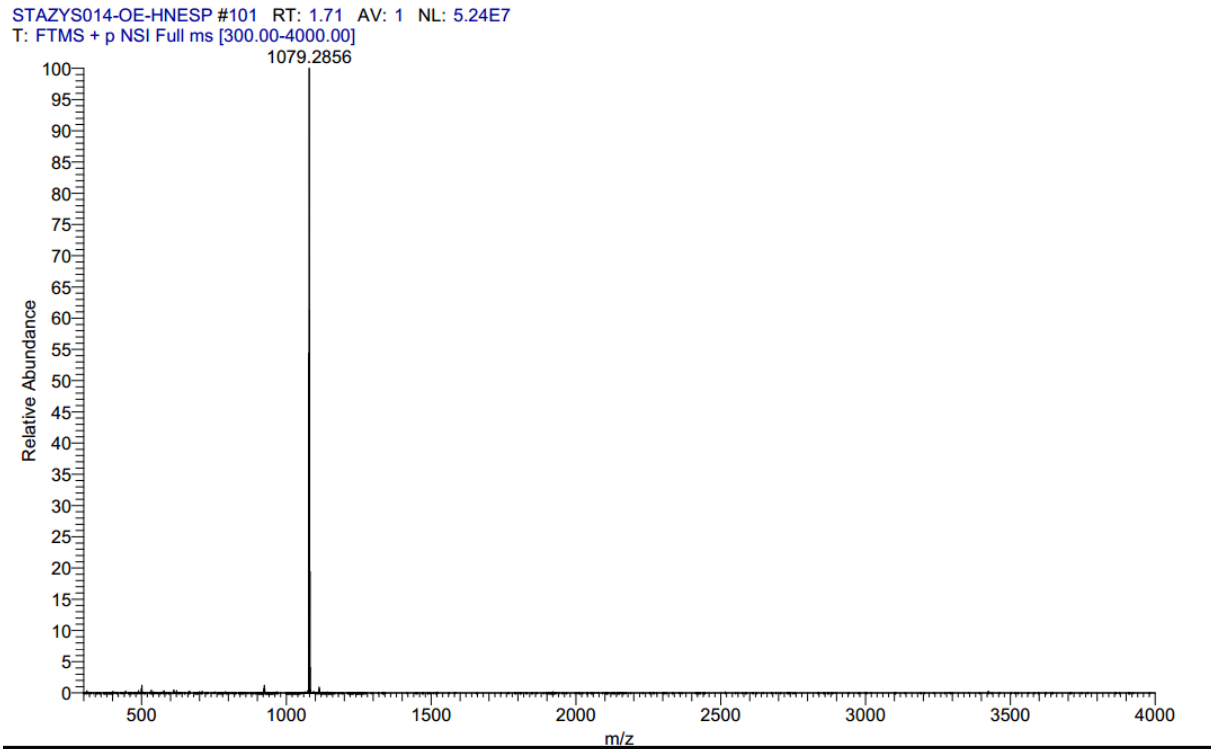

Figure **S19.** HR-MS spectrum of **[Ir(ppy)$_2$(xantphos)]PF$_6$ (1a).**

Iridium (III) bis[2-phenyl-4-(2,4,6-trimethylphenyl)pyridine]- 4,5-Bis(diphenylphosphino)-9,9-dimethylxanthene hexafluorophosphate, [Ir(mesppy)$_2$(xantphos)](PF$_6$) (2a)

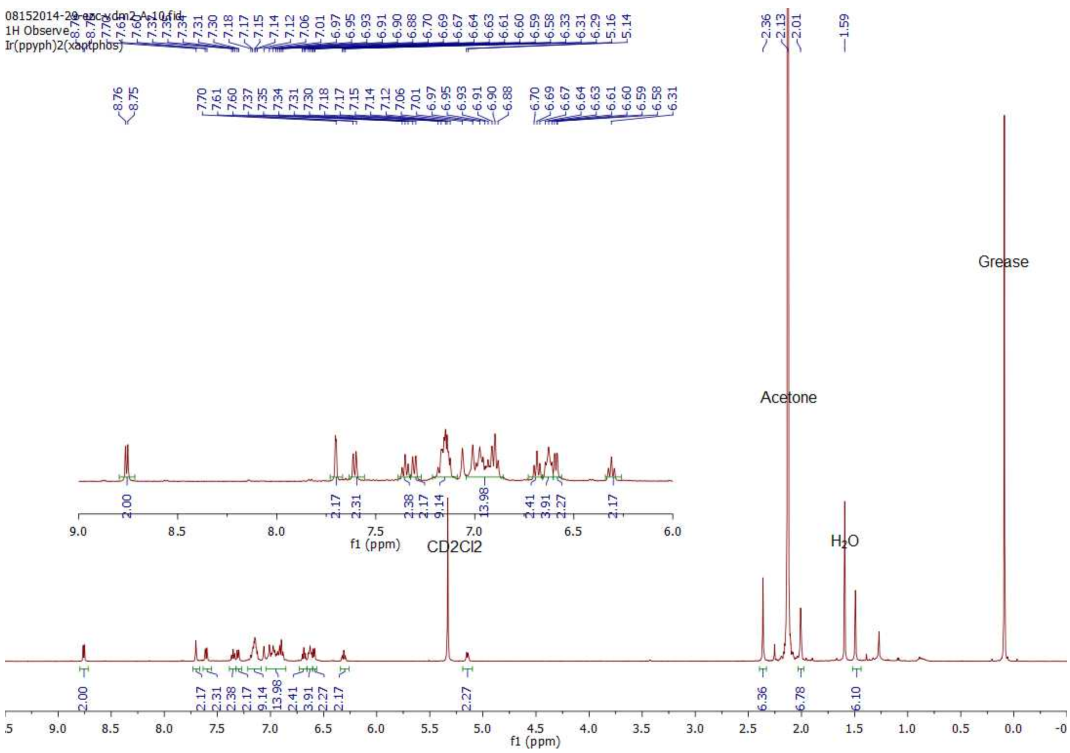

Figure **S20.** ^{1}H NMR spectrum of **[Ir(mesppy)$_2$(xantphos)]PF$_6$ (2a)** in CD_2Cl_2.

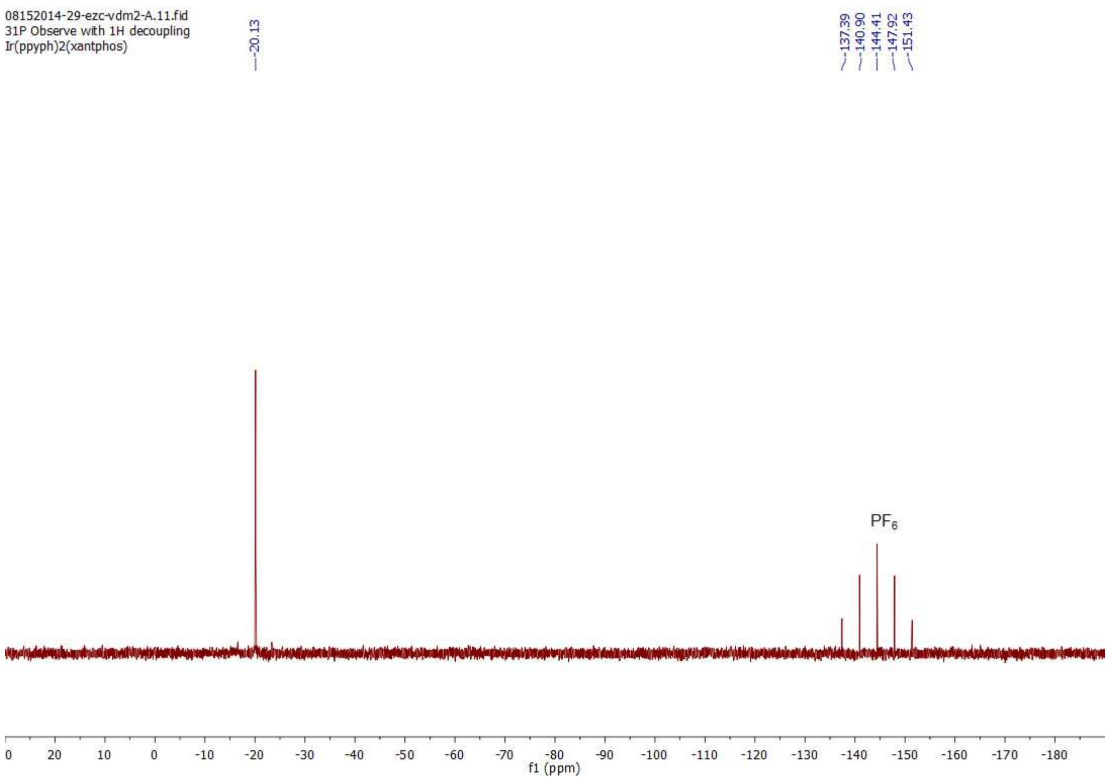

Figure **S21**. ^{31}P NMR spectrum of **[Ir(mesppy)$_2$(xantphos)]PF$_6$ (2a)** in CD_2Cl_2.

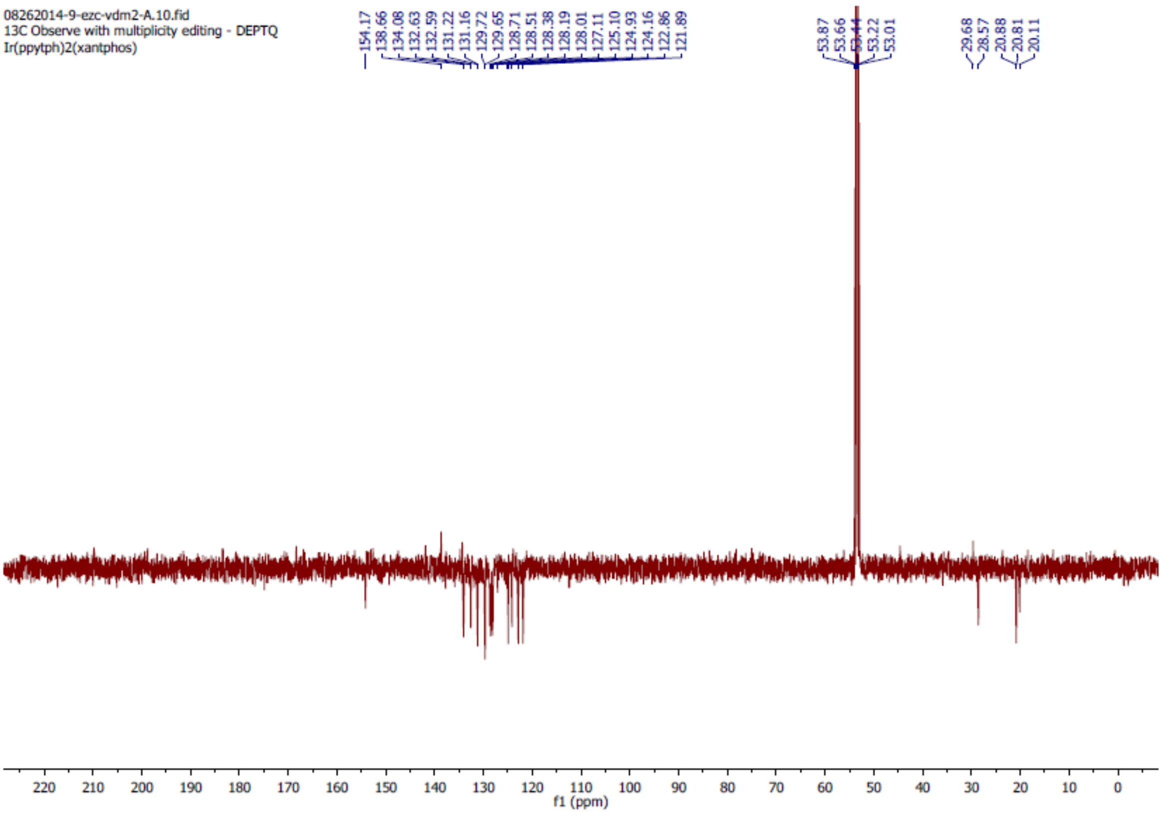

Figure **S22**. ^{13}C NMR spectrum of **[Ir(mesppy)$_2$(xantphos)]PF$_6$ (2a)** in CD_2Cl_2.

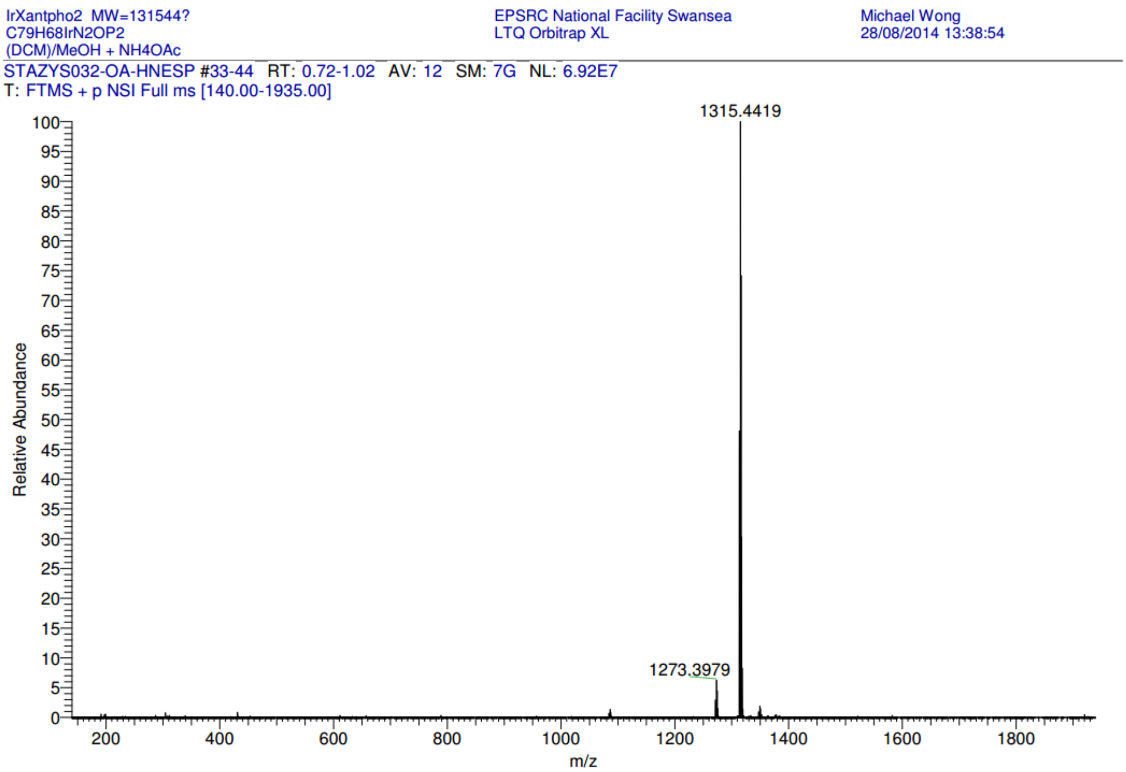

Figure **S23.** HR-MS spectrum of **[Ir(mesppy)$_2$(xantphos)]PF$_6$ (2a)**.

Iridium(III)bis[2-(2,4-difluoro)-phenyl-4-(2,4,6-trimethylphenyl)pyridinato]-4,5-bis(diphenylphosphino)-9,9-dimethylxanthene hexafluorophosphate, [Ir(dFmesppy)$_2$(xantphos)](PF$_6$) (4a)

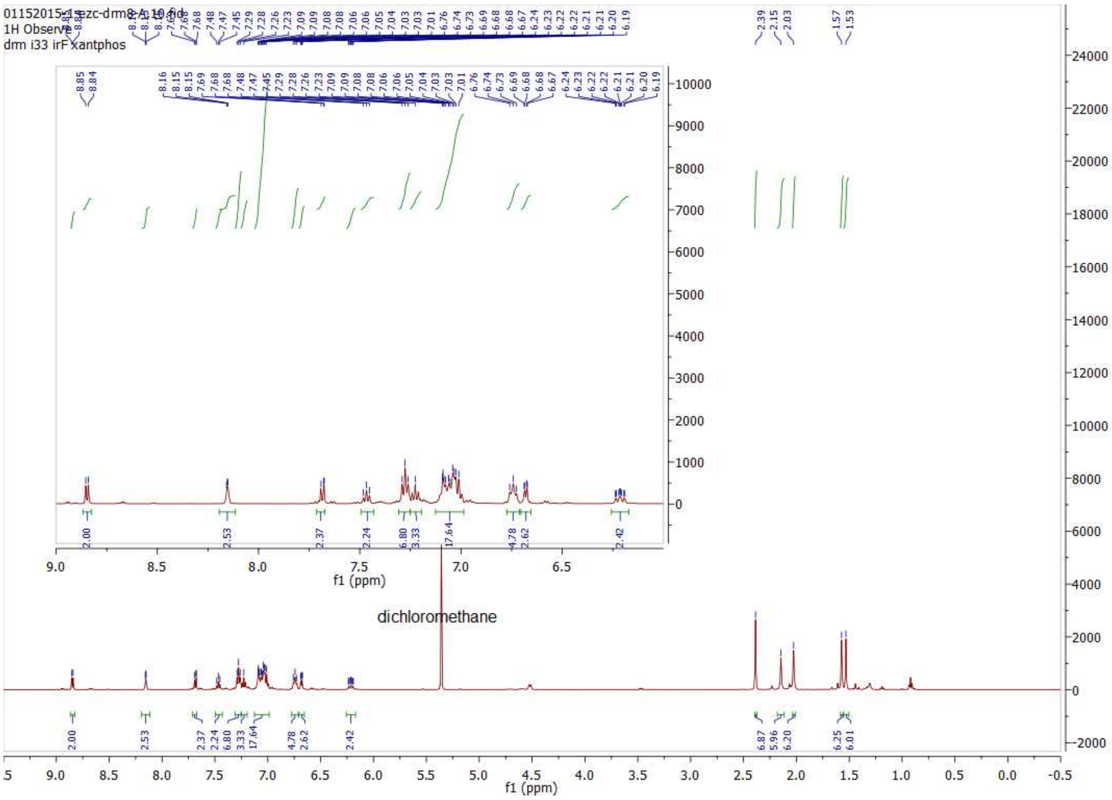

Figure **S24**. ^{1}H NMR spectrum of **[Ir(dFmesppy)$_2$(xantphos)]PF$_6$ (4a)** in CD_2Cl_2.

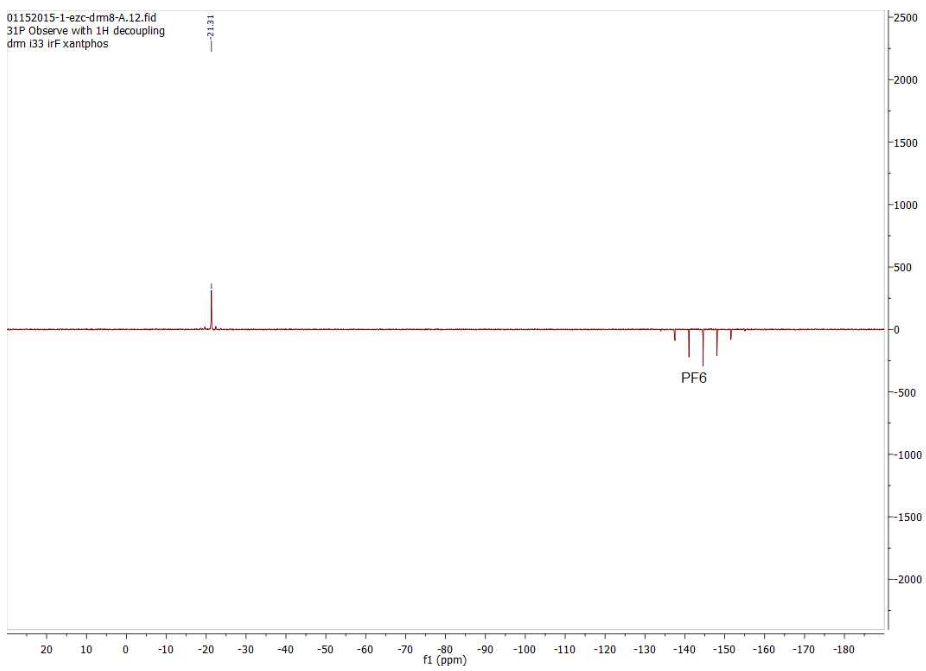

Figure **S25.** ^{31}P NMR spectrum of **[Ir(dFmesppy)$_2$(xantphos)]PF$_6$ (4a)** in CD_2Cl_2.

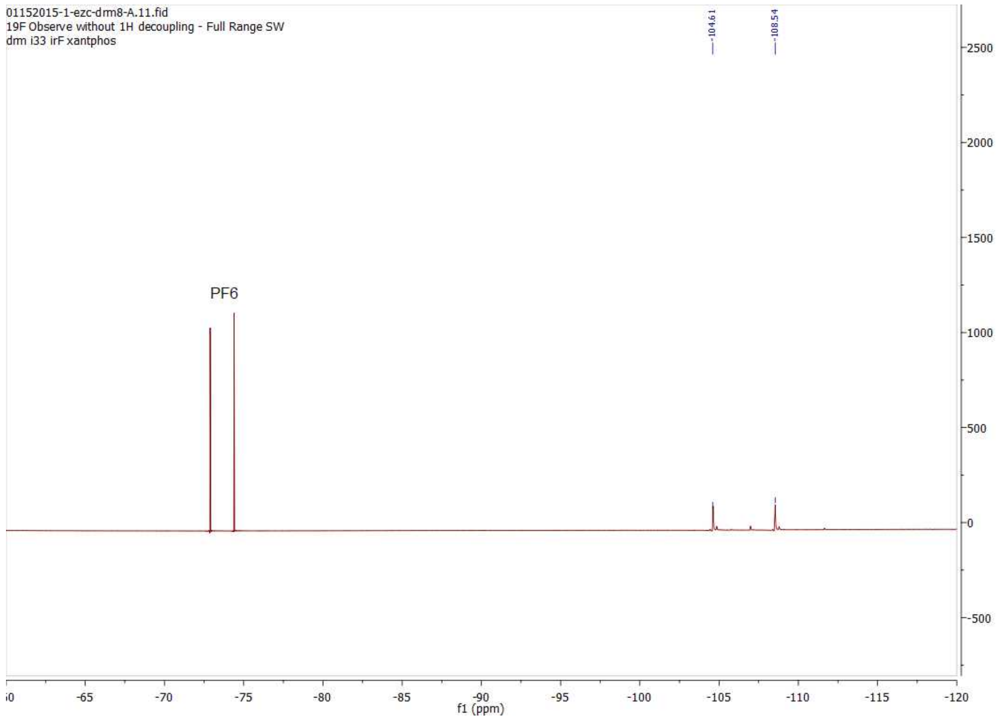

Figure **S26**. ^{19}F NMR spectrum of **$[Ir(dFmesppy)_2(xantphos)]PF_6$ (4a)** in CD_2Cl_2.

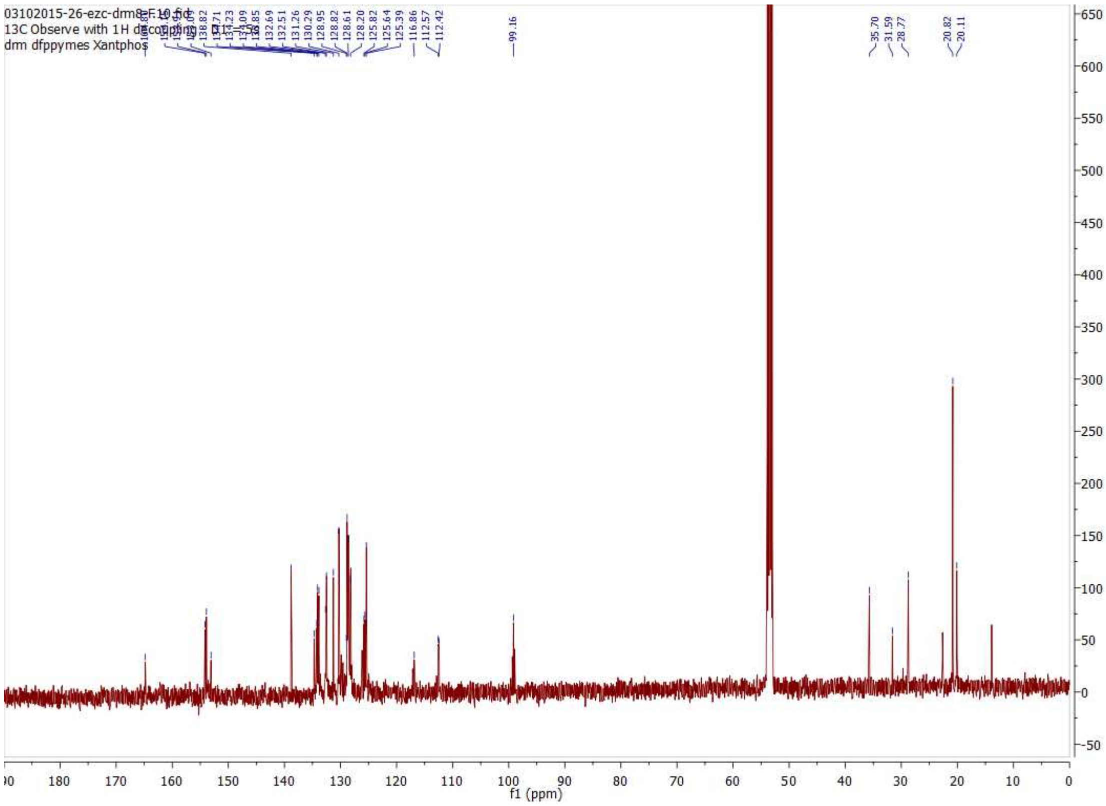

Figure **S27**. ^{13}C NMR spectrum of **$[Ir(dFmesppy)_2(xantphos)]PF_6$ (4a)** in CD_2Cl_2.

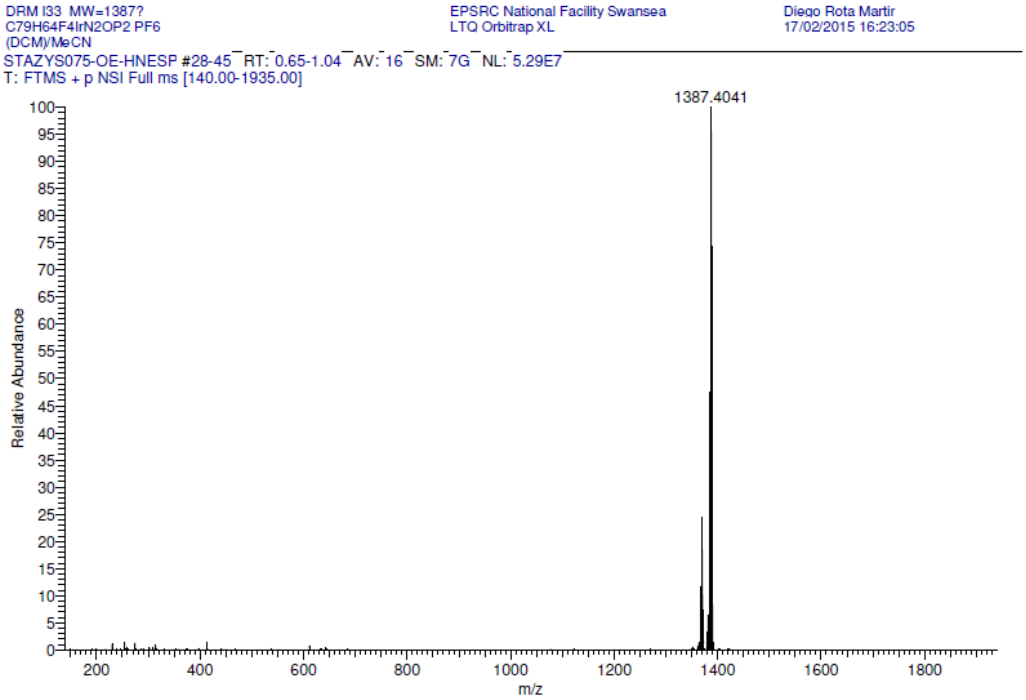

Figure **S28**. FT-MS spectrum of **[Ir(dFmesppy)$_2$(xantphos)]PF$_6$ (4a)**.

Iridium(III)bis[2-phenylpyridinato]-bis[(2-diphenylphosphino)phenyl]methane hexafluorophosphate, [Ir(ppy)$_2$(dpephos)](PF$_6$) (1b)

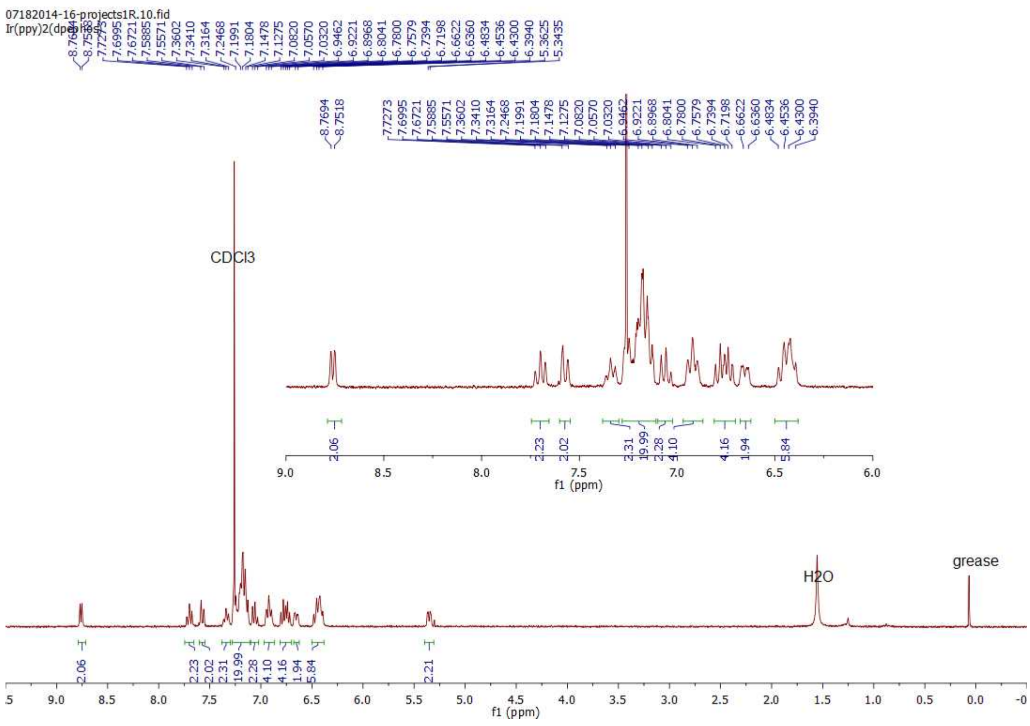

Figure **S29**. ^{1}H NMR spectrum of **[Ir(ppy)$_2$(dpephos)]PF$_6$ (1b)** in CD_2Cl_2.

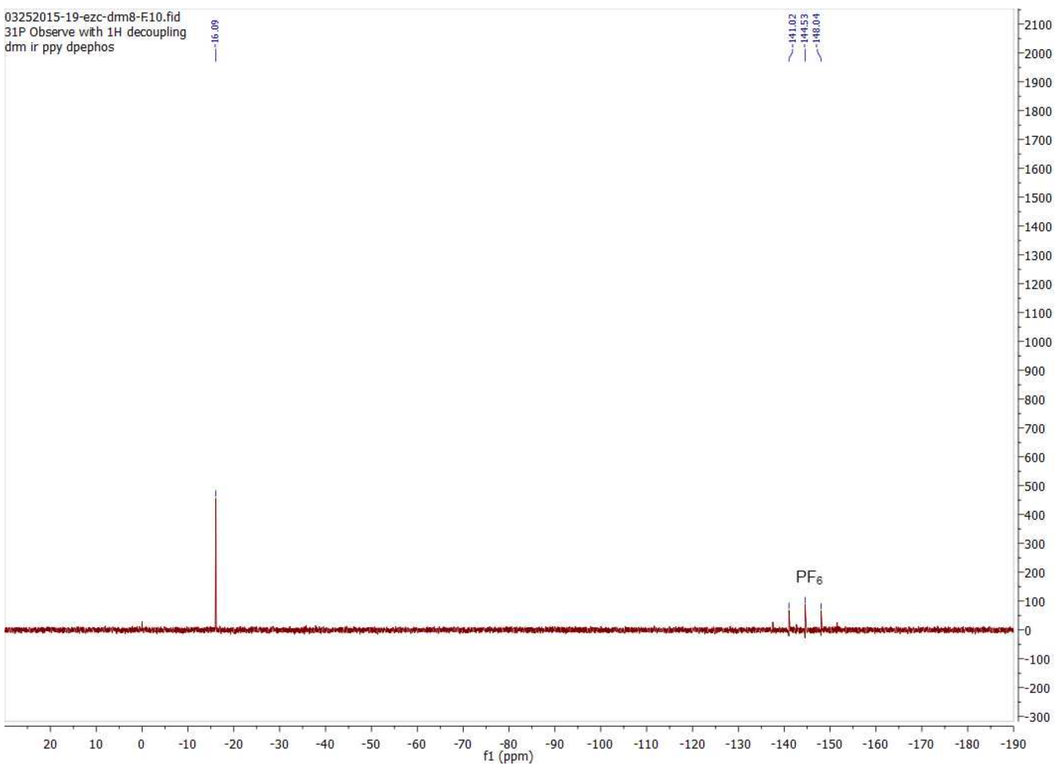

Figure **S30**. ^{31}P NMR spectrum of **[Ir(ppy)$_2$(dpephos)]PF$_6$ (1b)** in CD_2Cl_2.

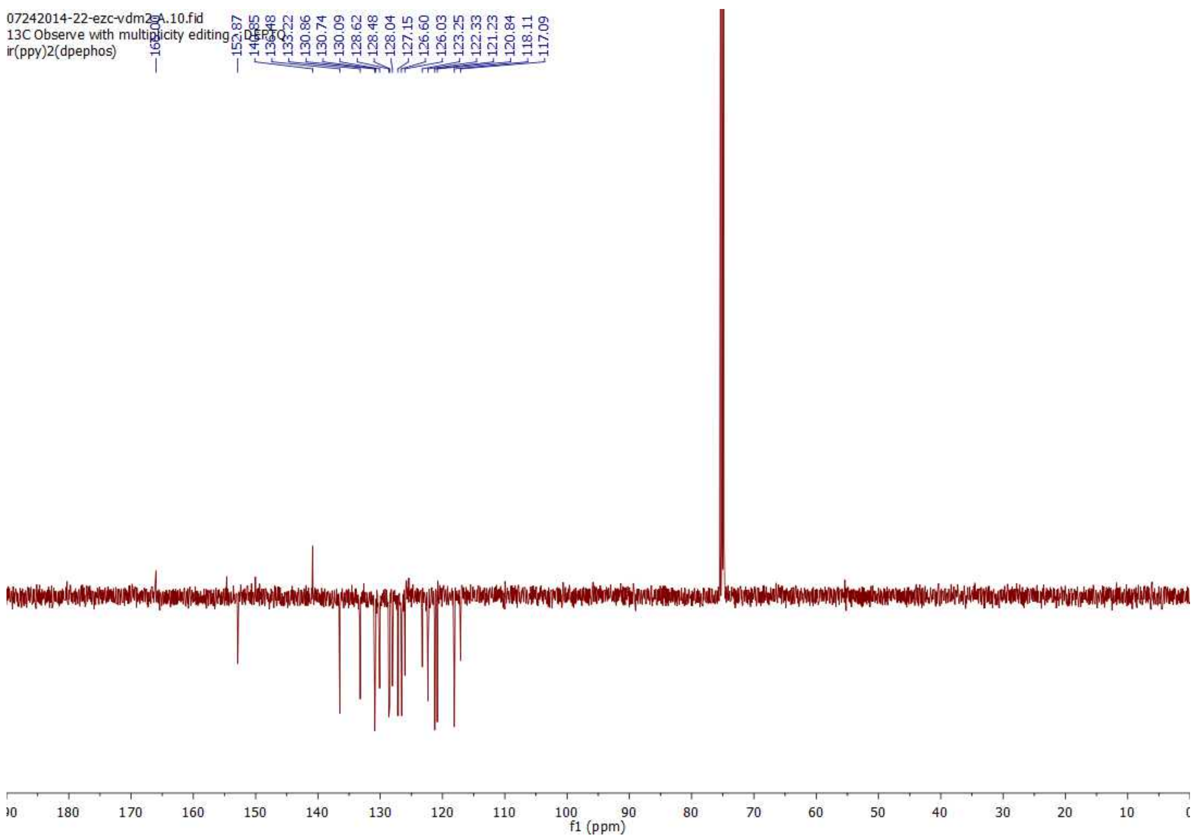

Figure **S31**. ^{13}C NMR spectrum of **[Ir(ppy)$_2$(dpephos)](PF$_6$) (1b)** in CD_2Cl_2.

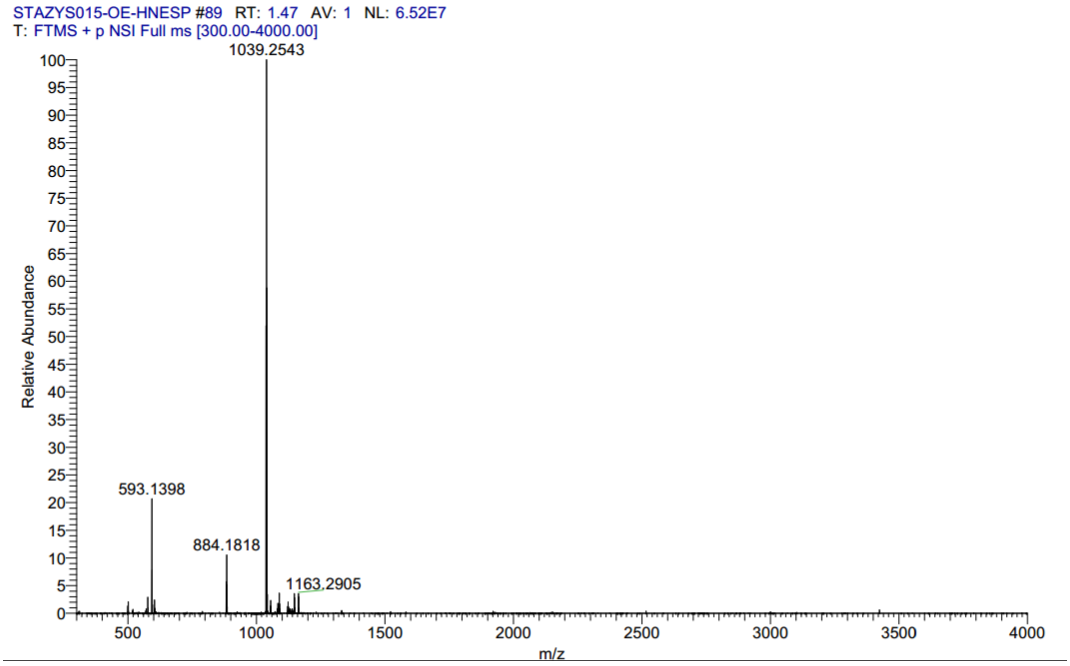

Figure **S32**. FT-MS spectrum of **[Ir(ppy)$_2$(dpephos)]PF$_6$ (1b)** in CD_2Cl_2.

Iridium(III)bis[2-phenyl-4-(2,4,6-trimethylphenyl)pyridinato]-bis[(2-diphenylphosphino)phenyl]methane hexafluorophosphate, [Ir(ppymes)$_2$(dpephos)](PF$_6$) (2b)

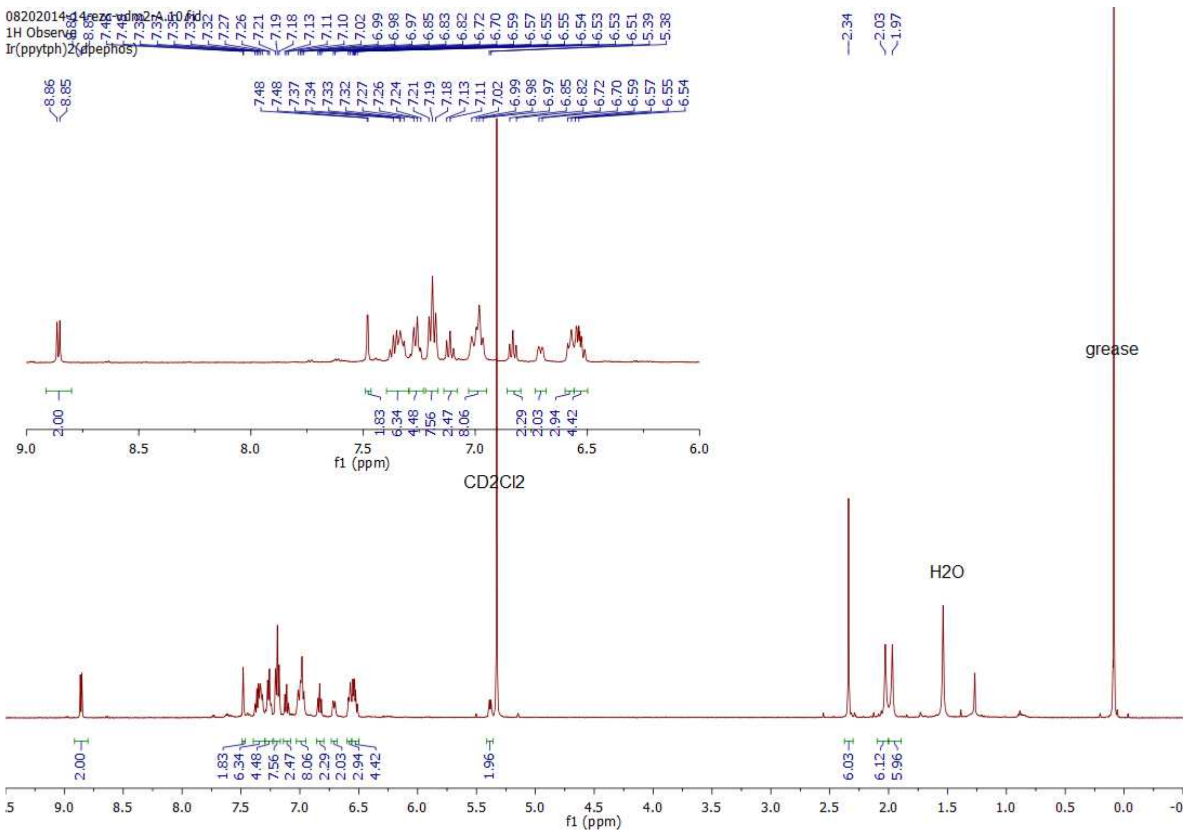

Figure **S33**. [1]H NMR spectrum of **[Ir(mesppy)$_2$(dpephos)]PF$_6$ (2b)** in CD_2Cl_2.

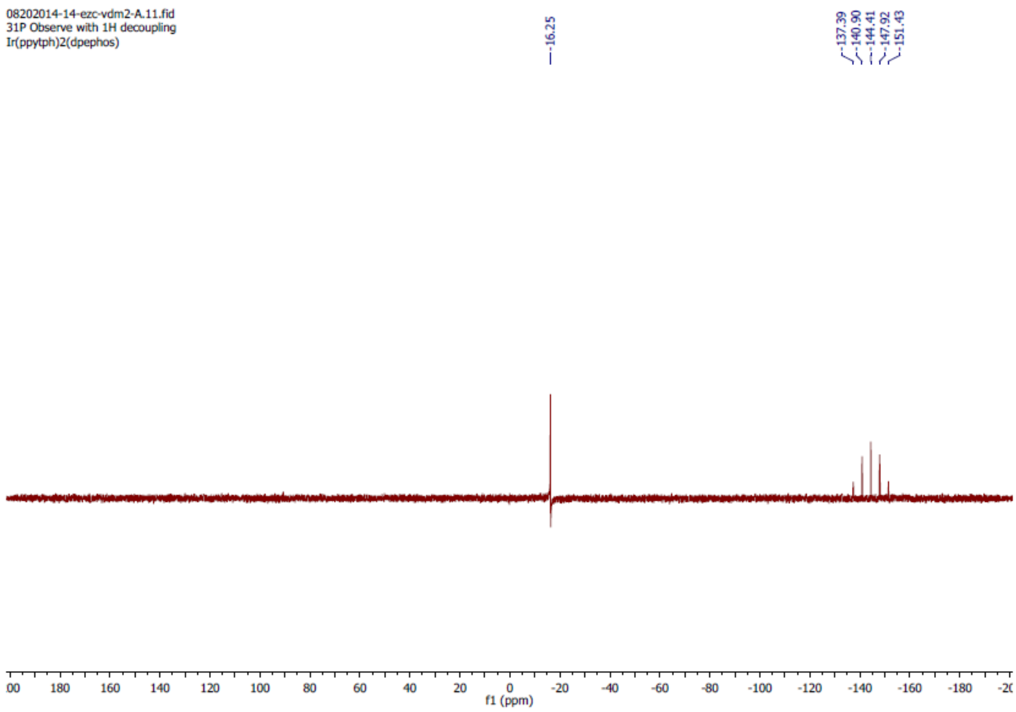

Figure **S34**. [31]P NMR spectrum of **[Ir(mesppy)$_2$(dpephos)]PF$_6$ (2b)** in CD_2Cl_2.

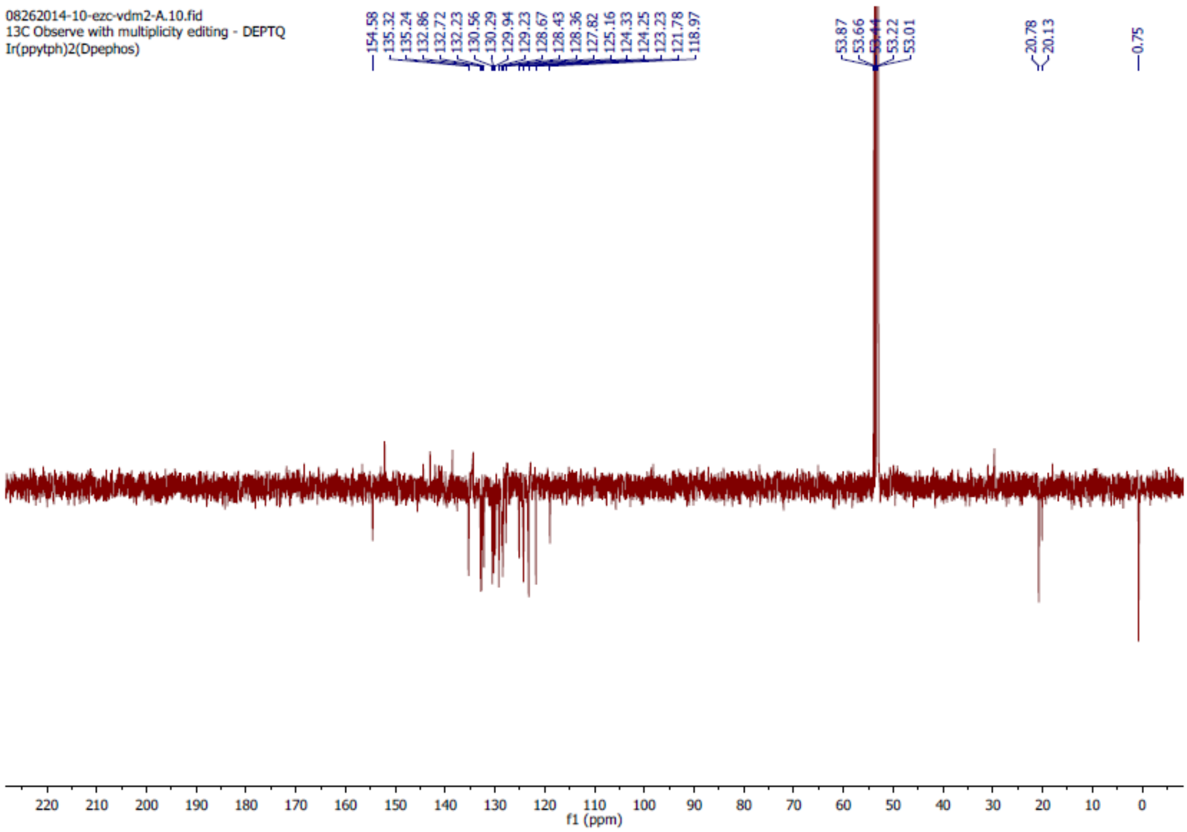

Figure **S35**. [13]C NMR spectrum of **[Ir(mesppy)$_2$(dpephos)](PF$_6$) (2b)** in CD_2Cl_2.

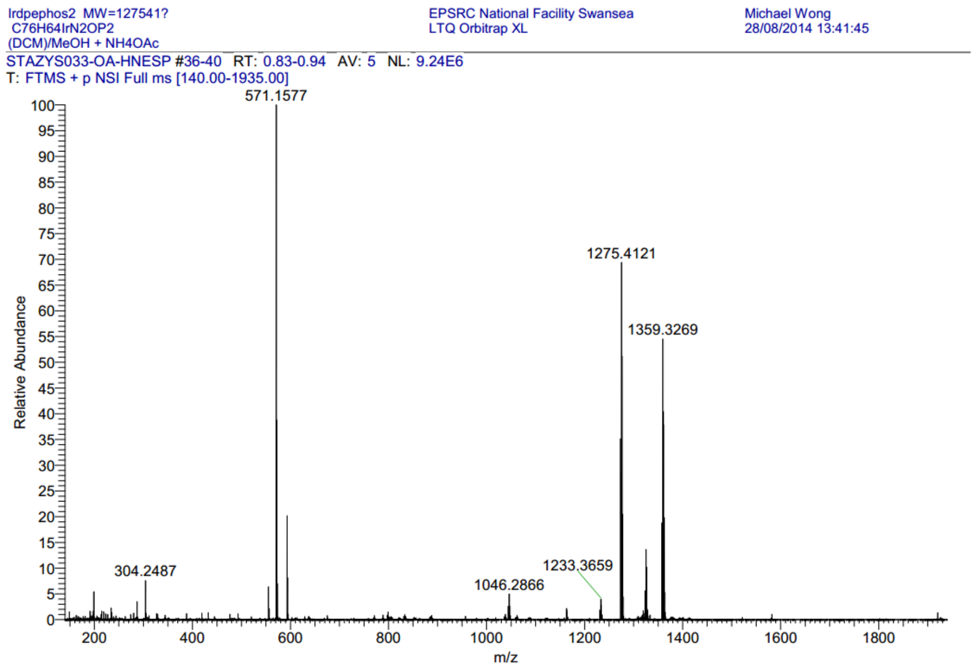

Figure **S36**. FT-MS spectrum of **[Ir(mesppy)$_2$(dpephos)]PF$_6$ (2b)**.

Iridium(III)bis[2-(2,4-difluorophenyl)-4-(2,4,6-trimethylphenyl)pyridinato]-bis[(2-diphenylphosphino)phenyl]methane hexafluorophosphate, [Ir(dFmesppy)$_2$(dpephos)]PF$_6$ (4b)

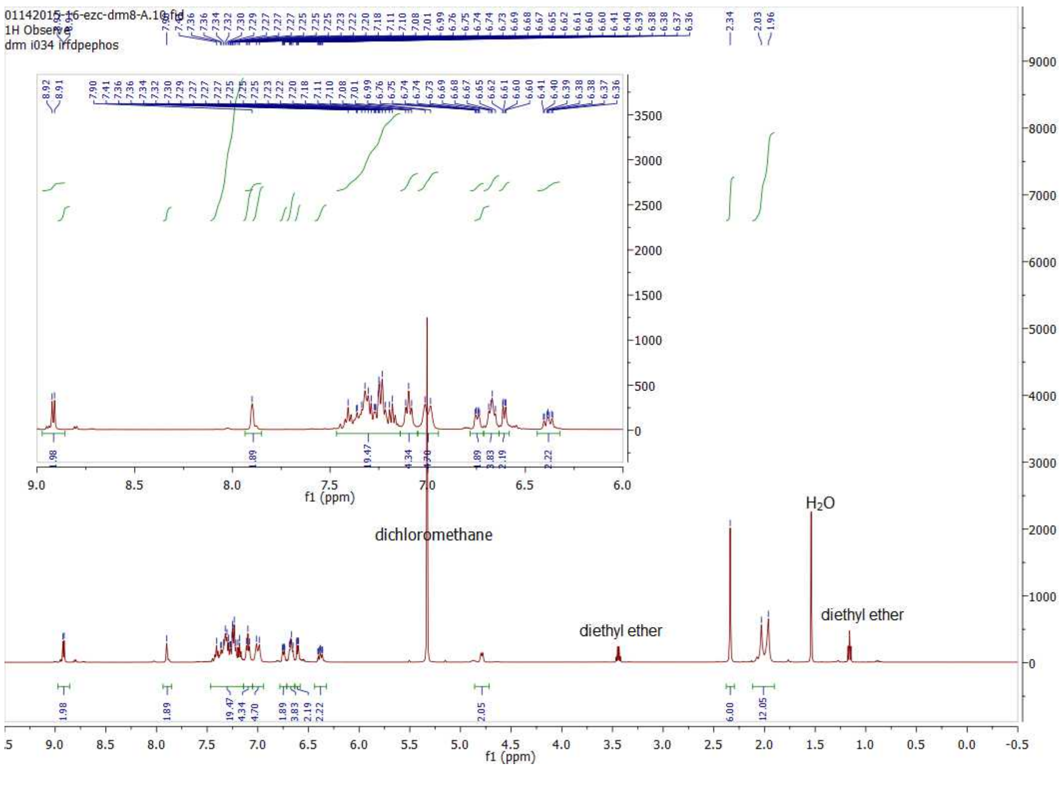

Figure **S37.** ^{1}H NMR spectrum of **[Ir(dFmesppy)$_2$(dpephos)]PF$_6$ (4b)** in CD_2Cl_2.

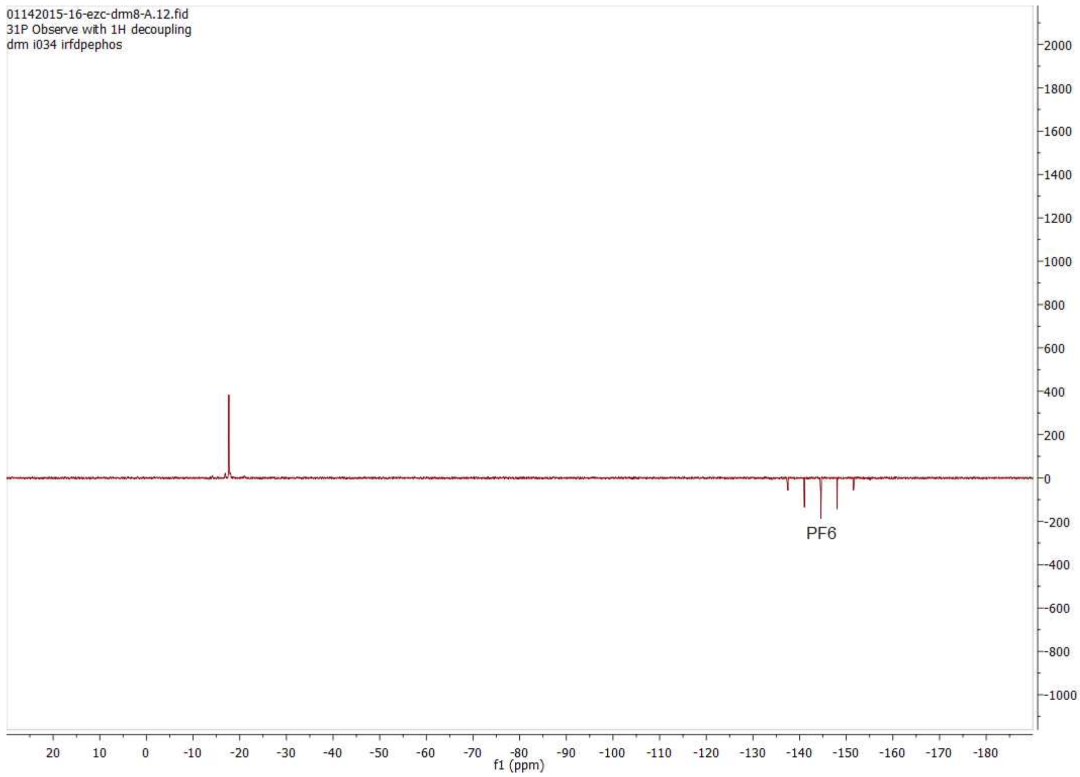

Figure **S38**. ^{31}P NMR spectrum of **[Ir(dFmesppy)$_2$(dpephos)]PF$_6$ (4b)** in CD_2Cl_2.

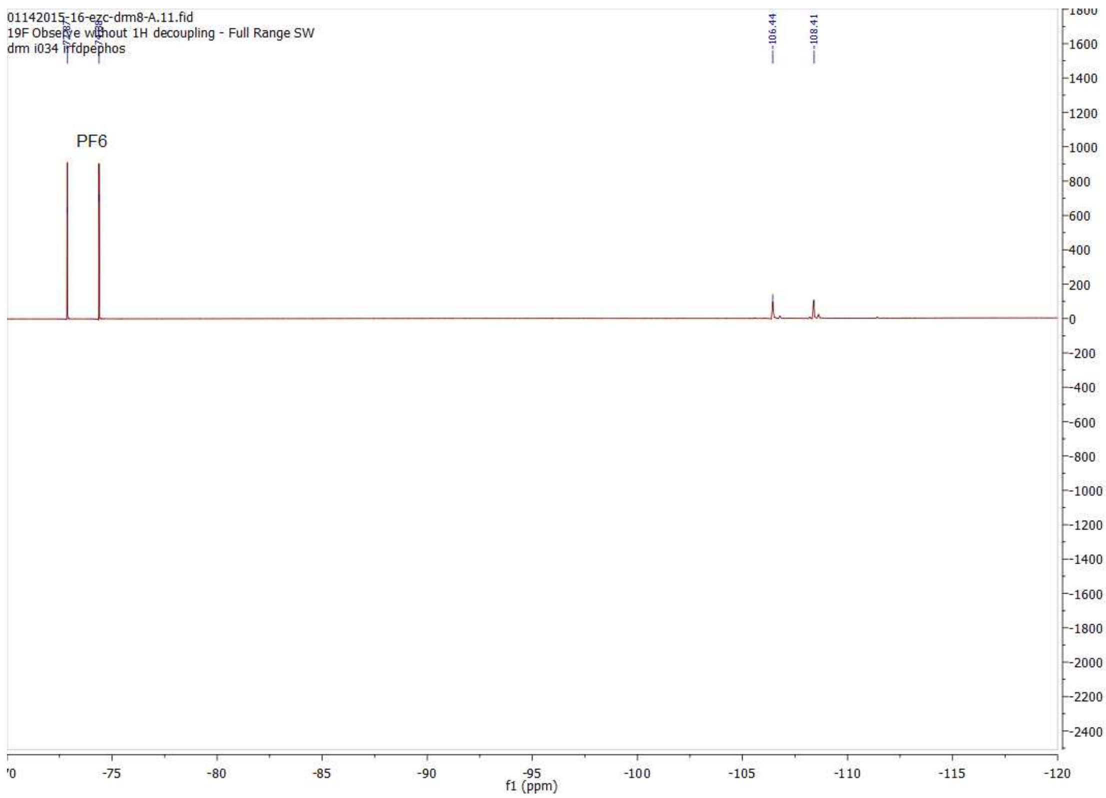

Figure **S39**. ^{19}F NMR spectrum of **[Ir(dFmesppy)$_2$(dpephos)]PF$_6$ (4b)** in CD_2Cl_2.

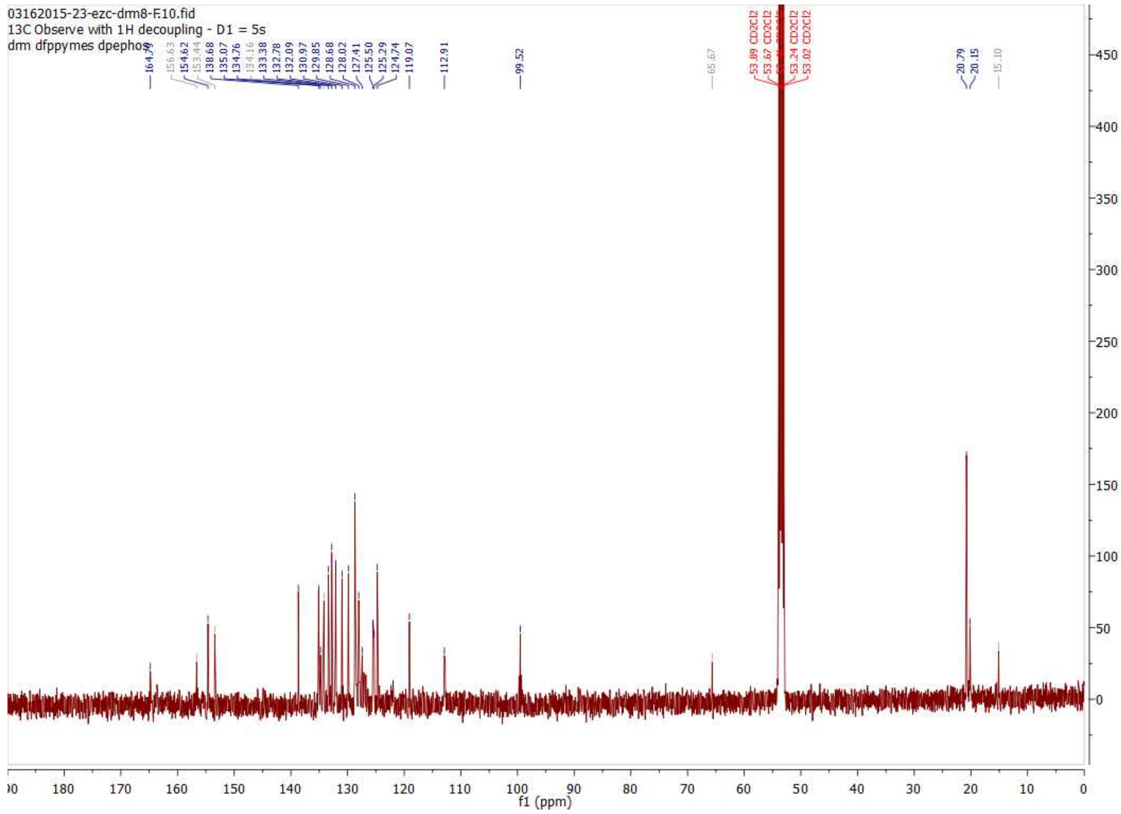

Figure S40. ^{13}C NMR spectrum of **[Ir(dFmesppy)$_2$(dpephos)]PF$_6$ (4b)** in CD_2Cl_2.

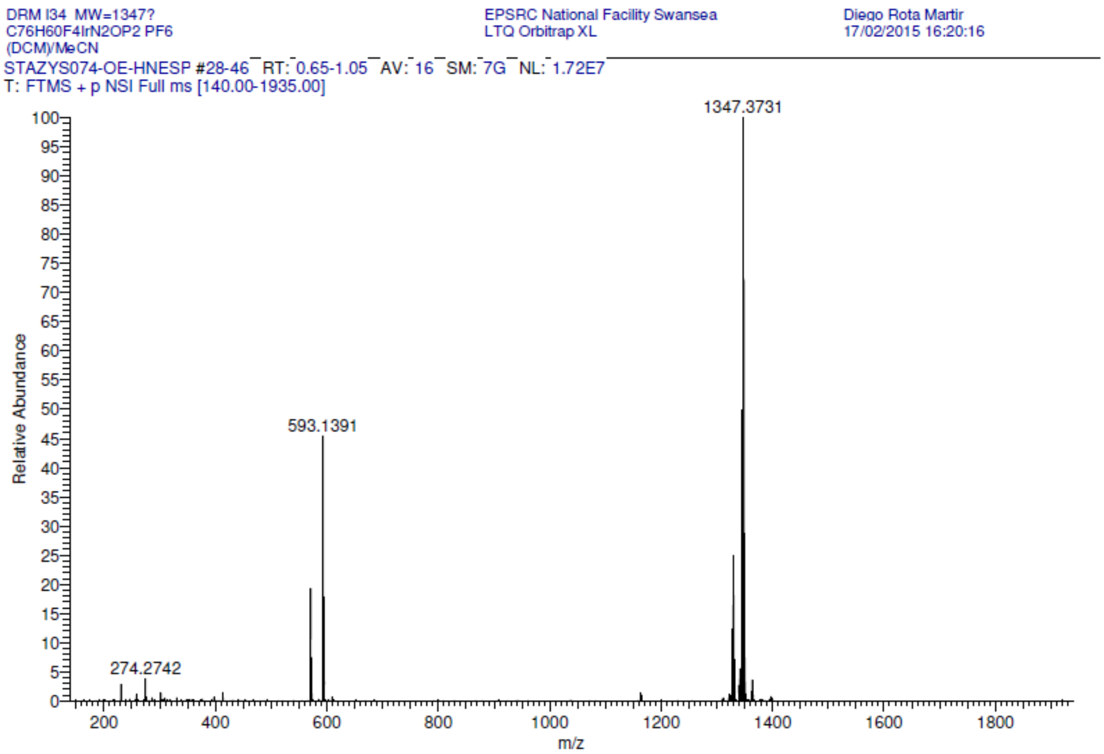

Figure **S41.** FT-MS spectrum of **[Ir(dFppymes)$_2$(dpephos)]PF$_6$ (4b)** in CD_2Cl_2.

Iridium(III)bis[2-phenylpyridinato]-bis[1,2-bis(diphenylphosphino)ethene] hexafluorophosphate, [Ir(ppy)$_2$(dppe)](PF$_6$) (1c).

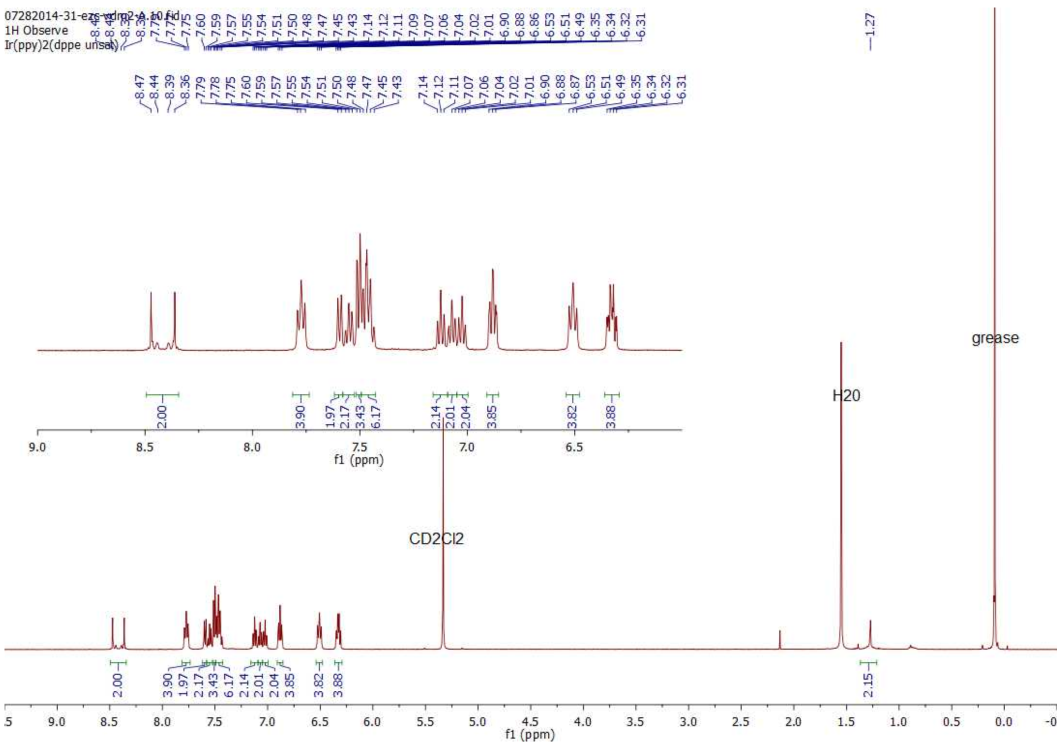

Figure **S42**. ^{1}H NMR spectrum of **[Ir(ppy)$_2$(dppe)]PF$_6$ (1c)** in CD_2Cl_2.

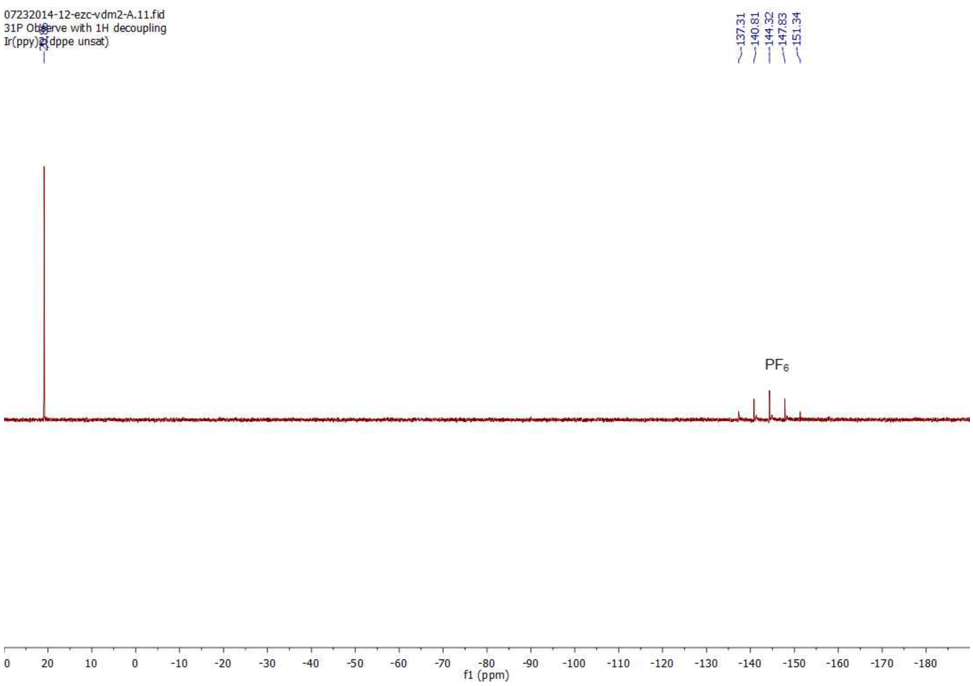

Figure **S43**. ^{31}P NMR spectrum of **[Ir(ppy)$_2$(dppe)]PF$_6$ (1c)** in CD_2Cl_2.

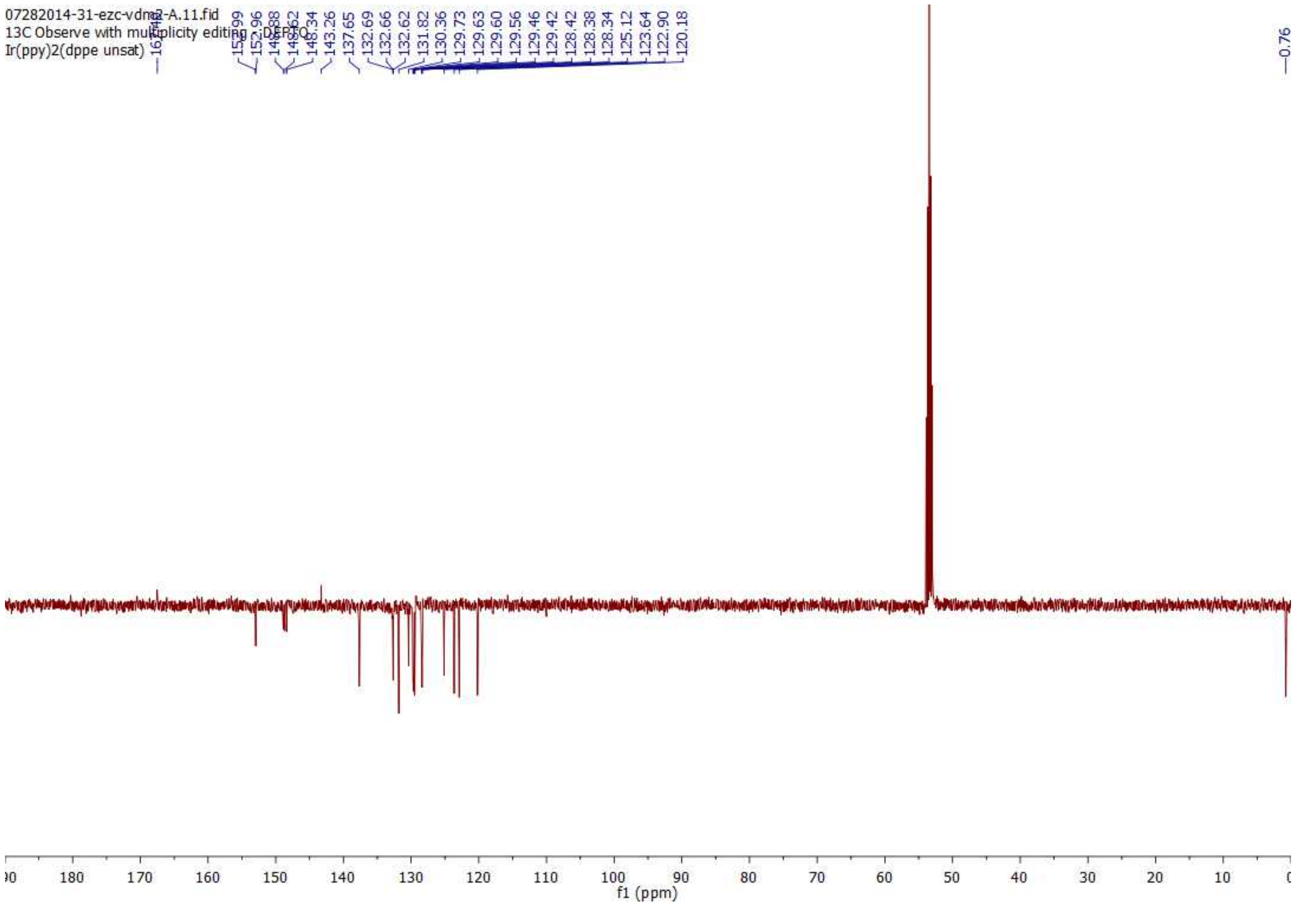

Figure **S44**. ^{13}C NMR spectrum of **[Ir(ppy)$_2$(dppe)]PF$_6$ (1c)** in CD_2Cl_2.

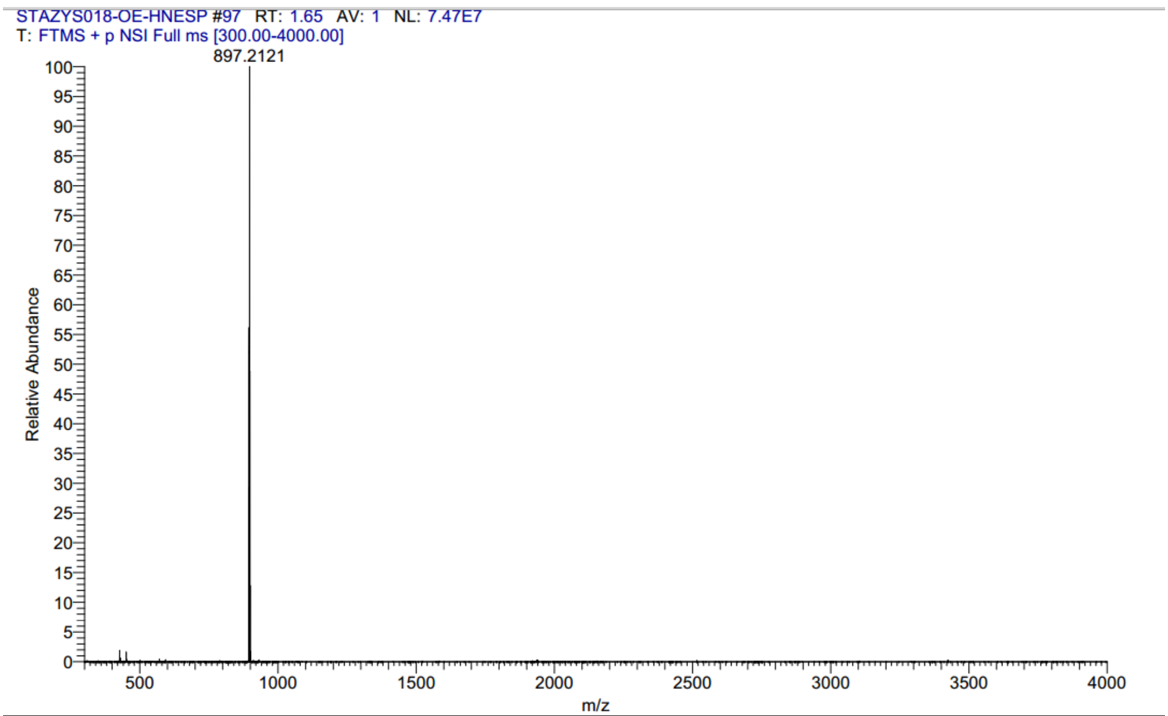

Figure **S45**. FT-MS spectrum of **[Ir(ppy)$_2$(dppe)]PF$_6$ (1c).**

Iridium(III)bis[2-phenyl-4-(2,4,6-trimethylphenyl)pyridinato]-bis[1,2-bis(diphenylphosphino)ethene] hexafluorophosphate, [Ir(mesppy)$_2$(dppe)](PF$_6$) (2c)

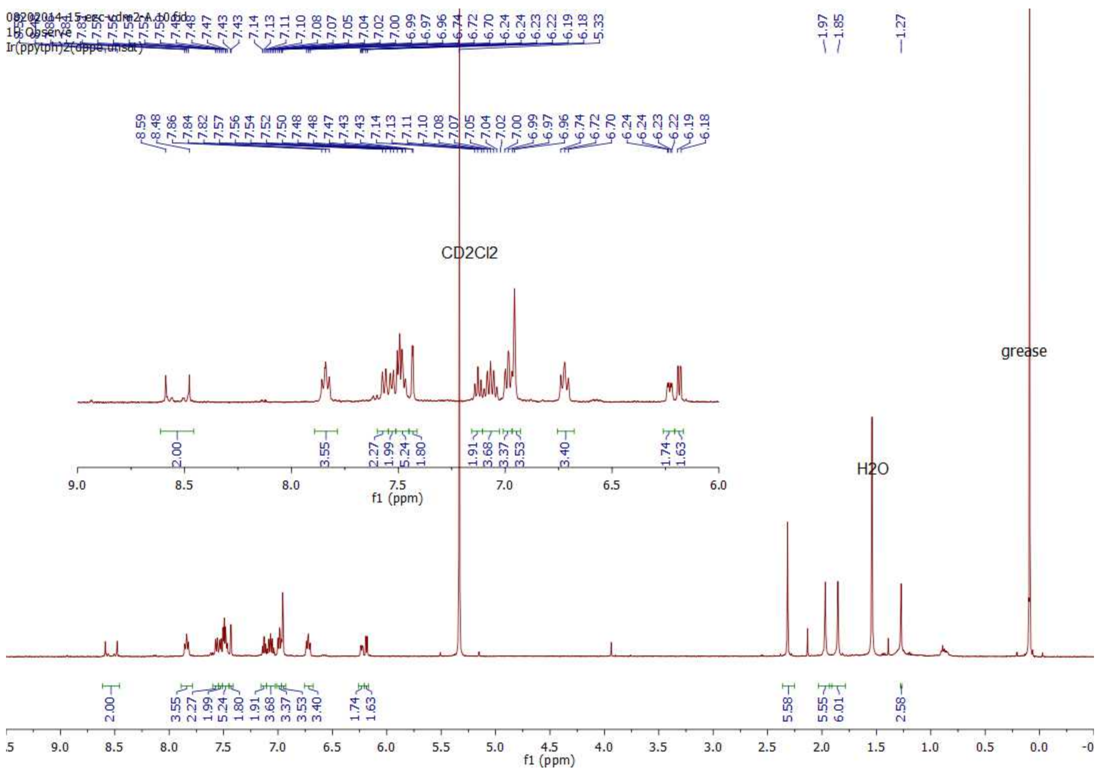

Figure **S46**. ^{1}H NMR spectrum of **[Ir(mesppy)$_2$(dppe)](PF$_6$) (2c)** in CD_2Cl_2.

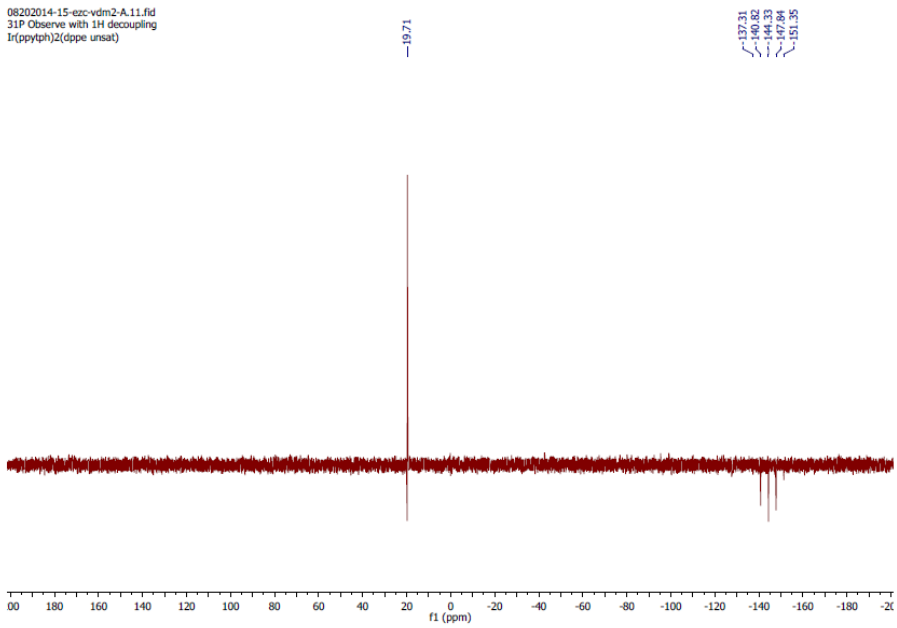

Figure **S47**. ^{31}P NMR spectrum of **[Ir(mesppy)$_2$(dppe)]PF$_6$ (2c)** in CD_2Cl_2.

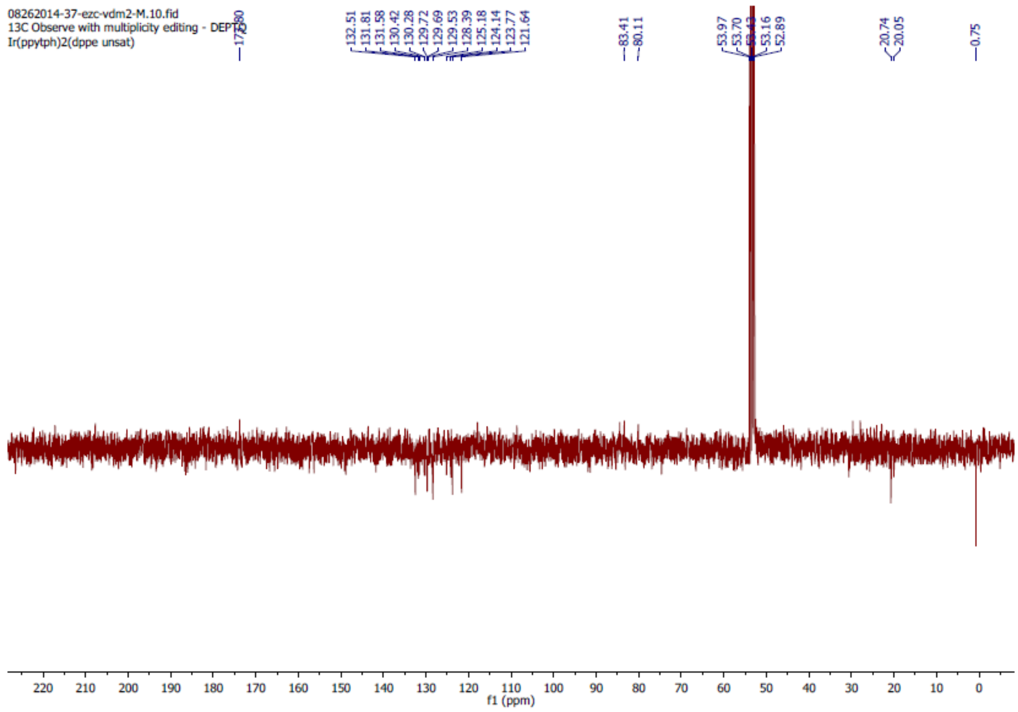

Figure **S48.** ^{13}C NMR spectrum of **[Ir(mesppy)$_2$(dppe)]PF$_6$ (2c)** in CD_2Cl_2.

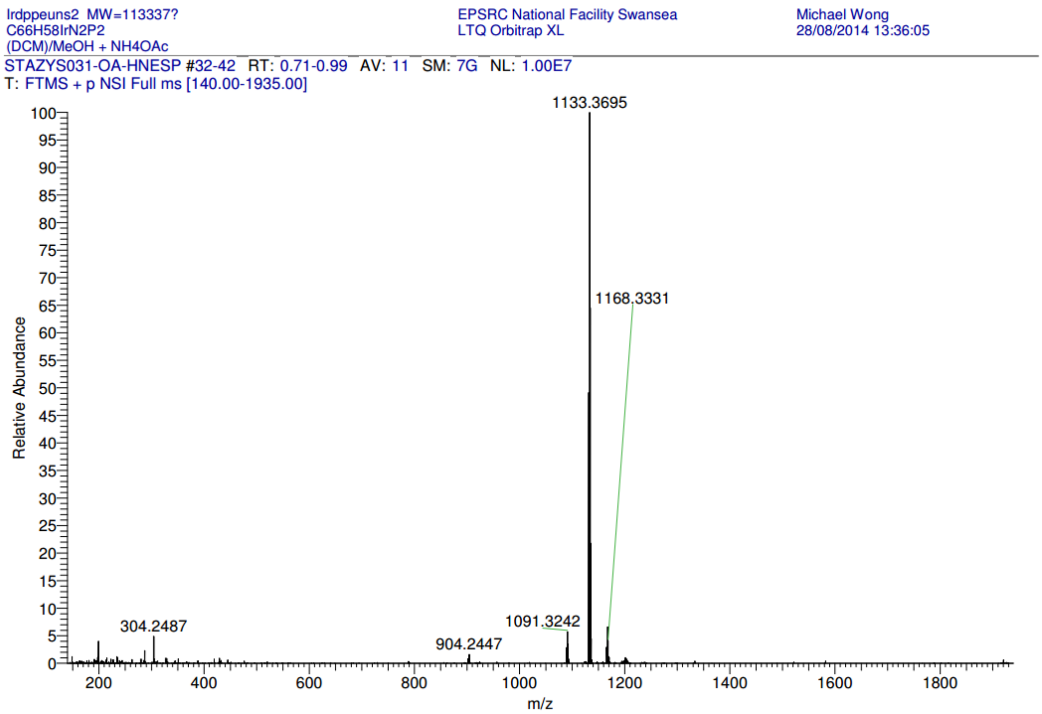

Figure **S49**. FT-MS spectrum of **[Ir(mesppy)$_2$(dppe)](PF$_6$) (2c).**

Iridium(III)bis[2-(2,4-difluorophenyl)-4-(2,4,6-trimethylphenyl)pyridinato]-bis[1,2-bis(diphenylphosphino)ethene] hexafluorophosphate, [Ir(dFmesppy)$_2$(dppe)](PF$_6$) (4c)

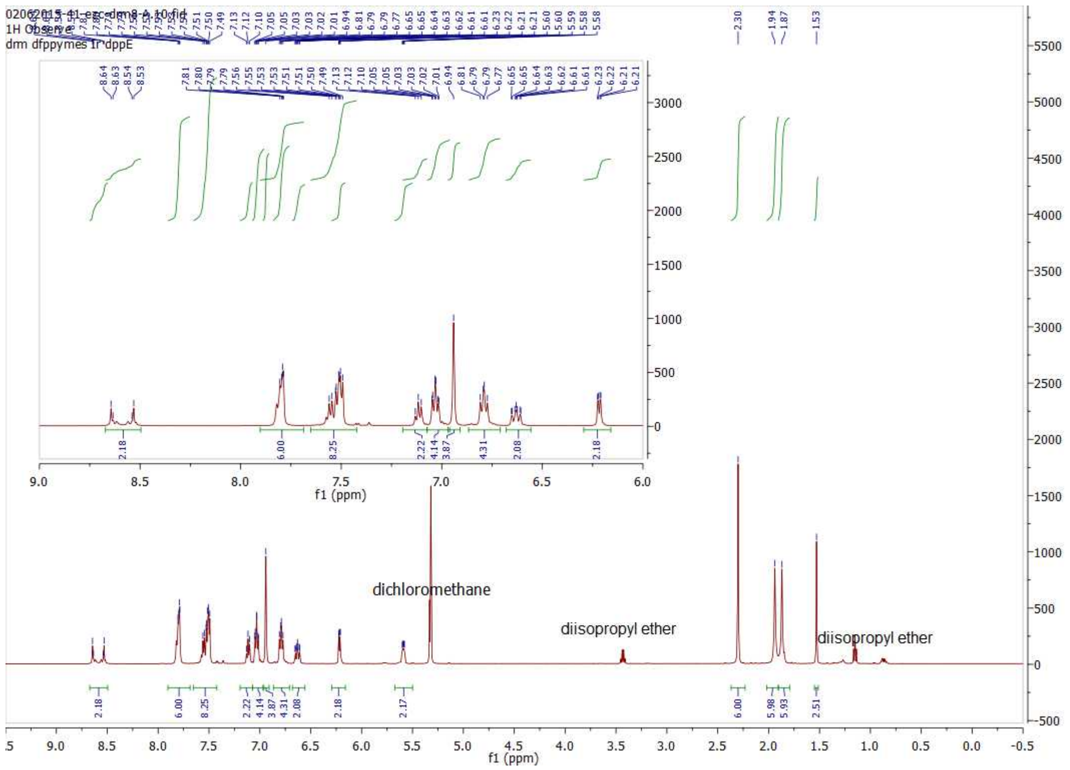

Figure **S50**. ^{1}H NMR spectrum of **[Ir(dFmesppy)$_2$(dppe)]PF$_6$ (4c)** in CD_2Cl_2.

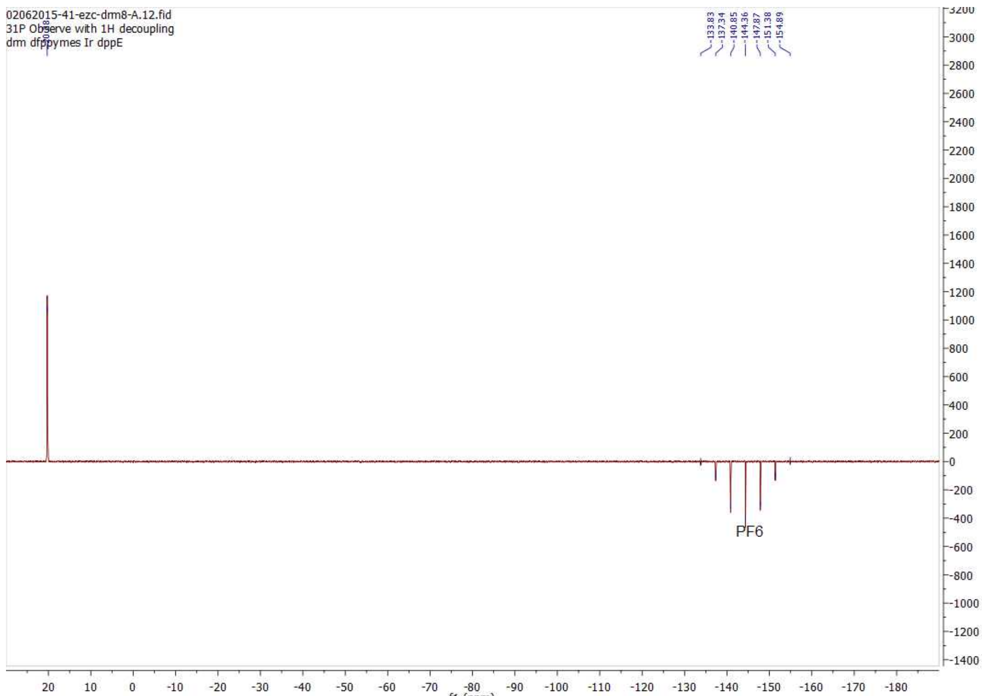

Figure **S51**. ^{31}P NMR spectrum of **[Ir(dFmesppy)$_2$(dppe)](PF$_6$) (4c)** in CD_2Cl_2.

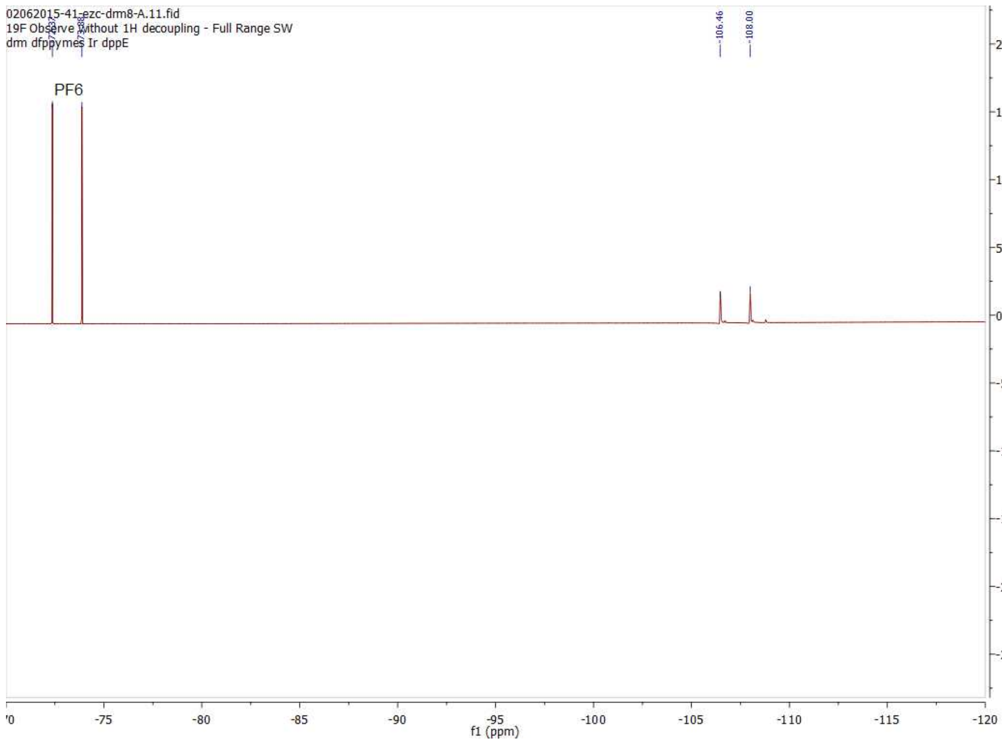

Figure **S52**. ^{19}F NMR spectrum of **$[Ir(dFmesppy)_2(dppe)]PF_6$ (4c)** in CD_2Cl_2.

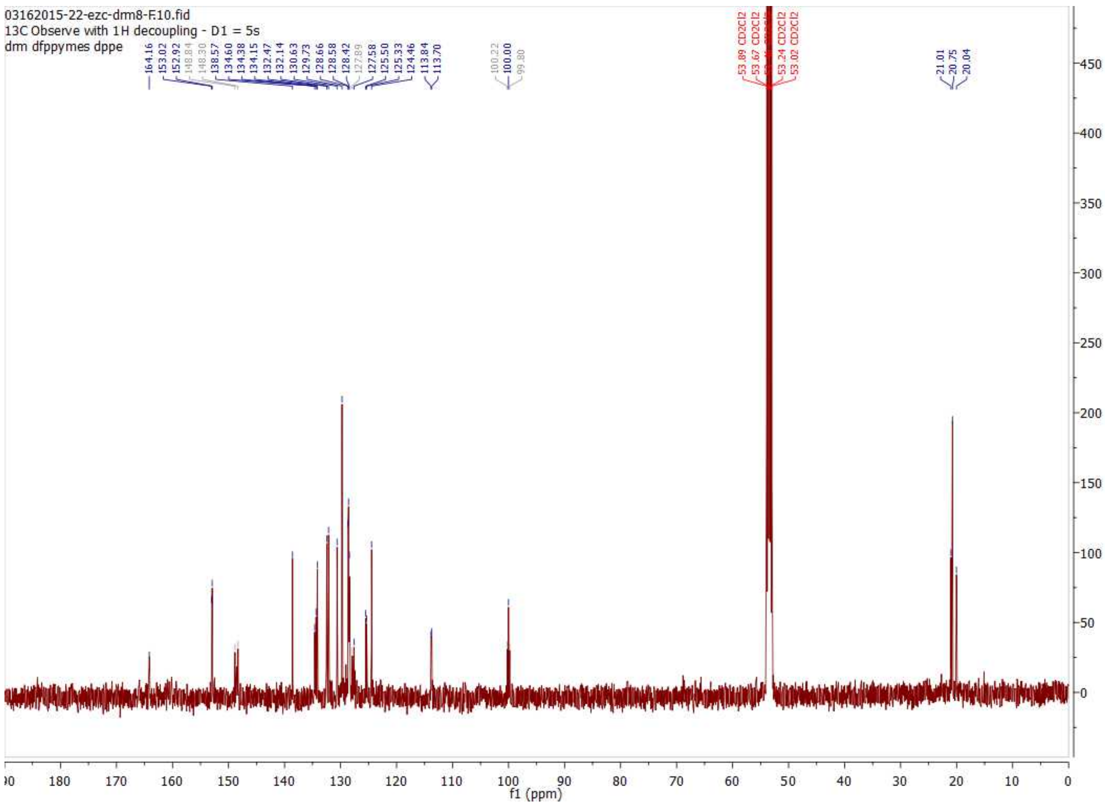

Figure **S53.** ^{13}C NMR spectrum of **$[Ir(dFmesppy)_2I(dppe)]PF_6$ (4c)** in CD_2Cl_2.

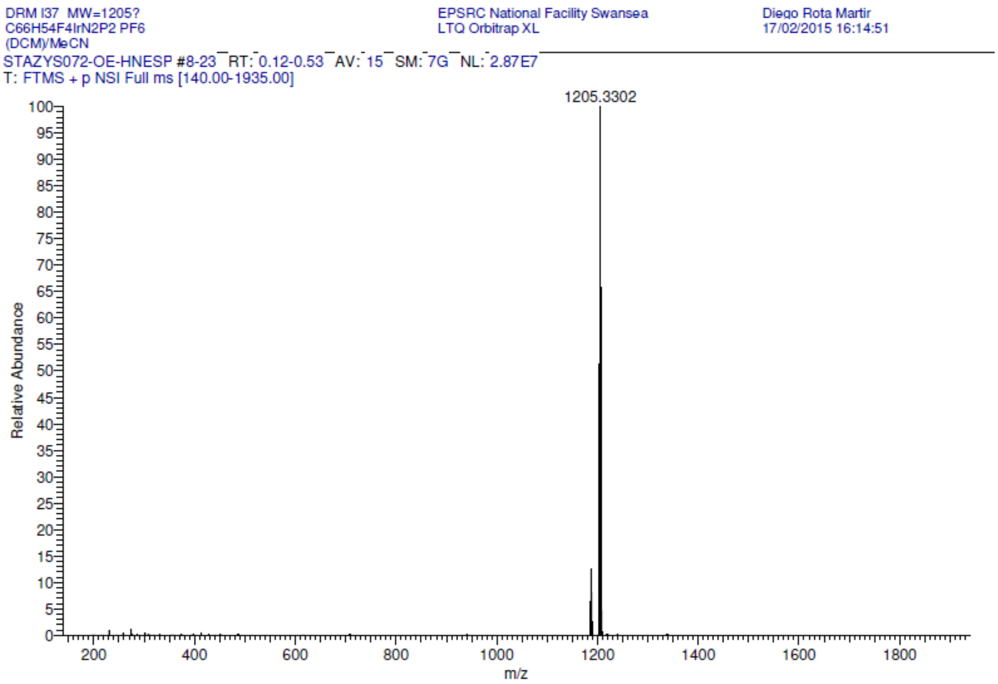

Figure **S54**. FT-MS spectrum of **[Ir(dFmesppy)$_2$(dppe)]PF$_6$ (4c)** in CD_2Cl_2.

Iridium(III)bis[2-(2,4-difluorophenyl)pyridinato]-bis[1,2-bis(diphenylphosphino)ethene] hexafluorophosphate, [Ir(dFppy)$_2$(dppe)](PF$_6$) (3c)

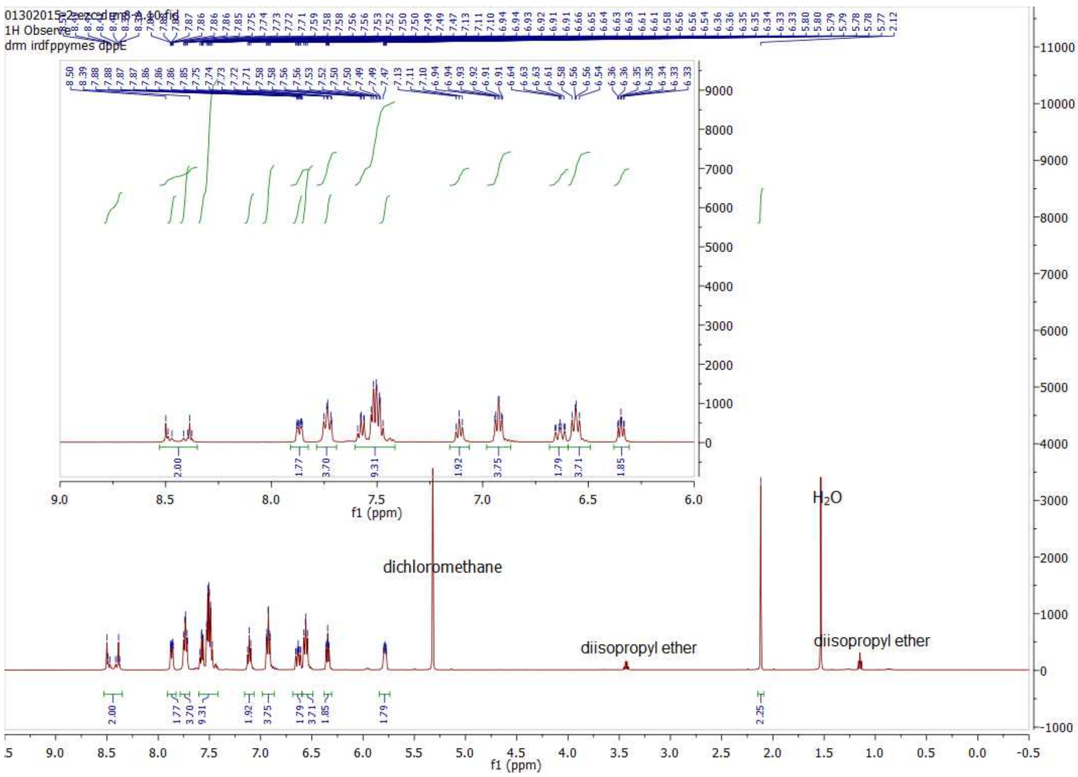

Figure **S55**. ^{1}H NMR spectrum of **[Ir(dFppy)$_2$(dppe)]PF$_6$ (3c)** in CD_2Cl_2.

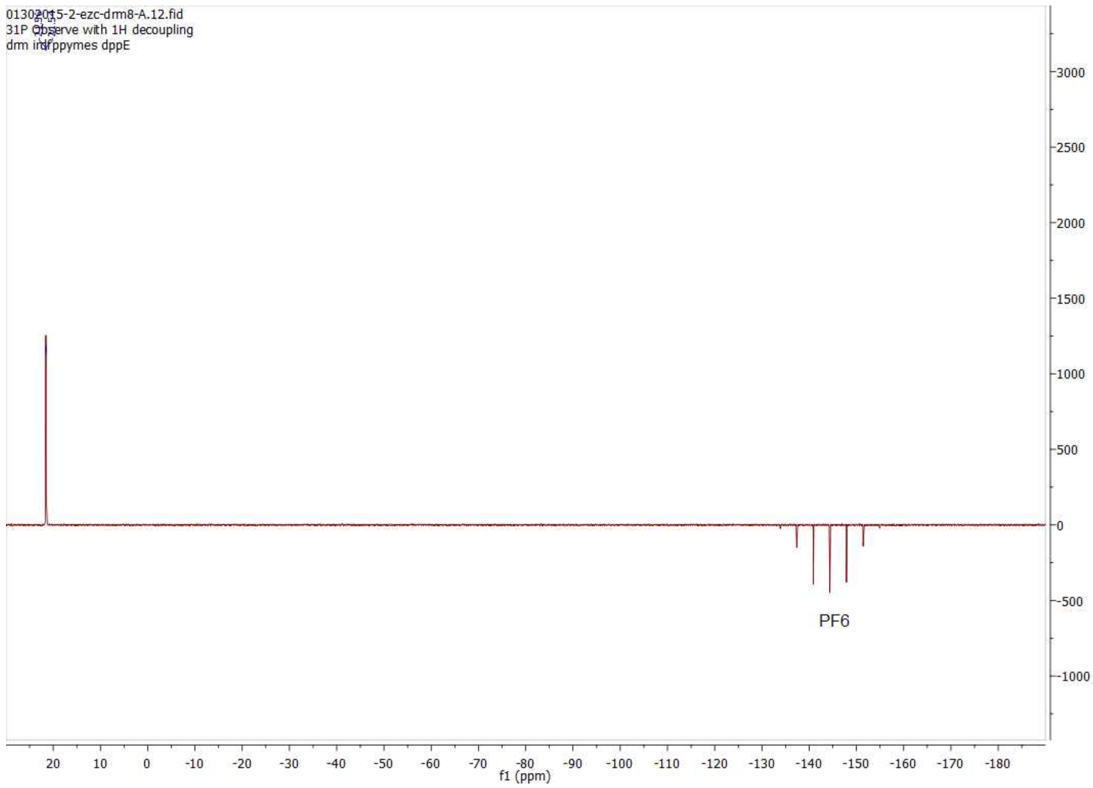

Figure **S56**. ^{31}P NMR spectrum of **[Ir(dFppy)$_2$(dppe)](PF$_6$) (3c)** in CD_2Cl_2.

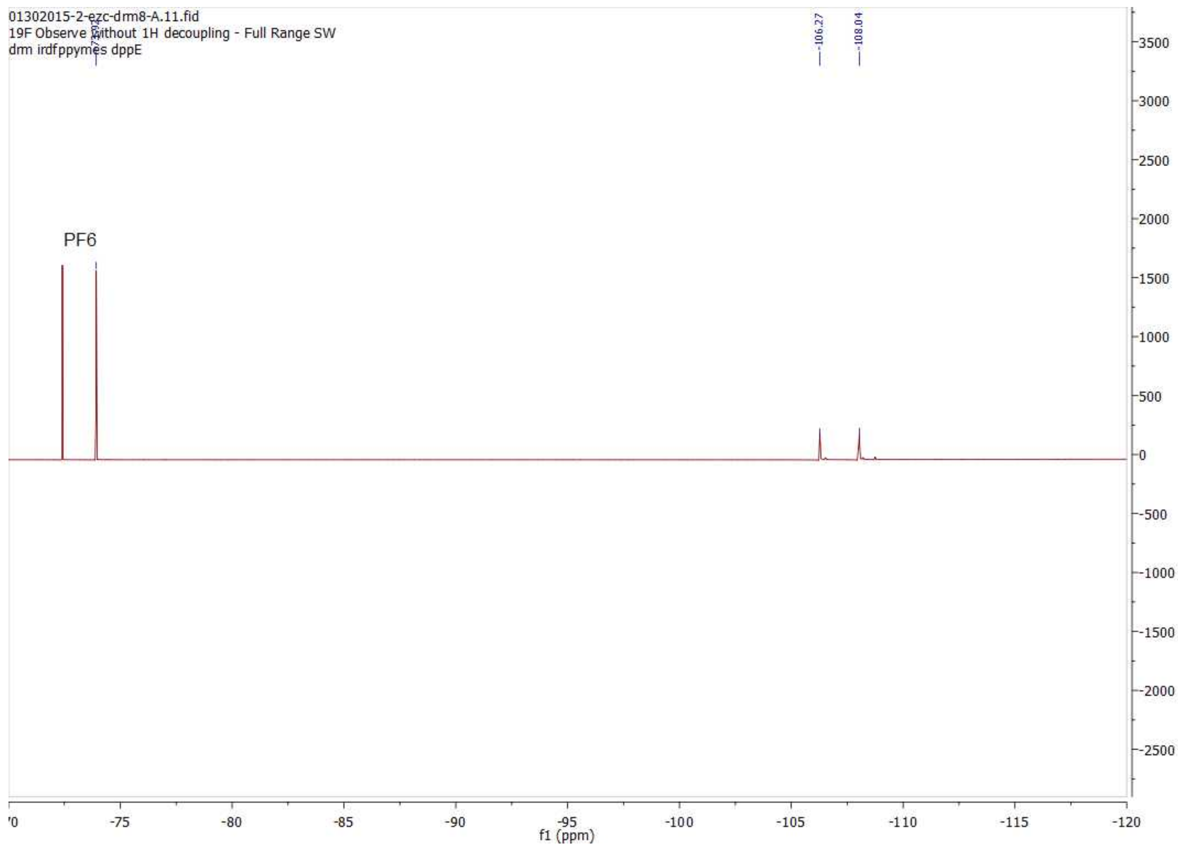

Figure **S57.** ^{19}F NMR spectrum of **[Ir(dFppy)$_2$(dppe)]PF$_6$ (3c)** in CD_2Cl_2.

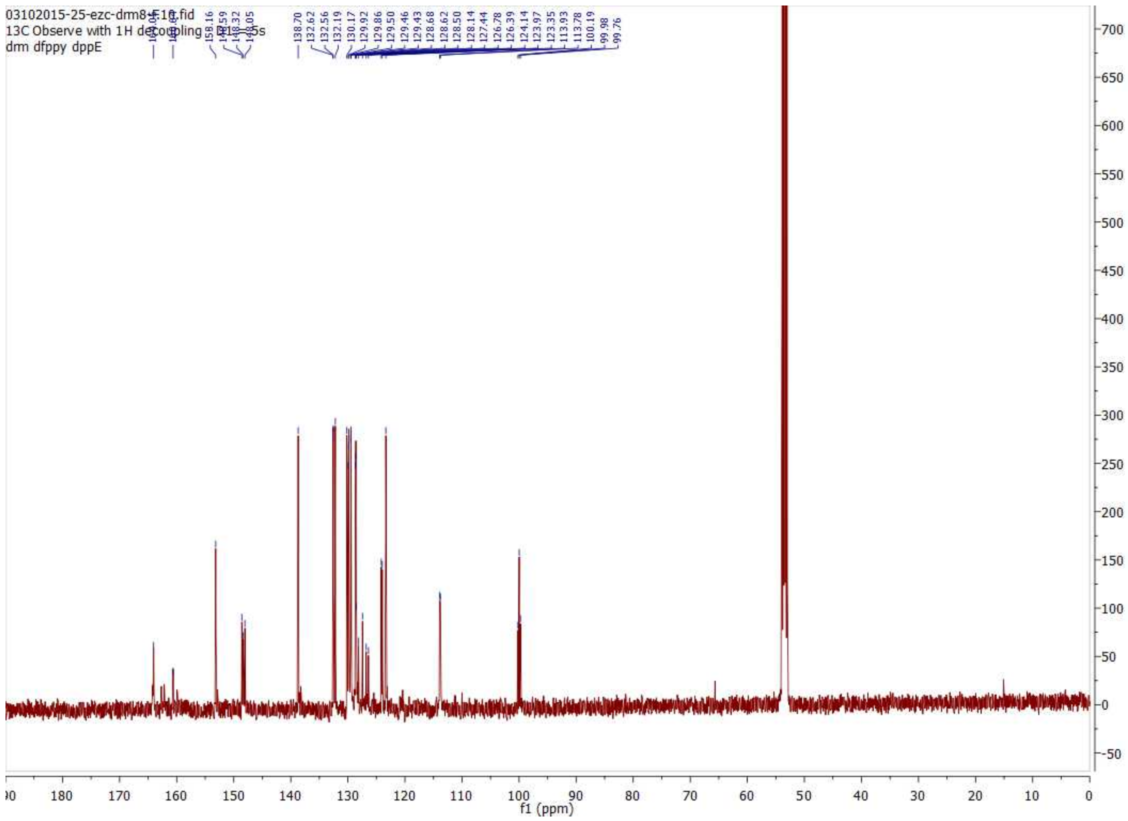

Figure **S58**. ^{13}C NMR spectrum of **$[Ir(dFppy)_2(dppe)]PF_6$ (3c)** in CD_2Cl_2.

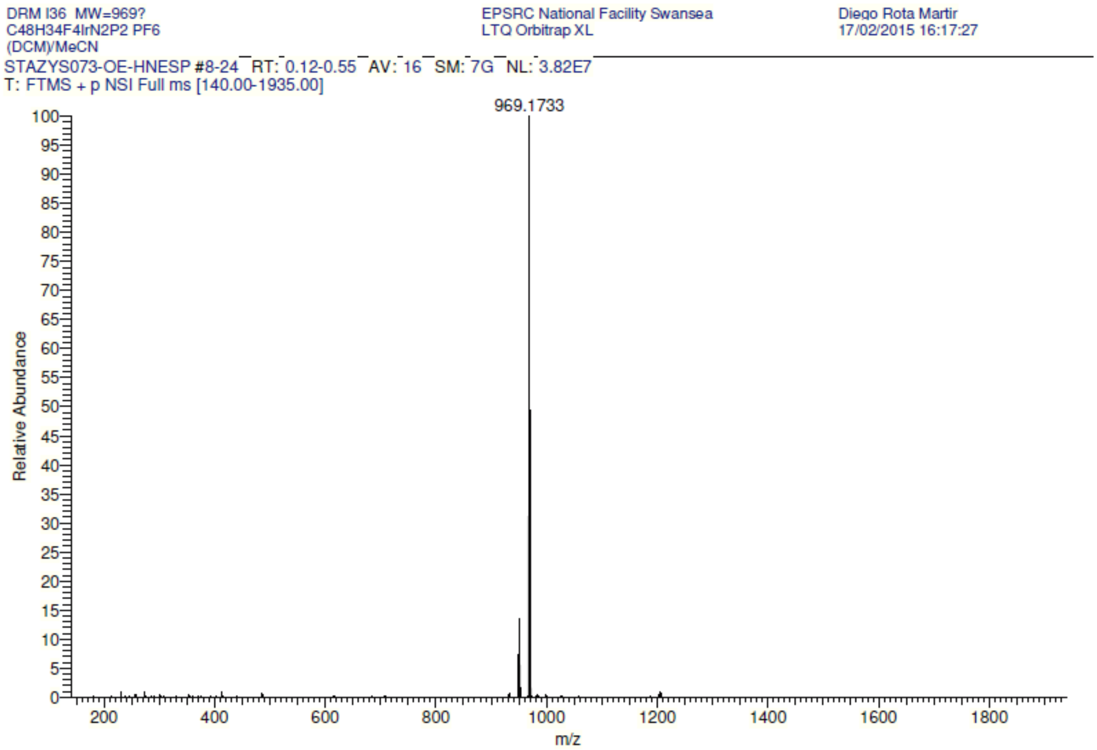

Figure **S59**. FT-MS spectrum of **$[Ir(dFppy)_2(dppe)]PF_6$ (3c)**.

Iridium(III)bis[2-phenylpyridinato]-bis[1,2-bis(diphenylphosphino)ethane] hexafluorophosphate, $[Ir(ppy)_2(Dppe)](PF_6)$ (1d)

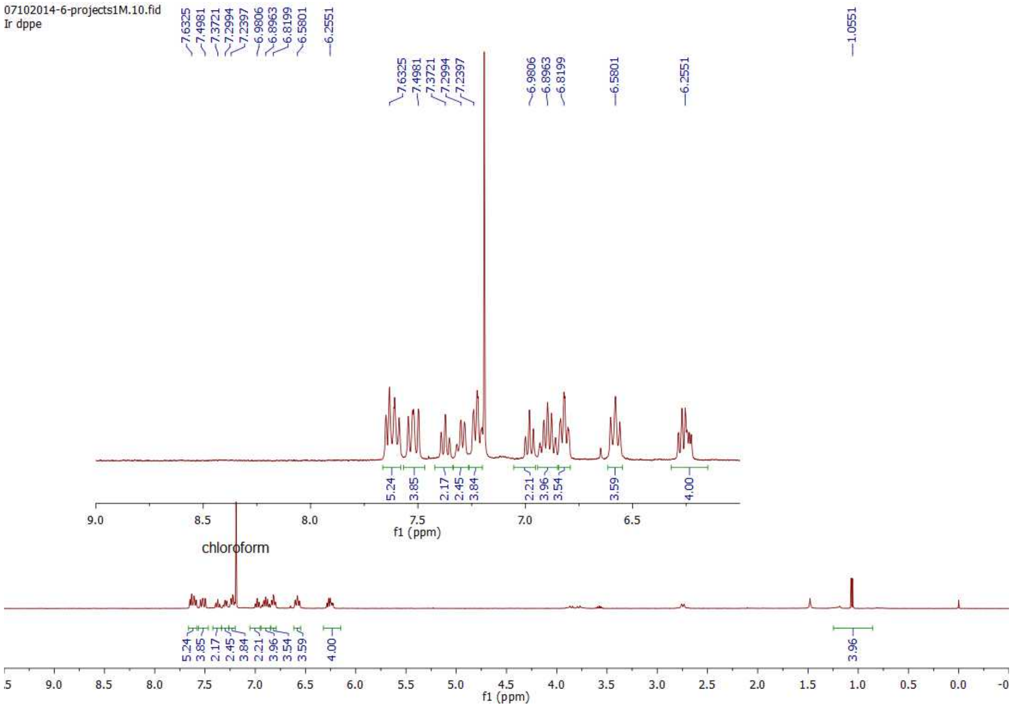

Figure **S60**. ^{1}H NMR spectrum of **$[Ir(ppy)_2(Dppe)]PF_6$ (1d)** in CD_2Cl_2.

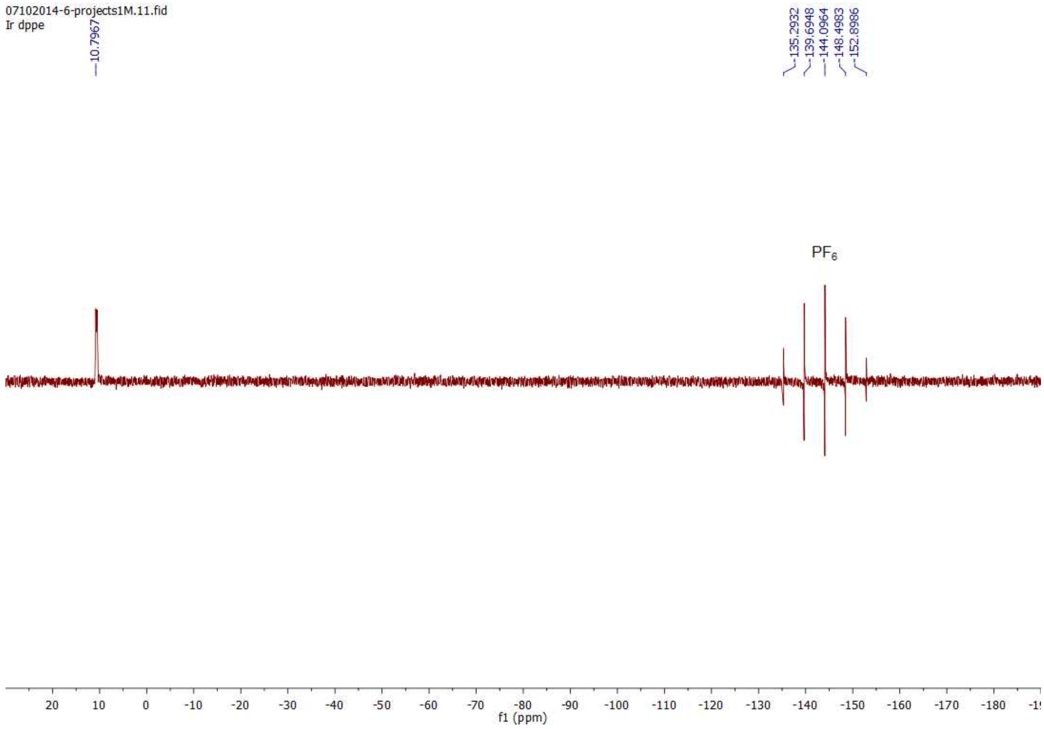

Figure **S61.** ^{31}P NMR spectrum of **$[Ir(ppy)_2(Dppe)]PF_6$ (1d)** in CD_2Cl_2.

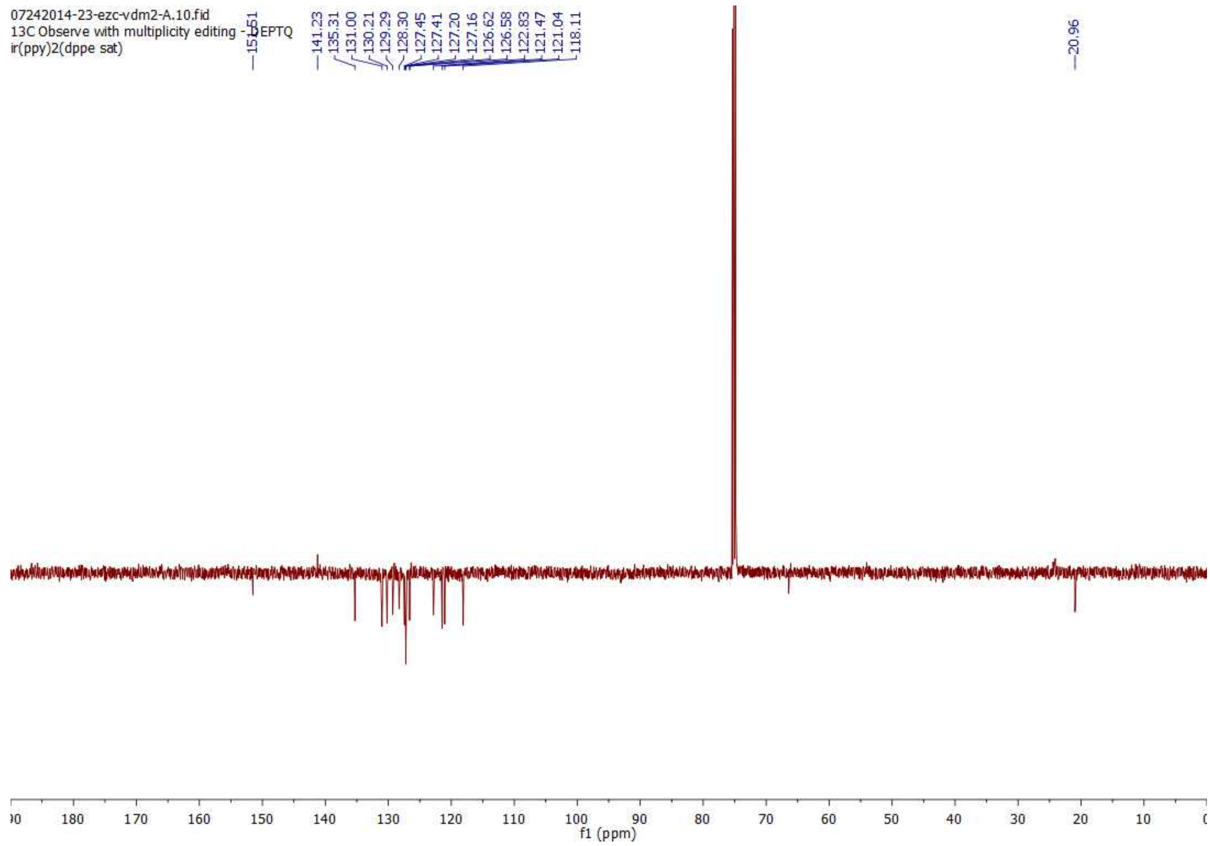

Figure **S62.** [13]C NMR spectrum of **[Ir(ppy)$_2$(Dppe)]PF$_6$ (1d)** in CD_2Cl_2.

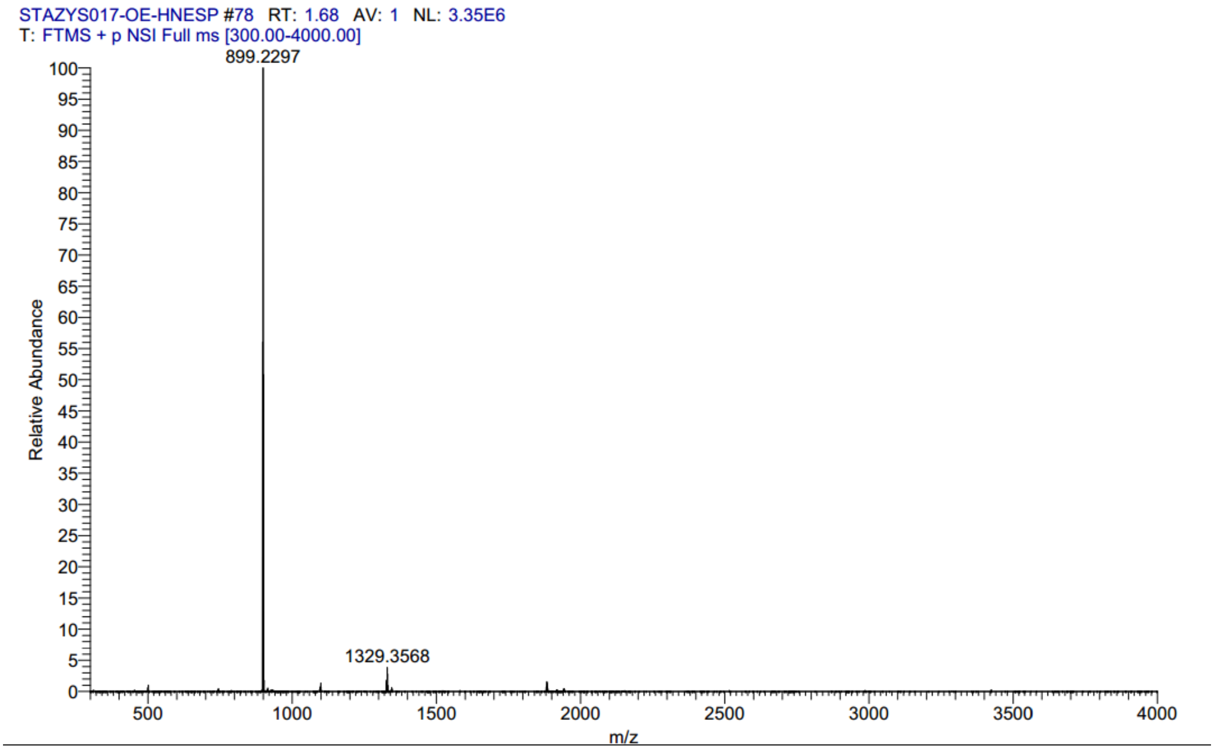

Figure S63. FT-MS spectrum of **[Ir(ppy)$_2$(Dppe)]PF$_6$ (1d).**

Iridium(III)bis[2-phenylpyridinato]-4,5-bis(diphenylphosphino)-9-isopropylxanthene hexafluorophosphate, [Ir(ppy)$_2$(isopropxantphos)](PF$_6$) (1f)

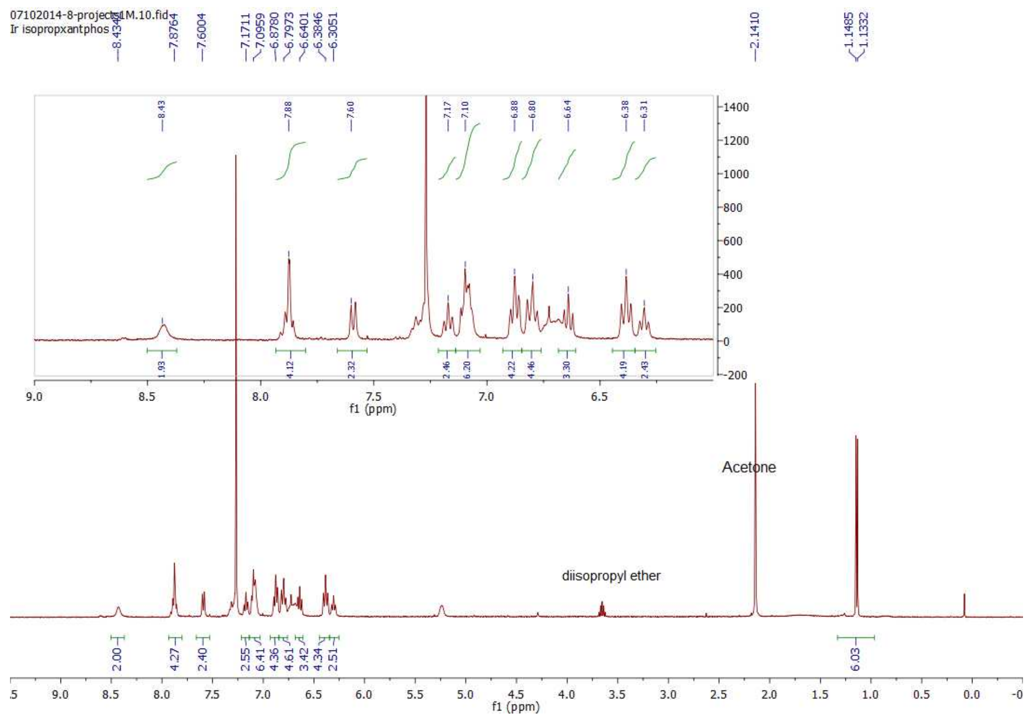

Figure **S64.** ^{1}H NMR spectrum of **[Ir(ppy)$_2$(isopropxantphos)]PF$_6$ (1f)** in CD_2Cl_2.

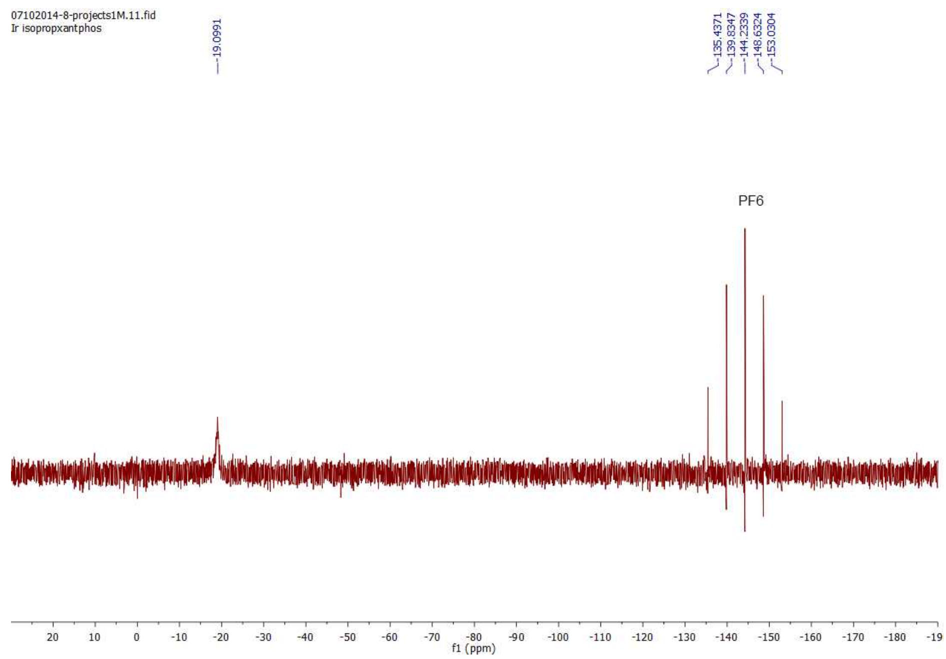

Figure **S65**. ^{31}P NMR spectrum of **[Ir(ppy)$_2$(isopropxantphos)]PF$_6$ (1f)** in CD_2Cl_2.

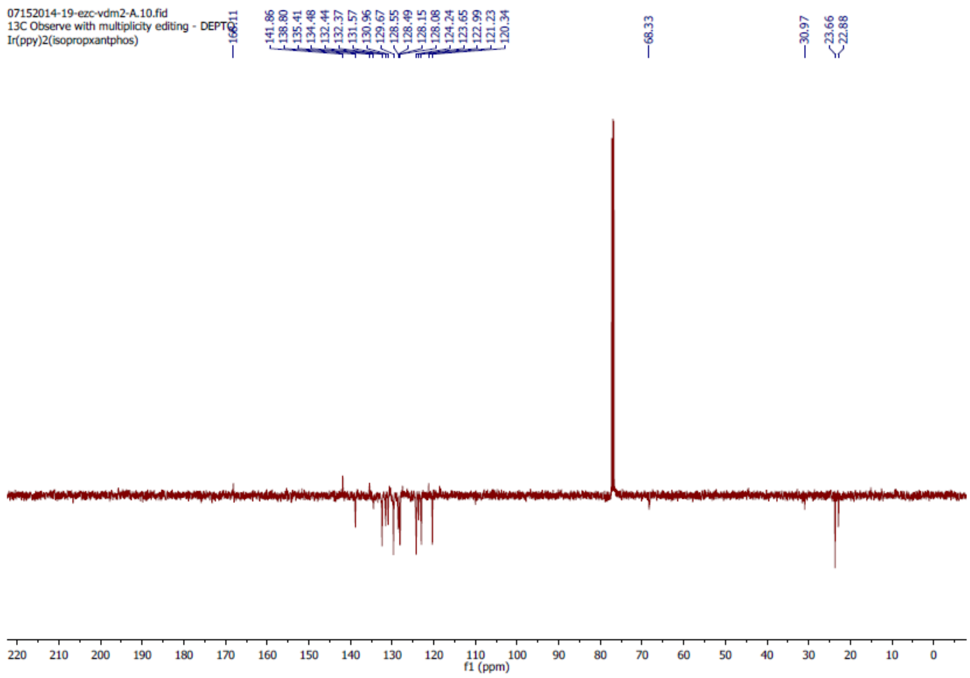

Figure **S66**. [13]C NMR spectrum of **[Ir(ppy)$_2$(isopropxantphos)]PF$_6$ (1f)** in CD_2Cl_2.

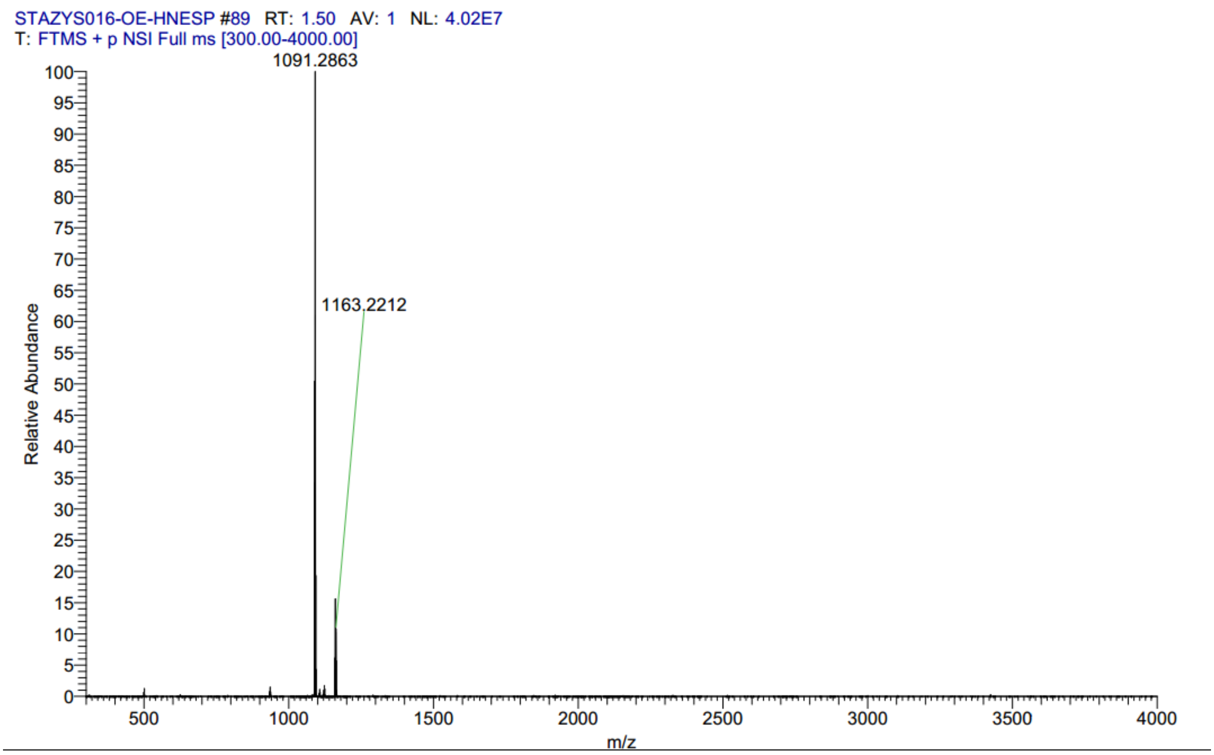

Figure **S67.** FT-MS spectrum of **[Ir(ppy)$_2$(isopropxantphos)]PF$_6$ (1f).**

Iridium(III)bis[2-phenylpyridinato]-4,6-bis(diphenylphosphino)phenoxazine hexafluorophosphate, [Ir(ppy)$_2$(nixantphos)](PF$_6$) (1e)

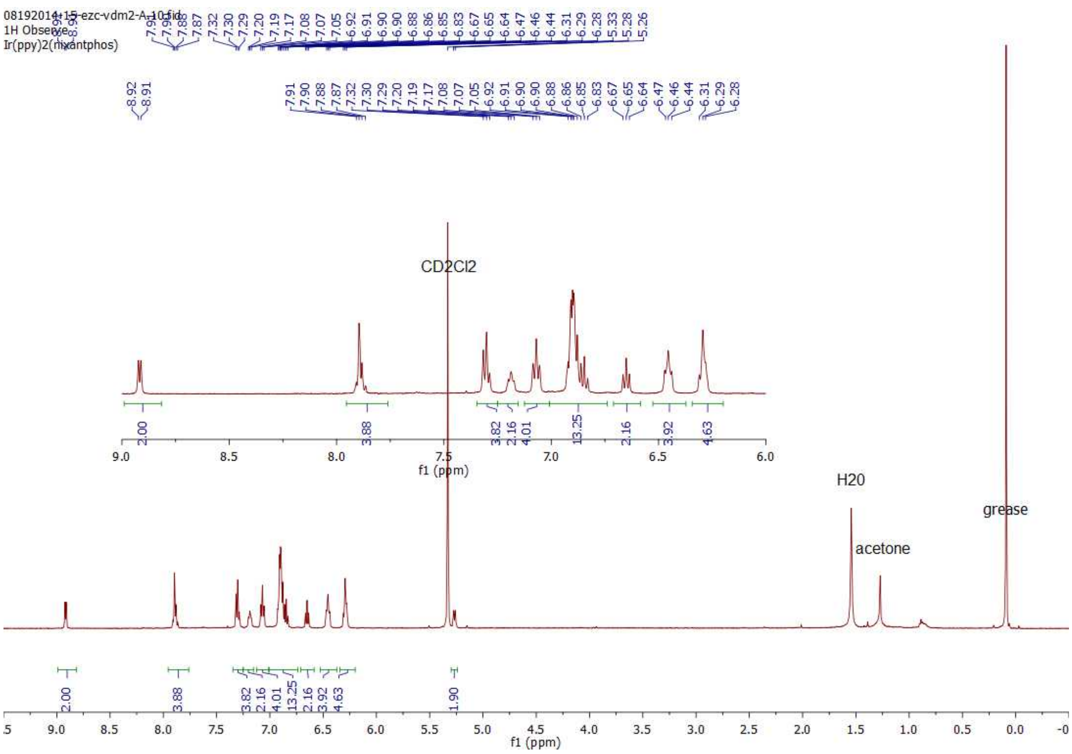

Figure **S68.** ^{1}H NMR spectrum of **[Ir(ppy)$_2$(nixantphos)]PF$_6$ (1e)** in CD_2Cl_2.

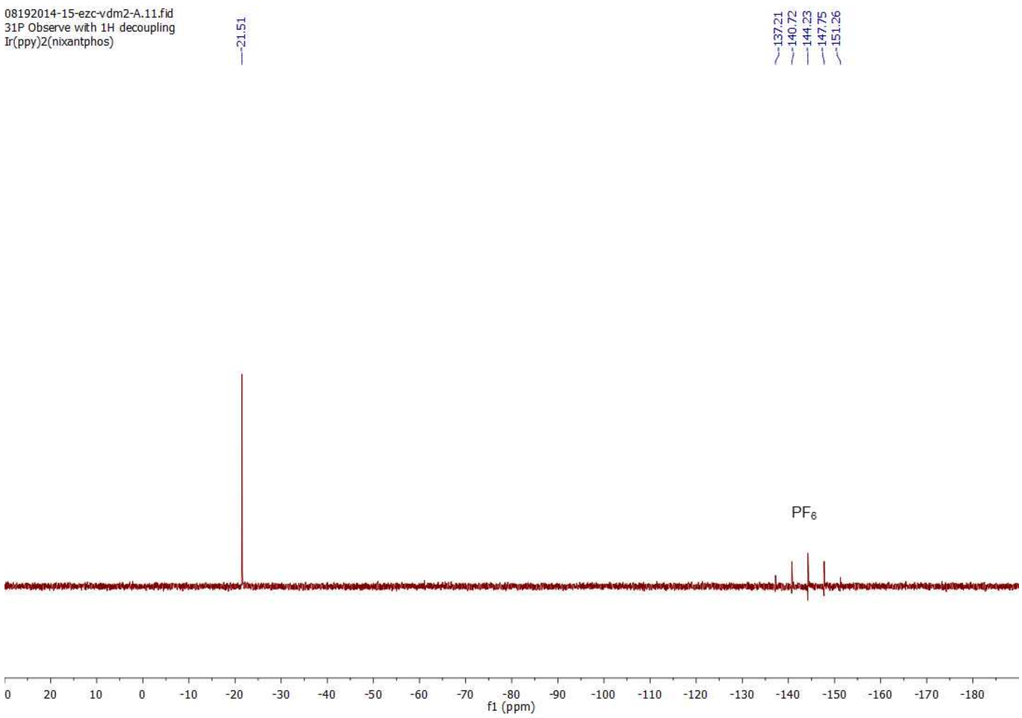

Figure **S69**. ^{31}P NMR spectrum of **[Ir(ppy)$_2$(nixantphos)]PF$_6$ (1d)** in CD_2Cl_2.

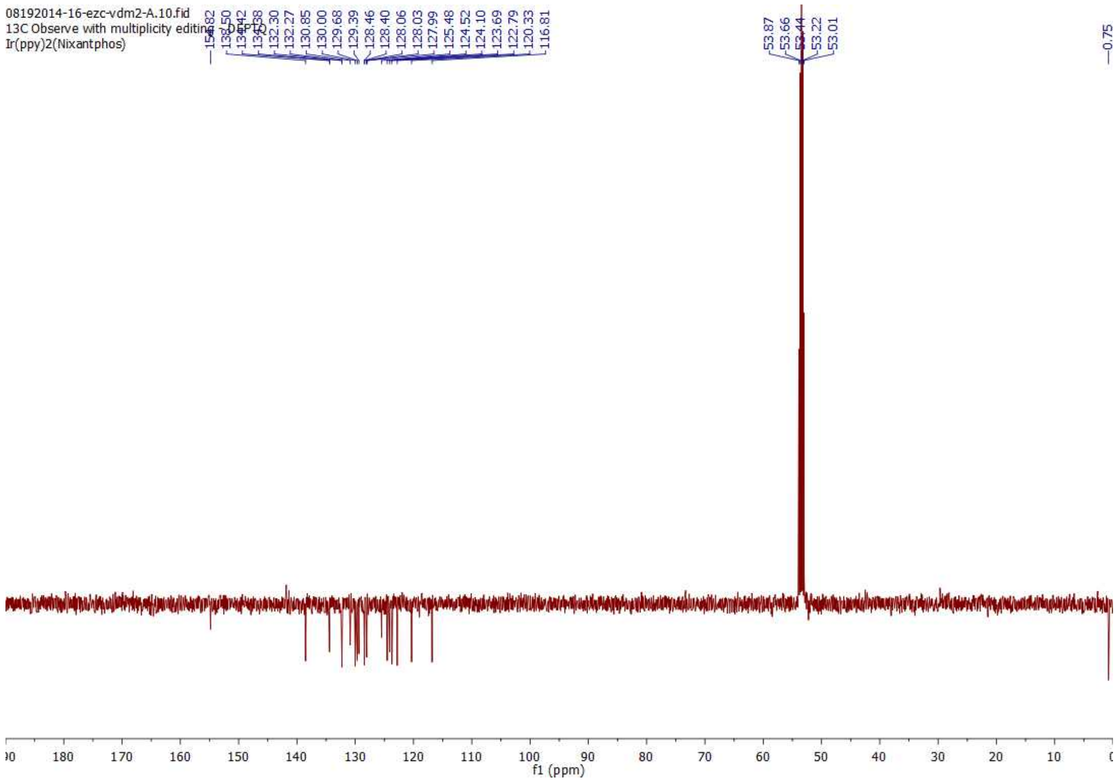

Figure **S70**. ^{13}C NMR spectrum of **[Ir(ppy)$_2$(nixantphos)]PF$_6$ (1e)** in CD_2Cl_2.

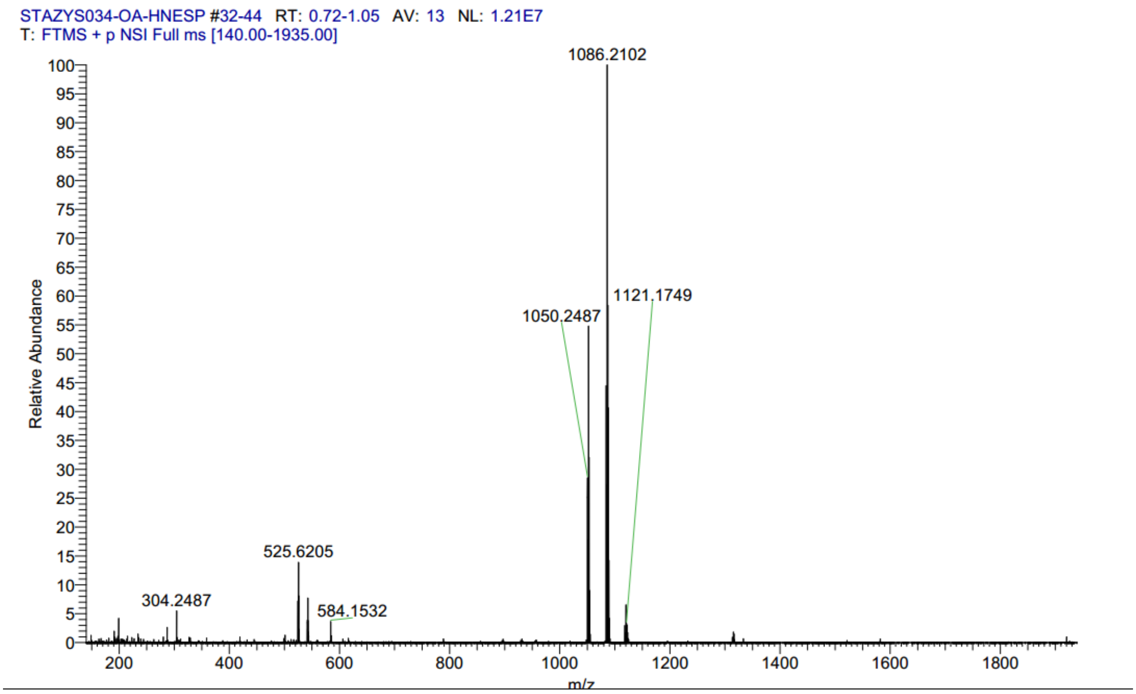

Figure **S71**. FT-MS spectrum of **[Ir(ppy)$_2$(nixantphos)]PF$_6$ (1e).**

Crystal Structures

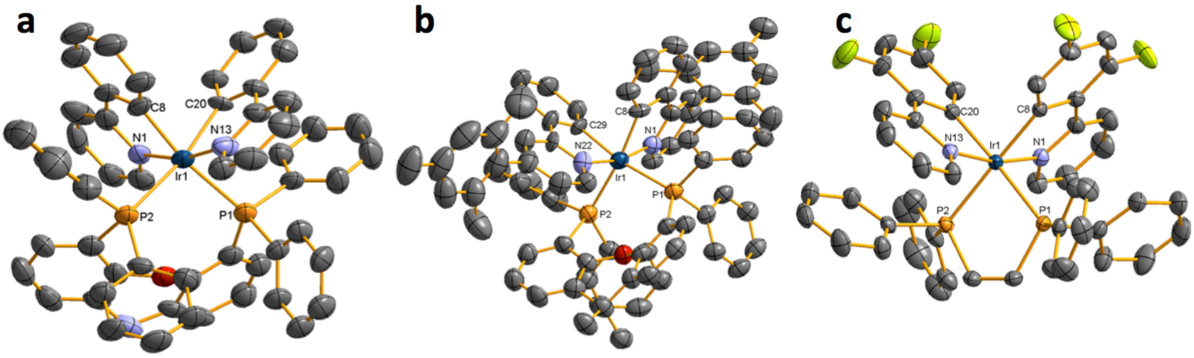

Figure **S72**. Crystal structure of (**a**) **1e**, (**b**) **2a** and **(c) 3c**. Hydrogen atoms, PF_6^- counterions, solvent molecules, minor components of disordered molecules and additional independent molecules are omitted for clarity. Selected bond lengths (Å) and angles (°): (**1e**) $Ir_1–N_1$ 2.082(9), $Ir_1–N_{13}$ 2.077(9), $Ir_1–C_8$ 2.049(11), $Ir_1–C_{20}$ 2.051(10), $Ir_1–P_1$ 2.526(3), $Ir_1–P_2$ 2.483(3), $Ir_{71}–N_{71}$ 2.093(9), $Ir_{71}–N_{83}$ 2.062(10), $Ir_{71}–C_{78}$ 2.036(11), $Ir_{71}–C_{90}$ 2.056(12), $Ir_{71}–P_{71}$ 2.529(3), $Ir_{71}–P_{72}$ 2.510(3), P_1-Ir_1-P_2: 102.10(9), $P_{71}–Ir_{71}–P_{72}$ 102.14(10); (**2a**) $Ir_1–N_1$ 2.071(6), $Ir_1–N_{22}$ 2.051(7), Ir_1-C_8 2.081(7), $Ir_1–C_{29}$ 2.065(7), $Ir_1–P_1$ 2.525(2), $Ir_1–P_2$ 2.477(2), P_1-Ir_1-P_2: 100.32(7); (**3c**) $Ir_1–N_1$: 2.0665(15), $Ir_1–N_{13}$ 2.0649(16), $Ir_1–C_8$ 2.0526(19), $Ir_1–C_{20}$ 2.0543(19), $Ir_1–P_1$ 2.3673(5), $Ir_1–P_2$ 2.3687(5), P_1-Ir_1-P_2: 83.623(18).

Supplementary Optoelectronic Characterization

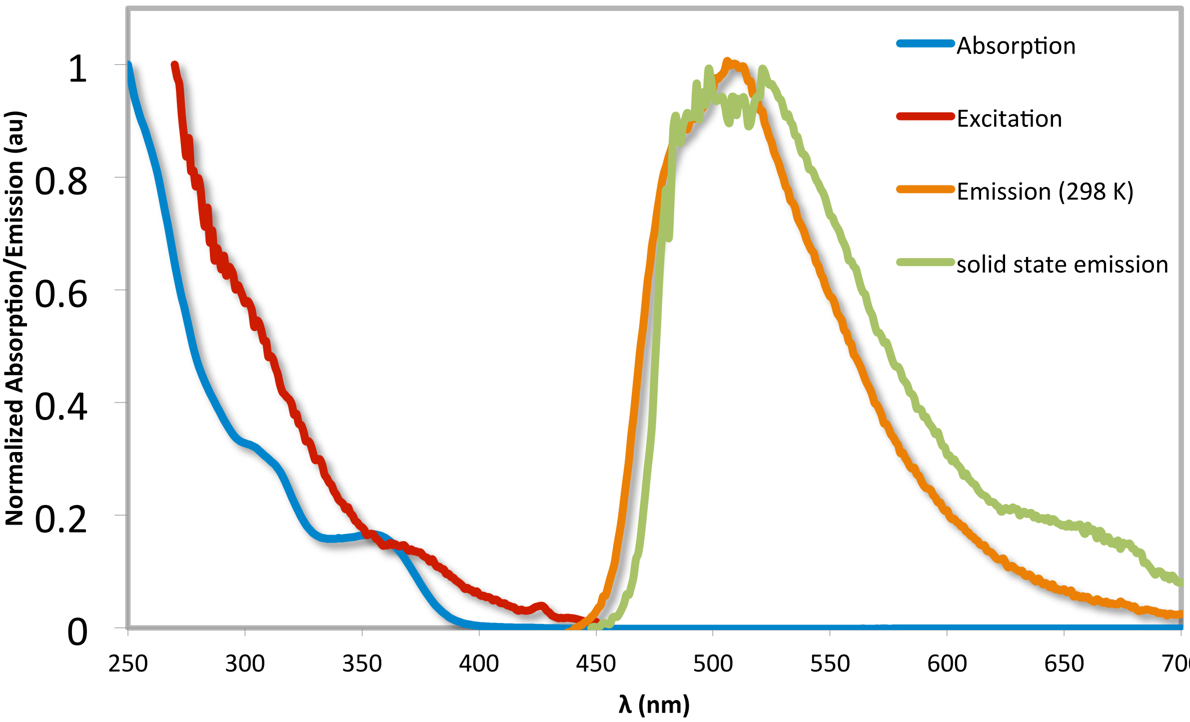

Figure **S73**. UV-Vis (in blue, in acetonitrile at 298 K), excitation (in red) and emission spectra (in orange, excitation wavelength: 360 nm, in degassed acetonitrile at 298 K) and solid state emission spectrum (in green, excitation wavelength: 360 nm, dip-coating deposition on pristine quartz substrate) of **[Ir(ppy)$_2$(xantphos)]PF$_6$ (1a)**.

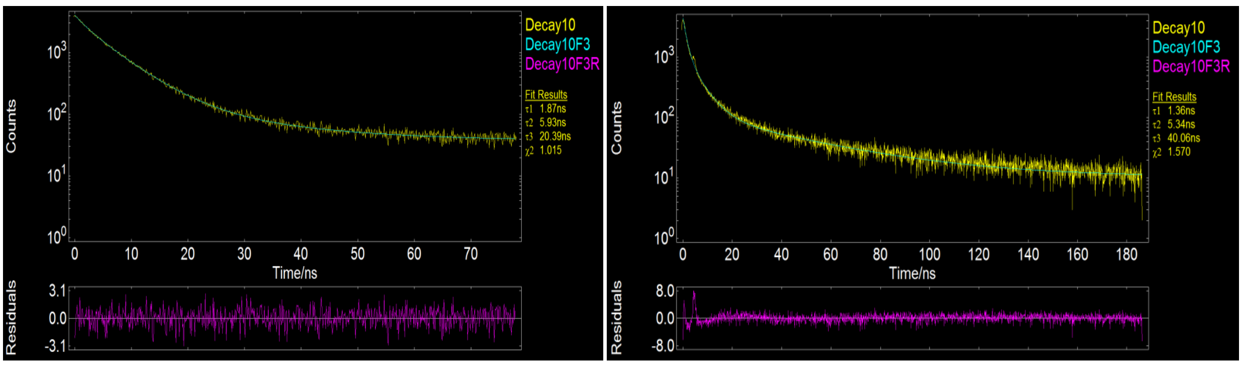

Figure **S74**. Lifetime decays of **[Ir(ppy)$_2$(xantphos)](PF$_6$) (1a)** after excitation at 379 nm; **left)** in degassed acetonitrile at 298 K; **right)** dip-coating deposition on pristine quartz substrate.

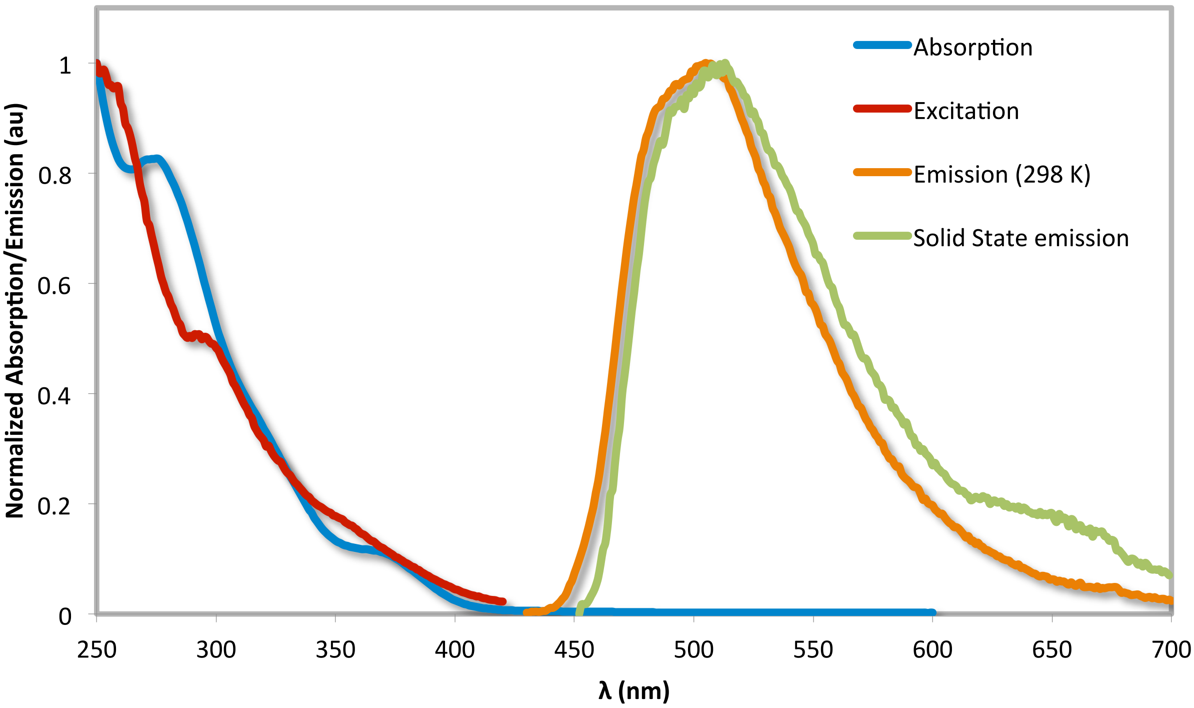

Figure **S75**. UV-Vis (in blue, in acetonitrile at 298 K), excitation (in red) and emission spectra (in orange, excitation wavelength: 360 nm, in degassed acetonitrile at 298 K) and solid state emission spectrum (in green, excitation wavelength: 360 nm, dip-coating deposition on pristine quartz substrate) of **[Ir(mesppy)$_2$(xantphos)]PF$_6$ (2a).**

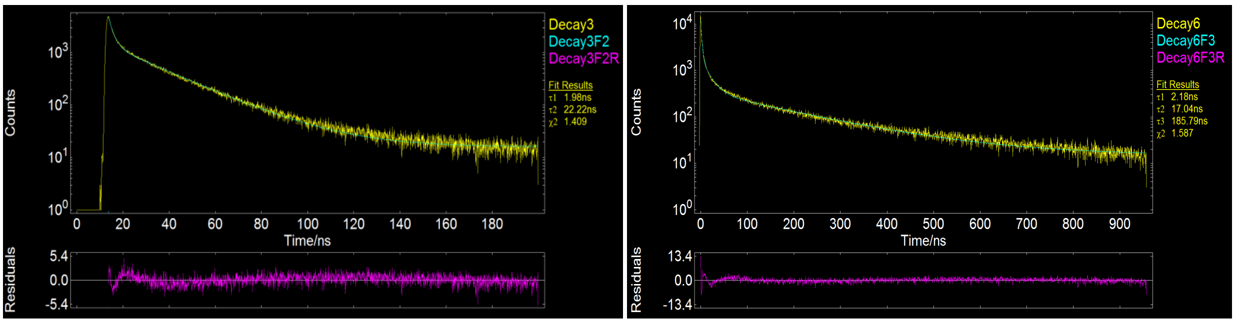

Figure **S76**. Lifetime decays of **[Ir(mesppy)$_2$(xantphos)](PF$_6$) (2a)** after excitation at 379 nm; **left)** in degassed acetonitrile at 298 K, **right)** dip-coating deposition on pristine quartz substrate.

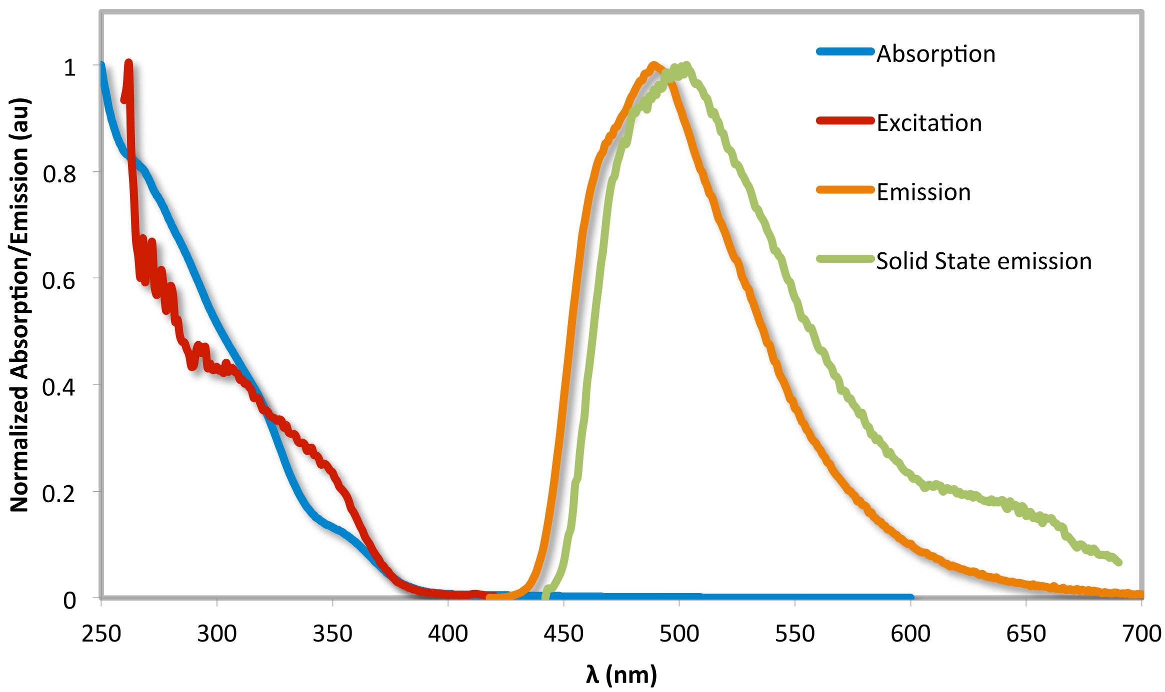

Figure **S77**. UV-Vis (in blue, in acetonitrile at 298 K), excitation (in red) and emission spectra (in orange, excitation wavelength: 360 nm, in degassed acetonitrile at 298 K) and solid state emission spectrum (in green, excitation wavelength: 360 nm, dip-coating deposition on pristine quartz substrate) of **[Ir(dFmesppy)$_2$(xantphos)]PF$_6$ (4a).**

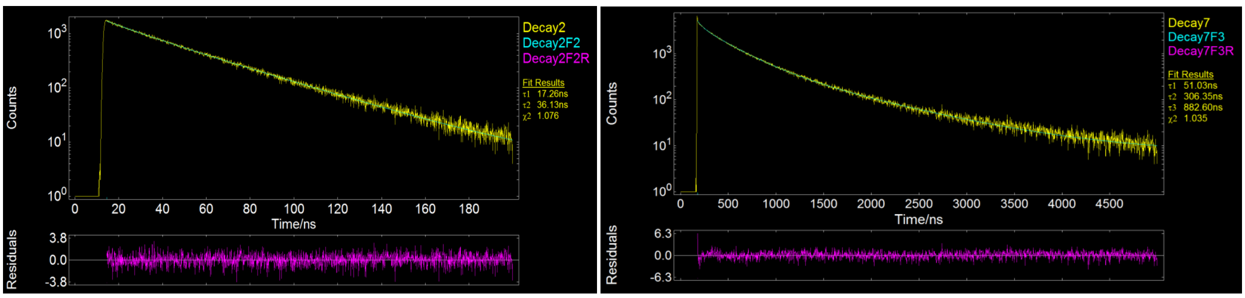

Figure **S78**. Lifetime decays of **[Ir(dFmesppy)$_2$(xantphos)]PF$_6$ (4a)** after excitation at 379 nm**; left)** in degassed acetonitrile at 298 K, **right)** dip-coating deposition on pristine quartz substrate.

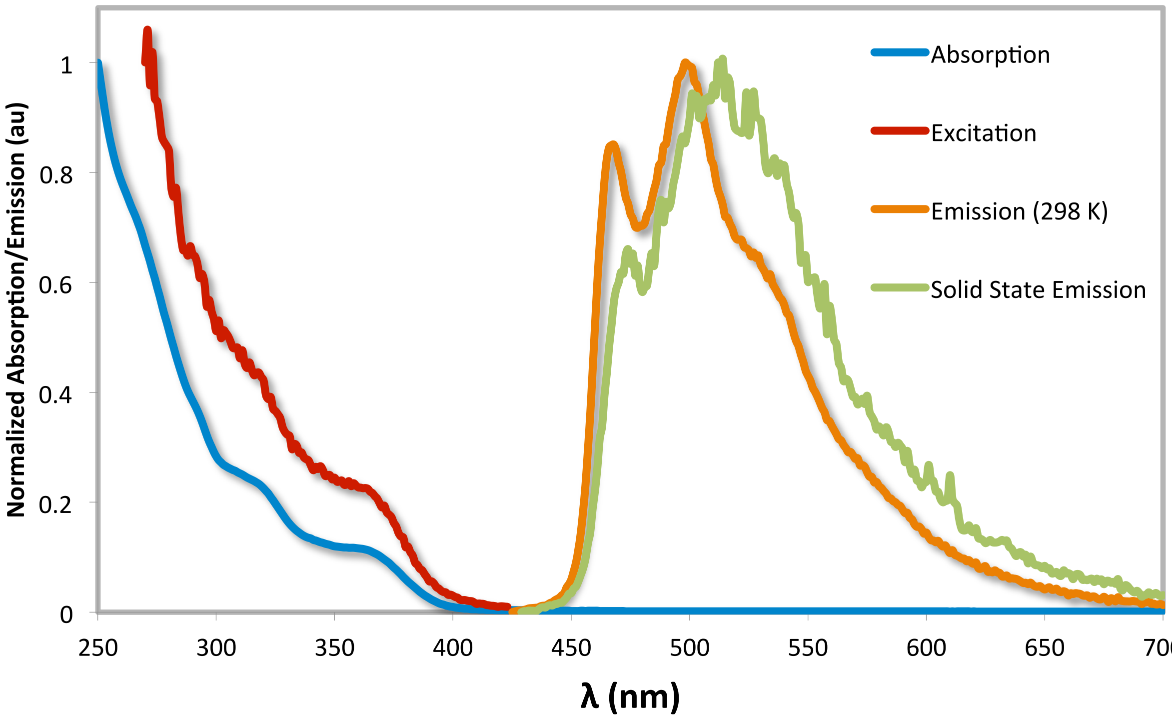

Figure **S79**. UV-Vis (in blue, in acetonitrile at 298 K), excitation (in red) and emission spectra (in orange, excitation wavelength: 360 nm, in degassed acetonitrile at 298 K) and solid state emission spectrum (in green, excitation wavelength: 360 nm, dip-coating deposition on pristine quartz substrate) of **[Ir(ppy)$_2$(dpephos)]PF$_6$ (1b).**

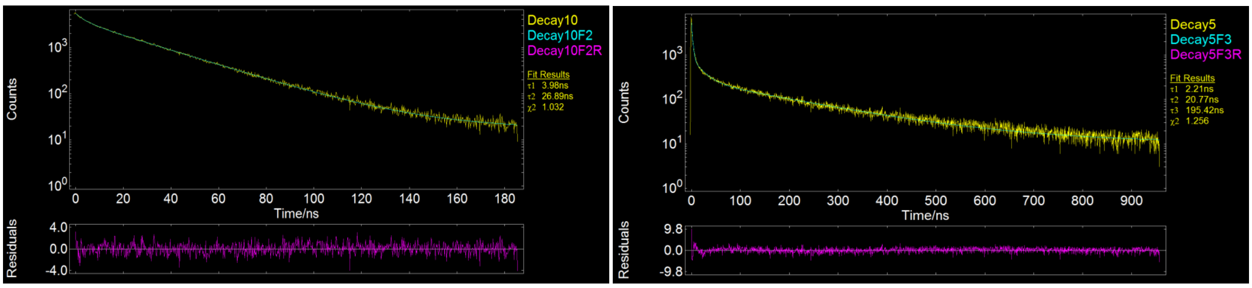

Figure **S80**. Lifetime decays of **[Ir(ppy)$_2$(dpephos)]PF$_6$ (1b)** after excitation at 379 nm; **left**) in degassed acetonitrile at 298 K, **right)** dip-coating deposition on pristine quartz substrate.

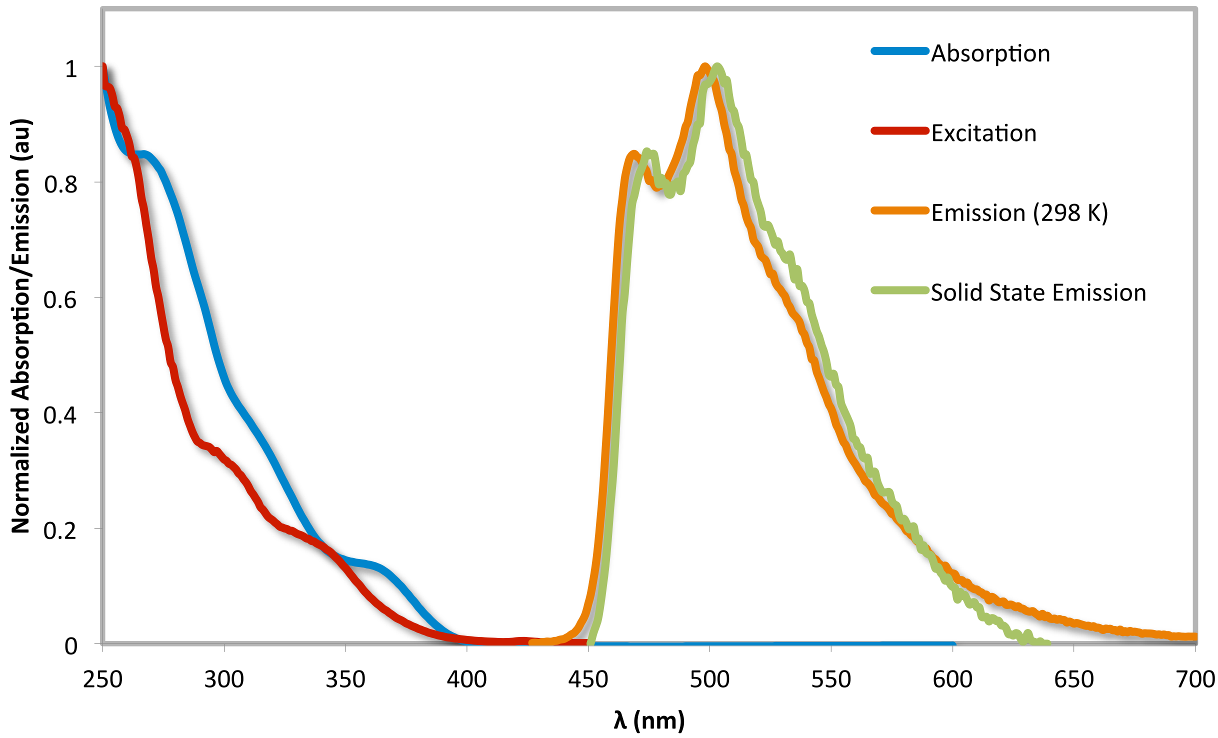

Figure **S81**. UV-Vis (in blue, in acetonitrile at 298 K), excitation (in red) and emission spectra (in orange, excitation wavelength: 360 nm, in degassed acetonitrile at 298 K) and solid state emission spectrum (in green, excitation wavelength: 360 nm, dip-coating deposition on pristine quartz substrate) of **[Ir(mesppy)$_2$(dpephos)]PF$_6$ (2b).**

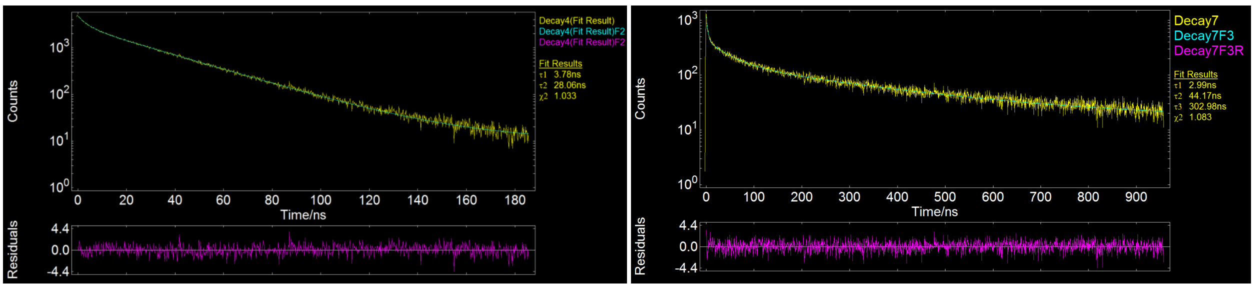

Figure **S82**. Lifetime decays of **[Ir(mesppy)$_2$(dpephos)]PF$_6$ (2b)** after excitation at 379 nm; **left)** in degassed acetonitrile at 298 K, **right)** dip-coating deposition on pristine quartz substrate.

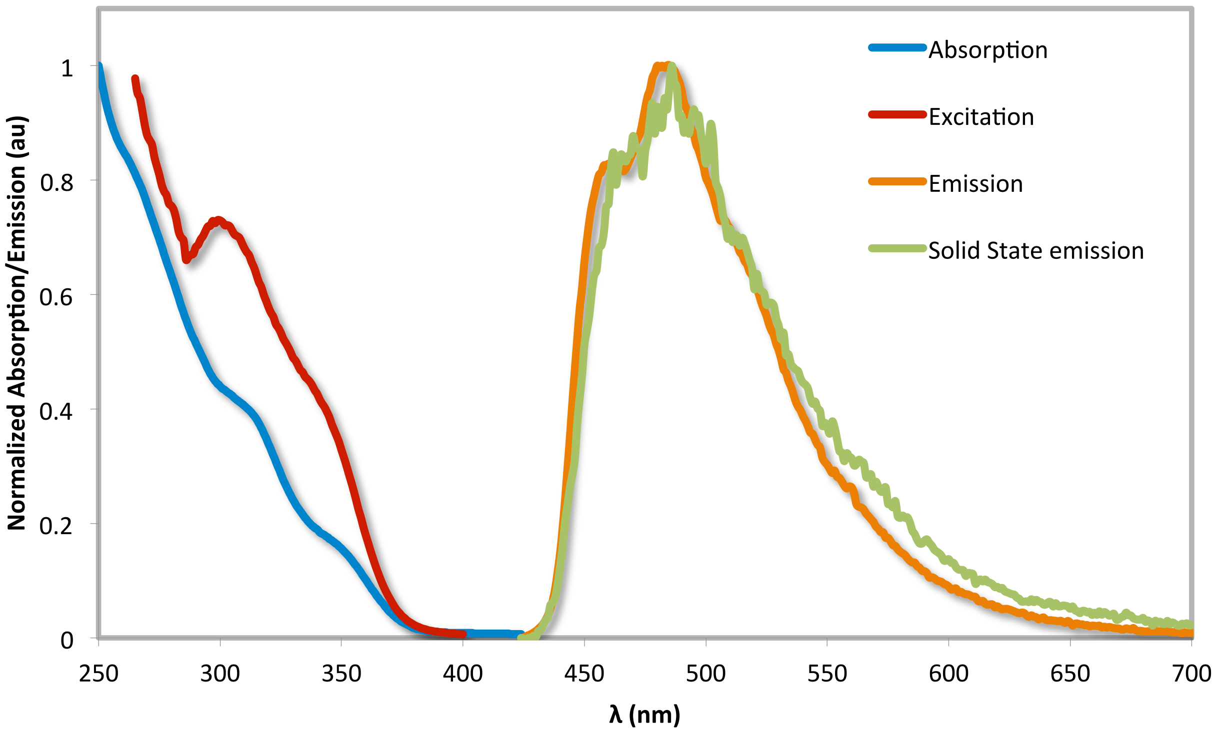

Figure **S83**. UV-Vis (in blue, in acetonitrile at 298 K), excitation (in red) and emission spectra (in orange, excitation wavelength: 360 nm, in degassed acetonitrile at 298 K) and solid state emission spectrum (in green, excitation wavelength: 360 nm, dip-coating deposition on pristine quartz substrate) of **[Ir(dFmesppy)$_2$(dpephos)]PF$_6$ (4b).**

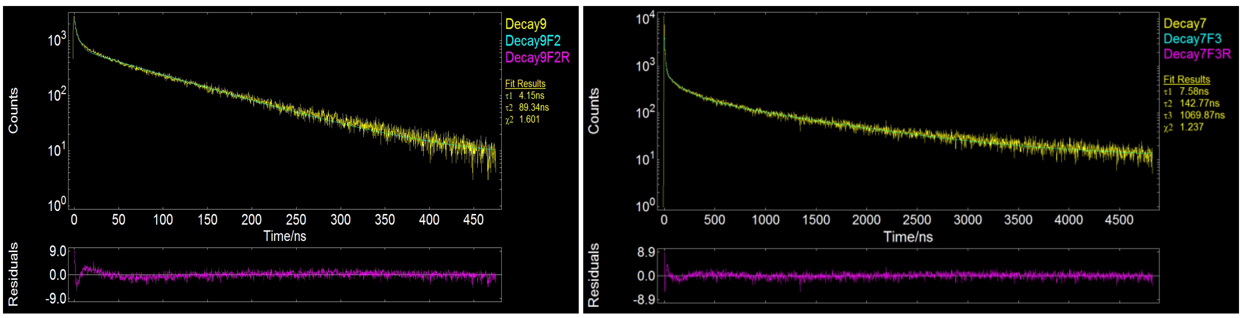

Figure **S84**. Lifetime decays of **[Ir(dFmesppy)$_2$(dpephos)]PF$_6$ (4b)** after excitation at 379 nm; **left)** in degassed acetonitrile at 298 K**, right)** dip-coating deposition on pristine quartz substrate.

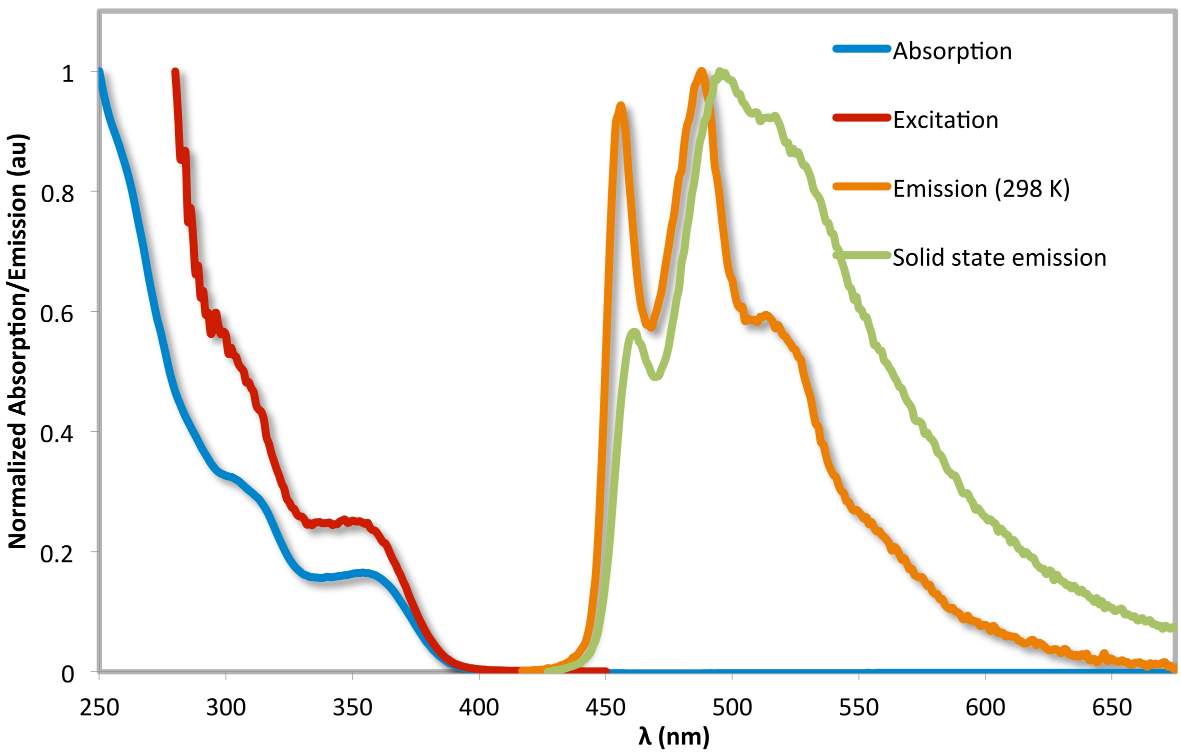

Figure **S85**. UV-Vis (in blue, in acetonitrile at 298 K), excitation (in red) and emission spectra (in orange, excitation wavelength: 360 nm, in degassed acetonitrile at 298 K) and solid state emission spectrum (in green, excitation wavelength: 360 nm, dip-coating deposition on pristine quartz substrate) of **[Ir(ppy)$_2$(dppe)]PF$_6$ (1c)**.

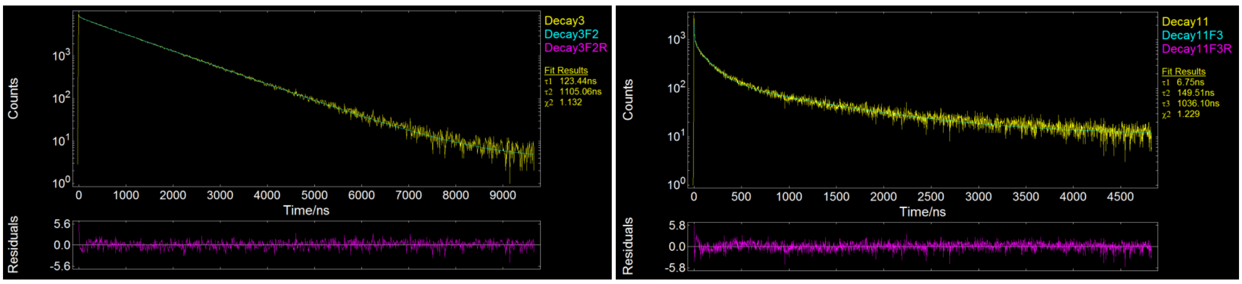

Figure **S86**. Lifetime decays of **[Ir(ppy)$_2$(dppe)](PF$_6$) (1c)** after excitation at 379 nm; **left)** in degassed acetonitrile at 298 K, **right)** dip-coating deposition on pristine quartz substrate.

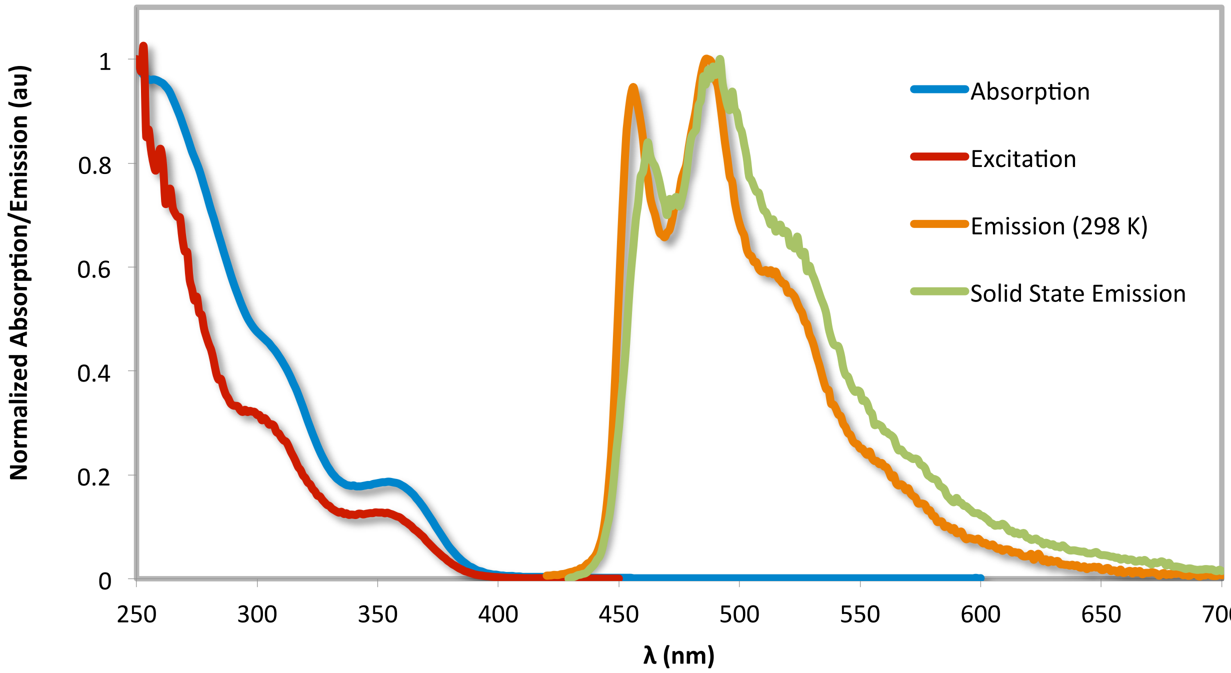

Figure **S87**. UV-Vis (in blue, in acetonitrile at 298 K), excitation (in red) and emission spectra (in orange, excitation wavelength: 360 nm, in degassed acetonitrile at 298 K) and solid state emission spectrum (in green, excitation wavelength: 360 nm, dip-coating deposition on pristine quartz substrate) of **[Ir(mesppy)$_2$(dppe)]PF$_6$ (2c)**.

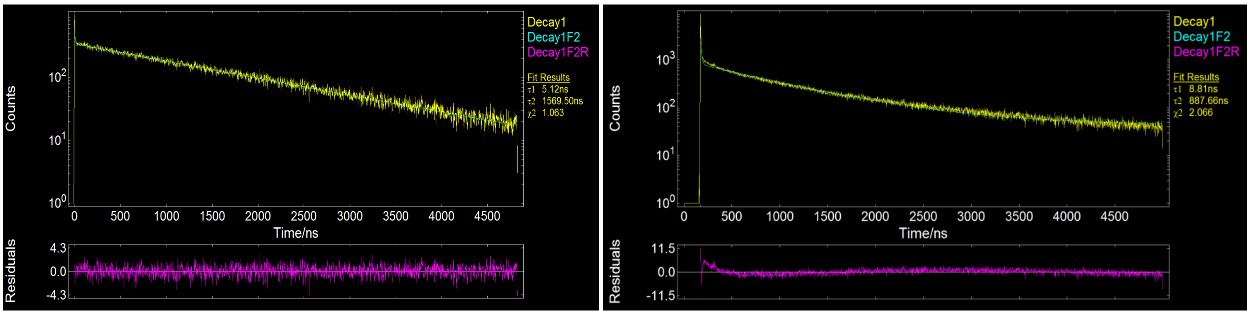

Figure **S88**. Lifetime decays of **[Ir(mesppy)$_2$(dppe)]PF$_6$ (2c)** after excitation at 379 nm; **left)** in degassed acetonitrile at 298 K, **right)** dip-coating deposition on pristine quartz substrate.

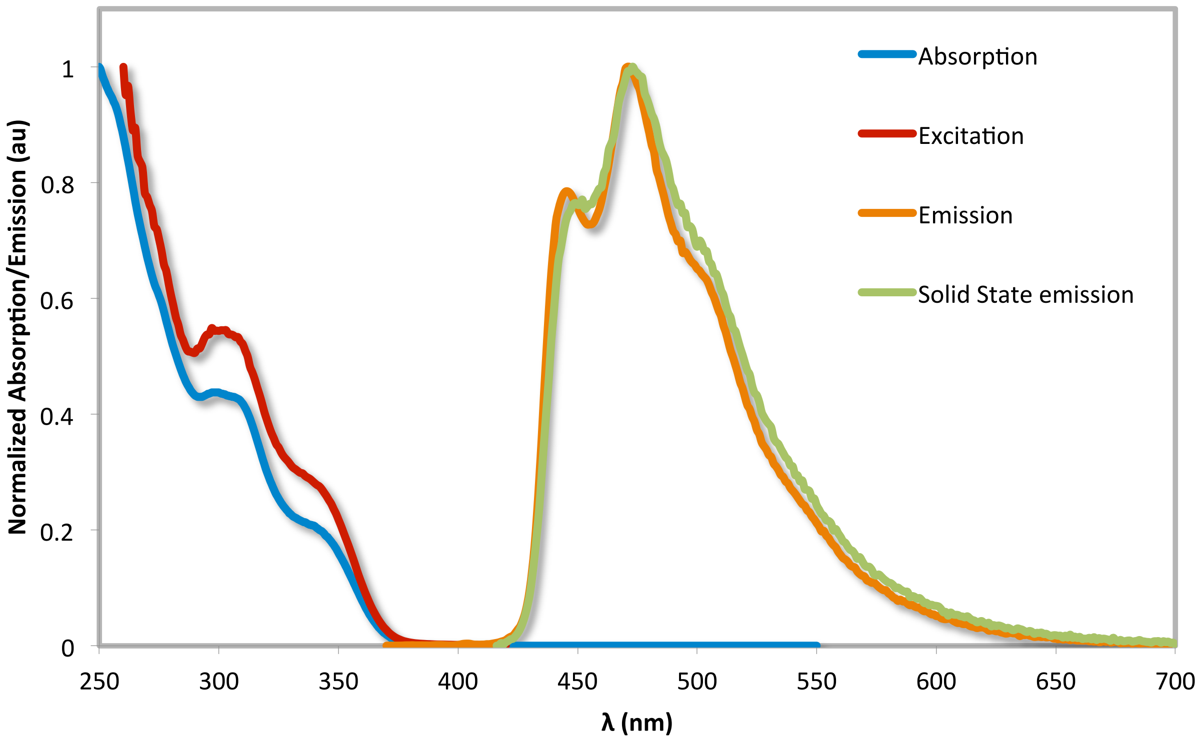

Figure **S89**. UV-Vis (in blue, in acetonitrile at 298 K), excitation (in red) and emission spectra (in orange, excitation wavelength: 360 nm, in degassed acetonitrile at 298 K) and solid state emission spectrum (in green, excitation wavelength: 360 nm, dip-coating deposition on pristine quartz substrate) of **[Ir(dFmesppy)$_2$(dppe)]PF$_6$ (4c)**.

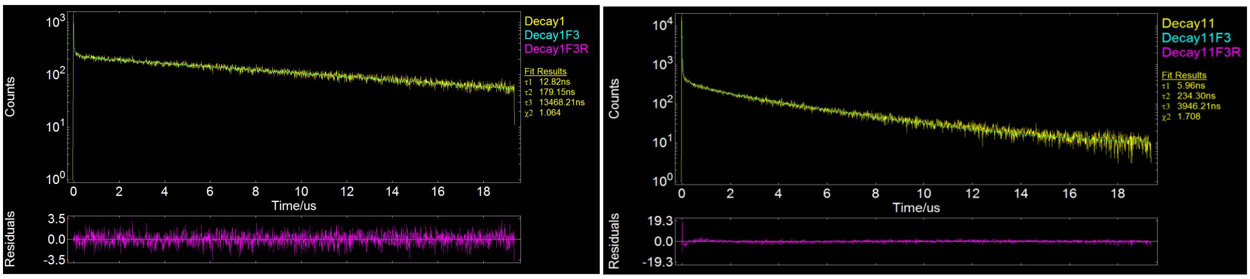

Figure **S90**. Lifetime decays of **[Ir(dFmesppy)$_2$(dppe)]PF$_6$ (4c)** after excitation at 379 nm; **left)** in degassed acetonitrile at 298 K, **right)** dip-coating deposition on pristine quartz substrate.

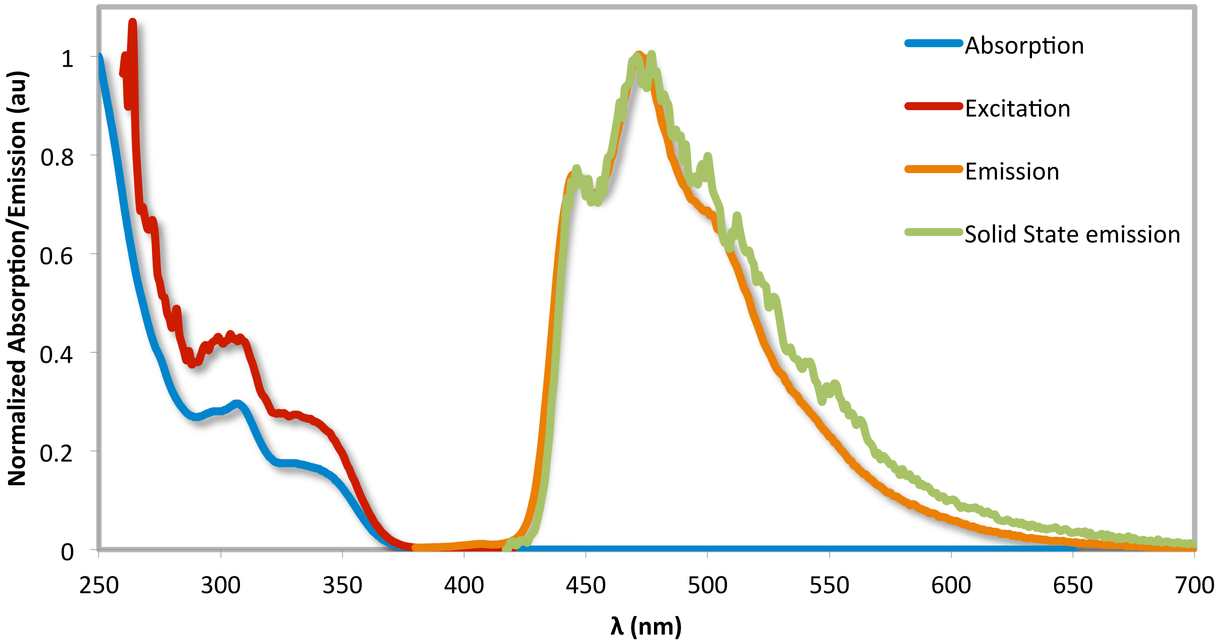

Figure **S91**. UV-Vis (in blue, in acetonitrile at 298 K), excitation (in red) and emission spectra (in orange, excitation wavelength: 360 nm, in degassed acetonitrile at 298 K) and solid state emission spectrum (in green, excitation wavelength: 360 nm, dip-coating deposition on pristine quartz substrate) of **[Ir(dFppy)$_2$(dppe)]PF$_6$ (3c)**.

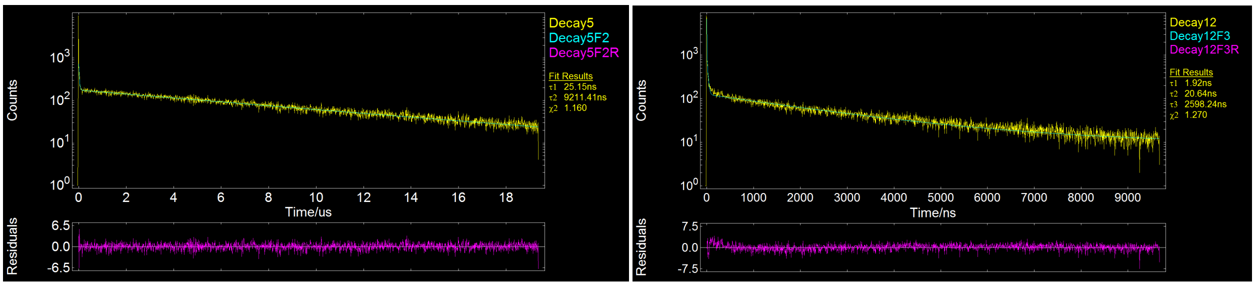

Figure **S92**. Lifetime decays of **[Ir(dFppy)$_2$(dppe)]PF$_6$ (3c)** after excitation at 379 nm; **left)** in degassed acetonitrile at 298 K, **right)** dip-coating deposition on pristine quartz substrate.

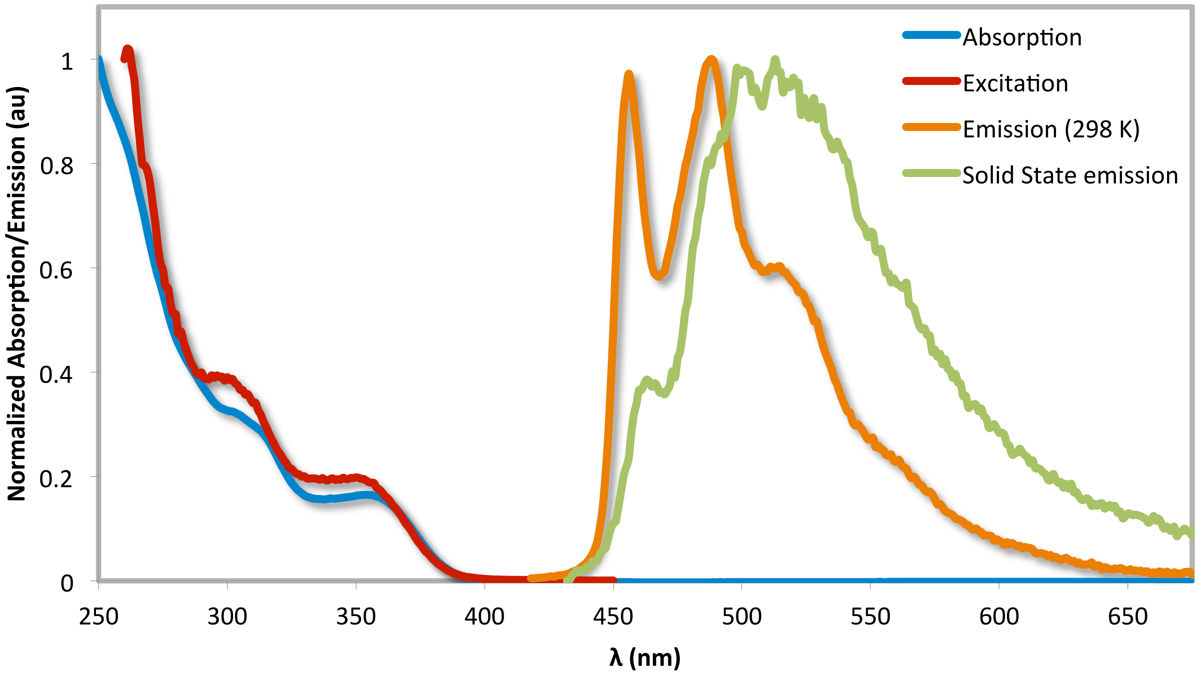

Figure **S93**. UV-Vis (in blue, in acetonitrile at 298 K), excitation (in red) and emission spectra (in orange, excitation wavelength: 360 nm, in degassed acetonitrile at 298 K) and solid state emission spectrum (in green, excitation wavelength: 360 nm, dip-coating deposition on pristine quartz substrate) of **[Ir(ppy)$_2$(Dppe)]PF$_6$ (1d)**.

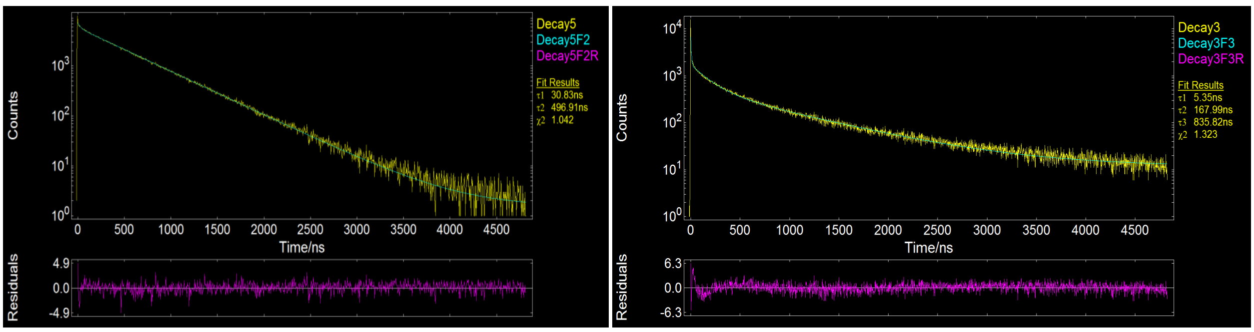

Figure **S94**. Lifetime decays of **[Ir(ppy)$_2$(Dppe)]PF$_6$ (1d)** after excitation at 379 nm; **left)** in degassed acetonitrile at 298 K, **right)** dip-coating deposition on pristine quartz substrate.

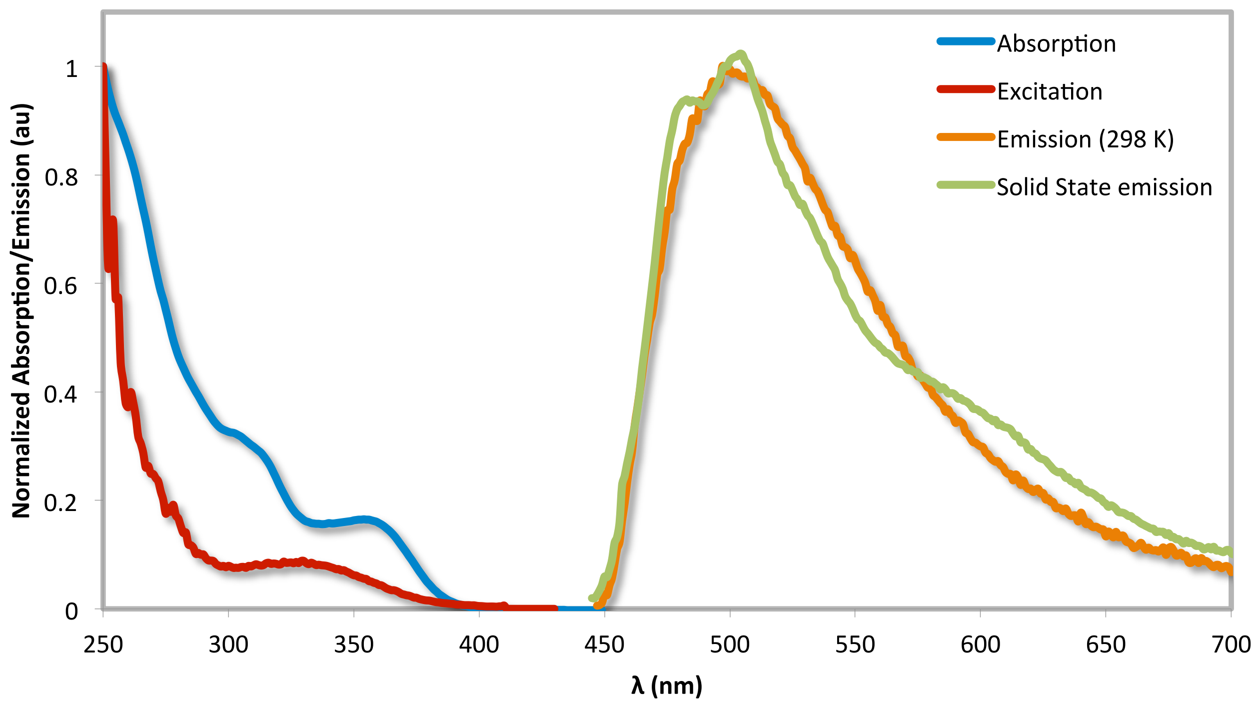

Figure **S95**. UV-Vis (in blue, in acetonitrile at 298 K), excitation (in red) and emission spectra (in orange, excitation wavelength: 360 nm, in degassed acetonitrile at 298 K) and solid state emission spectrum (in green, excitation wavelength: 360 nm, dip-coating deposition on pristine quartz substrate) of **[Ir(ppy)$_2$(isopropxantphos)]PF$_6$ (1f)**.

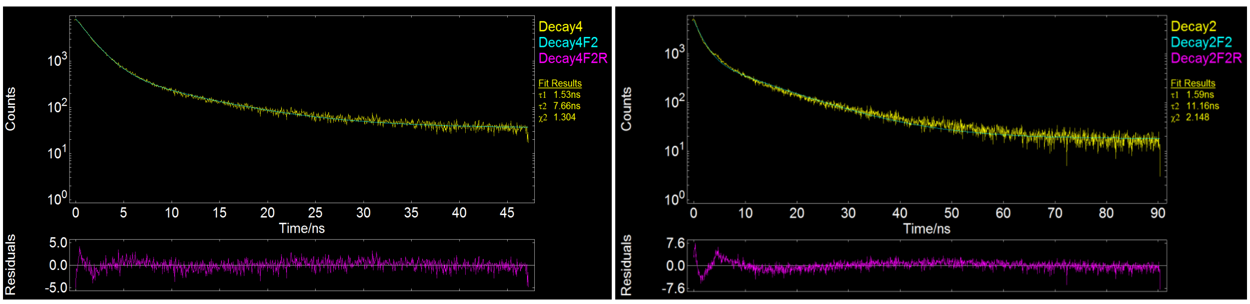

Figure **S96**. Lifetime decays of **[Ir(ppy)$_2$(isopropxantphos)]PF$_6$ (1f)** after excitation at 379 nm; **left)** in degassed acetonitrile at 298 K, **right)** dip-coating deposition on pristine quartz substrate.

Table **S1**. Supplementary Optoelectronic Characterization

complex	UV-Vis (nm) [ε(×10^3 M^{-1} cm^{-1})][a]	k_r (x10^5 s^{-1})[b]	k_{nr} (x10^7 s^{-1})[b]	*E-Chem*[c] E_{pa} (V)
1a	262 [25.4], 308 [9.5], 358 [5.1]	1.5	5.0	1.38
2a	276 [31.2], 316 [13.6], 368 [3.8]	2.1	3.6	1.40
4a	261 [32.5], 318 [1.7], 359 [4.7]	1.9	2.8	1.68
1b	293 [13.1],318 [8.3], 358 [4.2]	2.2	3.7	1.39
2b	269 [33.5], 317 [13.5], 365 [4.3]	3.2	3.5	1.41
4b	266 [24.4], 313 [12.8], 350 [4.9]	1.0	1.1	1.69
1c	260 [28.7], 308 [10.5], 358 [6.3]	0.38	0.087	1.42
2c	260 [32.8], 307 [15], 357 [6.3]	0.28	0.061	1.43
4c	266 [23.1], 313 [12.1], 350 [4.6]	0.39	0.0035	1.72
3c	276 [28.3], 309 [19.9], 342 [8.8]	0.19	0.0090	1.72
1d	260 [23.3], 306 [8.4], 356 [4.5]	0.32	0.20	1.44
1f	260 [19.9], 312 [6.8], 357 [4.3]	2.3	3.8	1.39
1e	270 [19.9], 320 [9.9]	-	-	1.42

[a] Measurements in acetonitrile at 298 K. [b] Crude calculations assuming emission only from the longest lived state. [c] Measurements performed at 50 mV s^{-1} in degassed acetonitrile solution using Fc/Fc$^+$ as an internal standard, and are referenced with respect to SCE (Fc/Fc$^+$ = 0.38 V in MeCN).

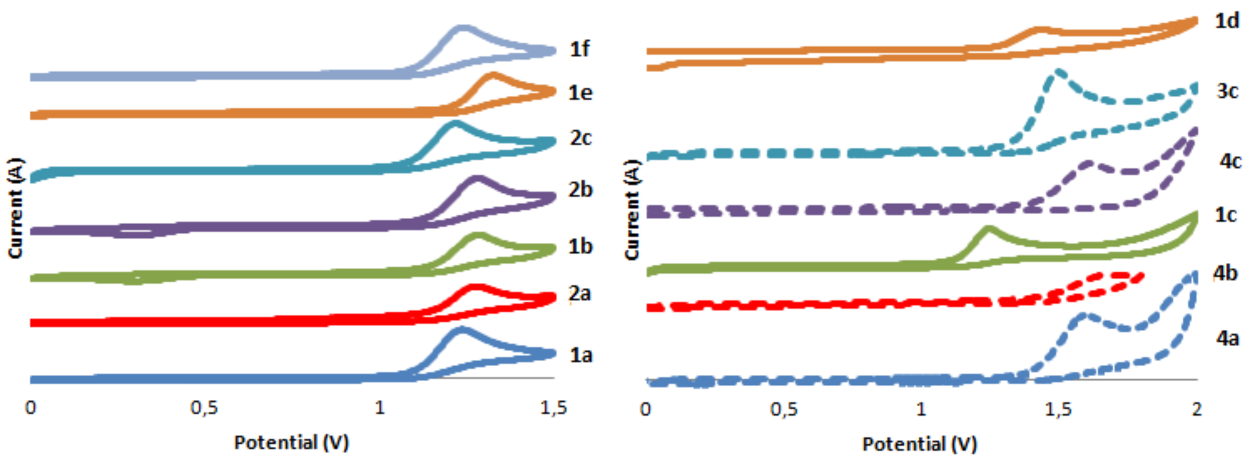

Figure **S98**. Oxidation processes of complexes **1 - 4** in MeCN with 0.1 M $TBAPF_6$ as the supporting electrolyte. Scan rate: 0.1V sec^{-1}

Electroluminescent devices (LEECs)

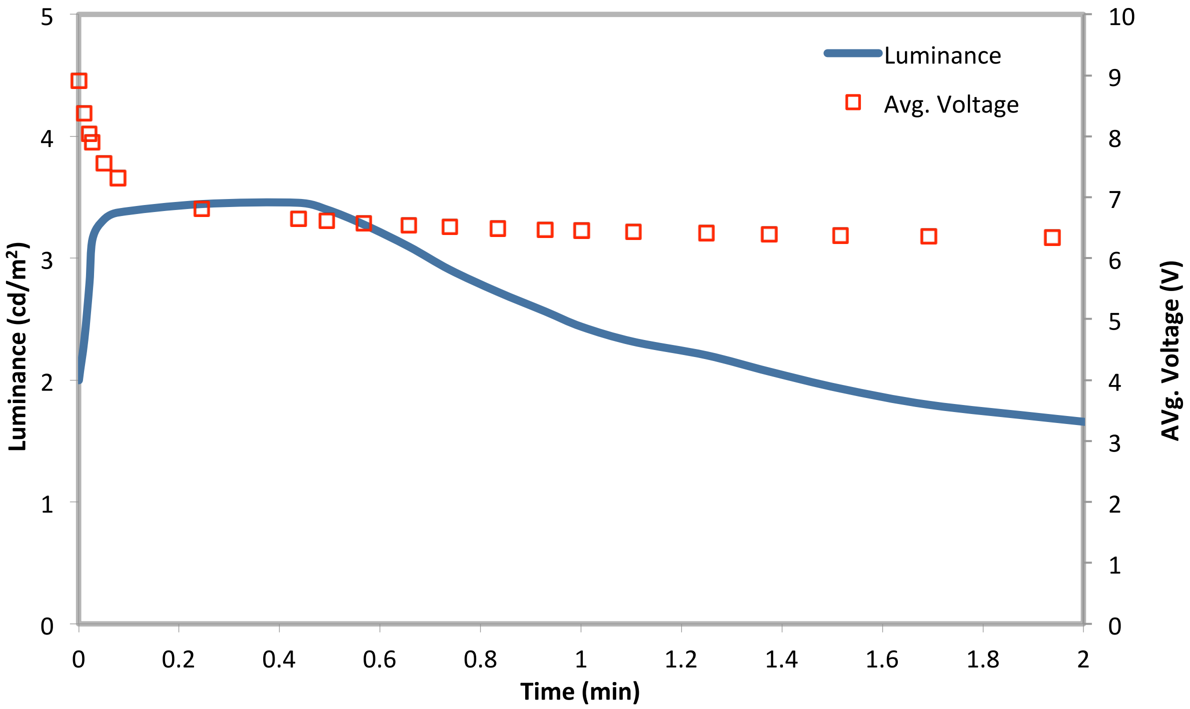

Figure **S99**. Luminance (solid blue line) and average voltage (open red squares) versus time for ITO/PEDOT:PSS/ **1b**:[Bmim][PF_6] 4:1/Al under a constant pulsed current (1000Hz, 50% duty cycle and block wave) of 765 A m^{-2} (average current density). [Bmim][PF_6] = 1-butyl-3-methylimidazolium hexafluorophosphate.

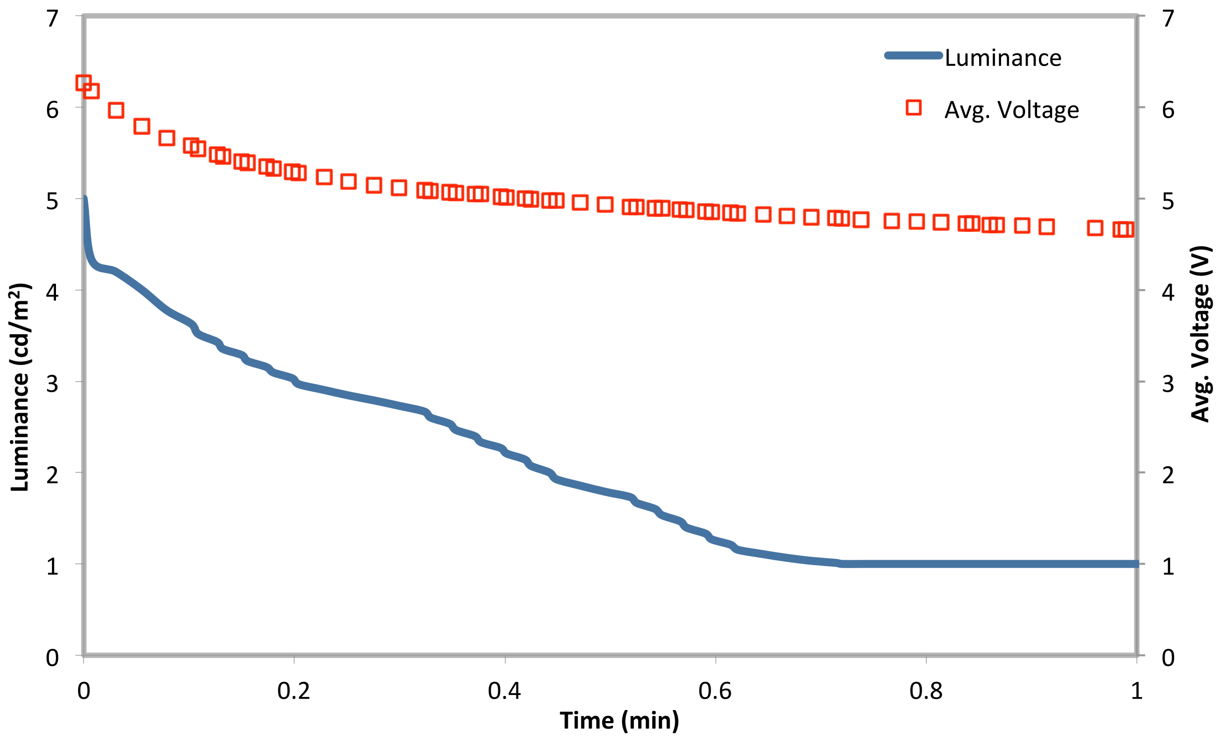

Figure **S100**. Luminance (solid blue line) and average voltage (open red squares) versus time for ITO/PEDOT:PSS/ **4a**:[Bmim][PF_6] 4:1/Al under a constant pulsed current (1000Hz, 50% duty cycle and block wave) of 765 A m-2 (average current density). [Bmim][PF_6] = 1-butyl-3-methylimidazolium hexafluorophosphate.

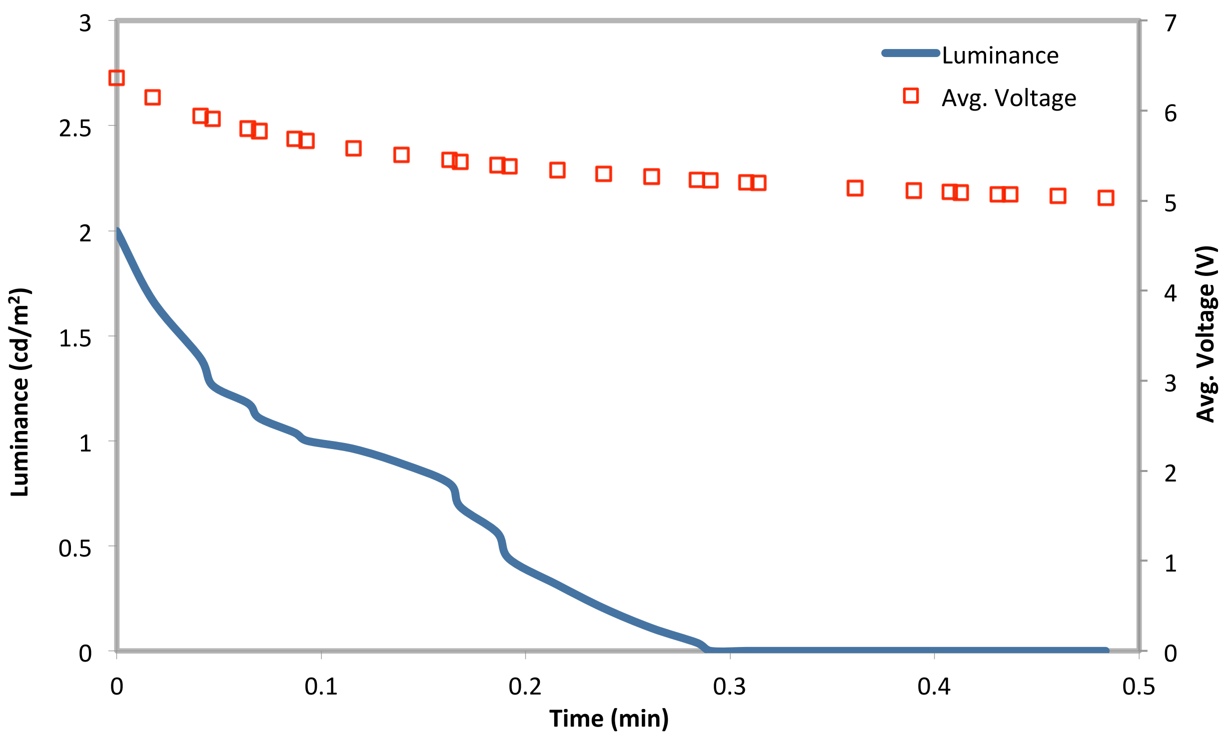

Figure **S101**. Luminance (solid blue line) and average voltage (open red squares) versus time for ITO/PEDOT:PSS/ **4b**:[Bmim][PF_6] 4:1/Al under a constant pulsed current (1000Hz, 50% duty cycle and block wave) of 765 A m-2 (average current density). [Bmim][PF_6] = 1-butyl-3-methylimidazolium hexafluorophosphate.

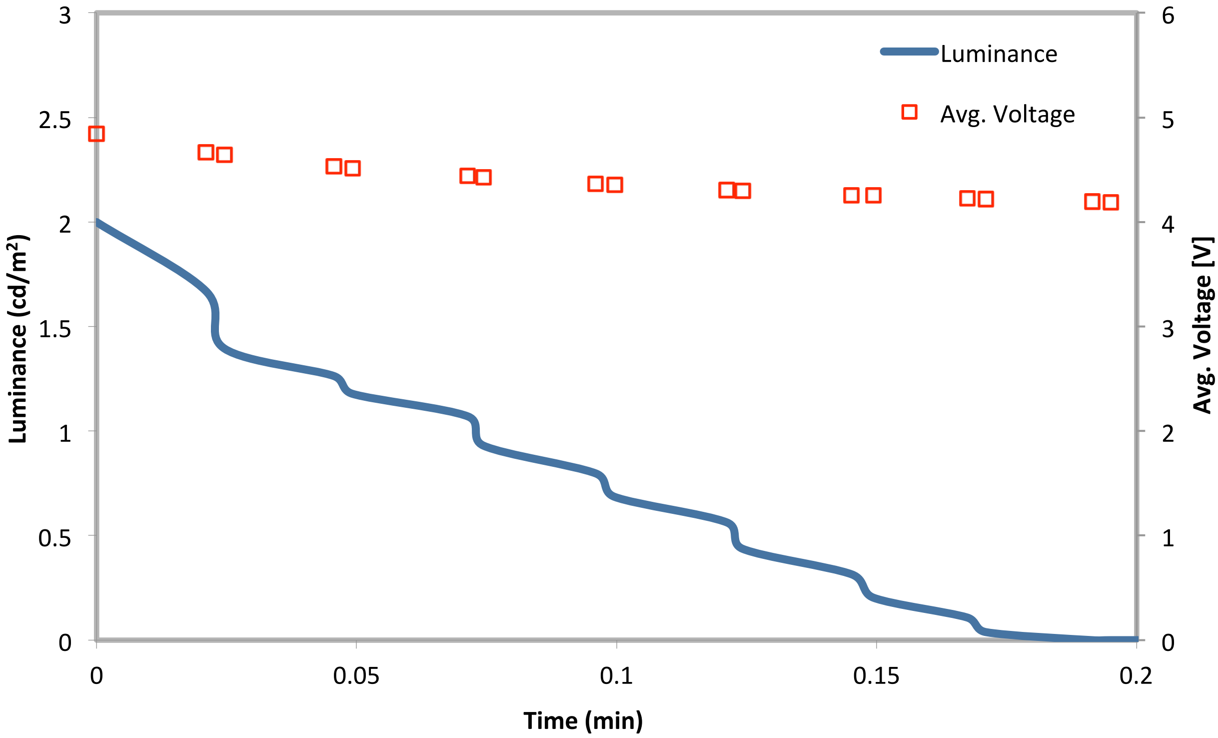

Figure **S102**. Luminance (solid blue line) and average voltage (open red squares) versus time for ITO/PEDOT:PSS/ **4c**:[Bmim][PF_6] 4:1/Al under a constant pulsed current (1000Hz, 50% duty cycle and block wave) of 765 A m-2 (average current density). [Bmim][PF_6] = 1-butyl-3-methylimidazolium hexafluorophosphate.